

# IFAC

INTERNATIONAL FEDERATION  
OF AUTOMATIC CONTROL



WARSZAWA 1969

## Pneumatic and Hydraulic Components

Fourth Congress of the International  
Federation of Automatic Control  
Warszawa 16–21 June 1969

TECHNICAL  
SESSION

# 14



Organized by  
Naczelna Organizacja Techniczna w Polsce

**INTERNATIONAL FEDERATION OF AUTOMATIC CONTROL**

# **Pneumatic and Hydraulic Components**

**TECHNICAL SESSION No 14**

**FOURTH CONGRESS OF THE INTERNATIONAL  
FEDERATION OF AUTOMATIC CONTROL  
WARSZAWA 16 – 21 JUNE 1969**



**Organized by  
Naczelna Organizacja Techniczna w Polsce**



Biblioteka  
Politechniki Białostockiej



1181040

K-1289

### Contents

Paper No		Page
14.1	H - A.Boros - Natural Oscillations of Pneumatic Power Amplifiers and a Solution for Their Elimination.....	3
14.2	GB - J.J.Hunter - The Dynamic Behaviour of Hydraulic Components.....	16
14.3	GB - H.R.Martin, A.Lichtarowicz - Small Amplitude Response Characteristics in Hydraulic Servomechanisms.....	31
14.4	USA - W.J.Thayer - Redundant Electrohydraulic Servo-actuators.....	52
14.5	USA - B.L.Ho - Mechanical Transmission Ratio Requirements in Minimum-Time Positioning Servos.....	88
14.6	D - R.Müller - Experimental Method of Sizing Final Control Elements /Control Valves/ for Process Plants.....	97
	/GDR/	

Wydawnictwa Czasopism Technicznych NOT - Polska

Zakład Poligraficzny WCT NOT. Zam. 108/69.

# NATURAL OSCILLATIONS OF PNEUMATIC POWER AMPLIFIERS AND A SOLUTION FOR THEIR ELIMINATION

Dr. A. Boros

Hungarian Academy of Science, Research Institute  
for Automation

Budapest - Hungary

## 1) Introduction

It is generally known that the pneumatic signal changers function on a low performance level and that, at the same time, their coupling elements represent, in general, a capacitive load.

The dynamic characteristics of the pneumatic control circuit can be highly improved if a power-boosting element is connected. The purpose of this element is to keep large quantities of air in motion at the outlet according to the instantaneous level of the signal changer stress. Thus, the power amplifier fulfills a coupling task, i.e., it enables coupling a load of low impedance (especially a capacitive load) to a generator with high internal resistance.

It is also known that the pneumatic power amplifiers may be of the following types according to their functions:

- 1) Amplifiers with continuous air consumption
- 2) Amplifiers with intermittent air consumption.

The power amplifiers mentioned under 1) are characterised by the phenomenon that a continuous air stream is moving at the inlet and outlet valves, even in the stationary state. This disadvantageous characteristic is compensated only to a small degree by making the performance of this type smoother with a lower tendency to oscillate, in comparison to Type 2 where an air stream occurs only during the transient process.

In this paper we publish part of our studies which



have been carried out with the widely applied power compensating amplifier which has intermittent air consumption and is provided with a loose twin diaphragm.

Main characteristics of this type are high accuracy of signal imitation, sensitivity and tendency to produce self-excited oscillations of relatively high frequency.

Our studies have been mainly directed towards the generation of oscillations as well as the possibilities of their avoidance and, meanwhile, we have handed in a suggestion for a design modification which shall be briefly mentioned in this paper.

## 2) Physical Description of the Oscillatory Process

Figure 1 represents the general model which has been studied by us both theoretically and experimentally.

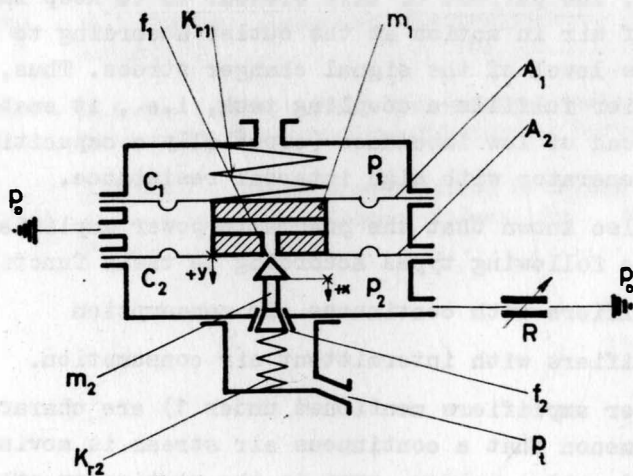


Fig. 1

It shows the special load we have chosen to study the continuous oscillations, i.e.,  $R$  is adjustable (however, is fixed for a given test series) while the capacitive load component  $C = \infty$ ; i.e., the atmosphere itself enables it to

keep the consumption constant in contrast, for instance, to a load of limited capacity where - after replenishment of the load - the consumption of the amplifier and, thus, its oscillations come to a stop.

At this point, we would like to mention that prerequisite [2] - namely, that the oscillations of the amplifier are to be studied in the case of a closed outlet - is mainly of theoretical importance. In our experience, self-excited oscillations in amplifiers with closed outlet do never occur.

At the beginning of our studies we tried to assume that the masses which are designated with  $m_1$  and  $m_2$  in Figure 1 do not separate during oscillations and, thus, form an oscillatory system having one mass ( $m_1 + m_2$ ).

For the purpose of studying the kinematic and initial conditions of the oscillations we have carried out analysis of motion using a film. The amplifier was made of plexiglass to provide transparency. The film which was taken with image frequencies between 2000 c/s and 100 c/s and from different angles made clear that the two masses separate and collide, respectively. Evaluation of the film by means of an analyzer is a very exact method but, at the same time, requires a lot of work. Therefore, we have, on

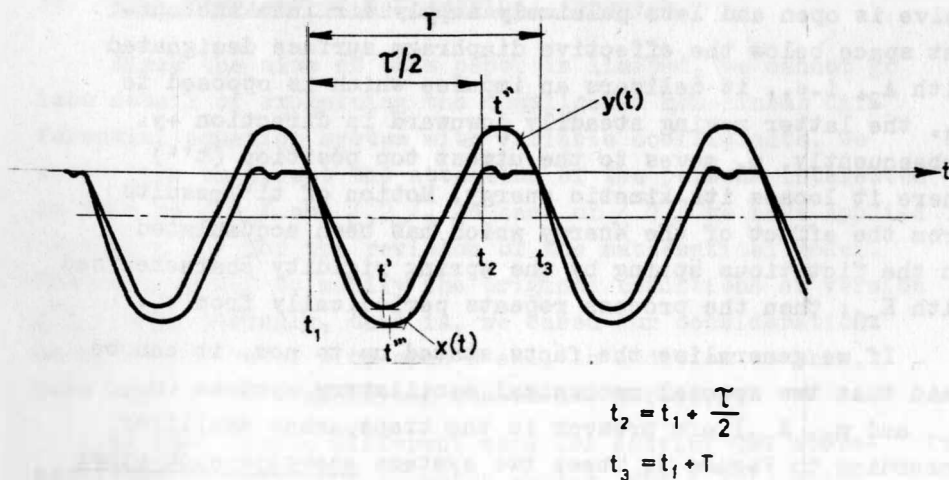


Fig. 2

the basis of more detailed studies, chosen another way. Two special capacitive instrument transducers have been manufactured for the available DISA Universal Indicators. They have been installed in the power amplifier so that the time responses of coordinates  $x$  and  $y$  in Figure 1 became simultaneously visible on the screen of the double-beam oscilloscope. The produced image is visible in Figure 2.

The sinusoidal curve is designated with  $y(t)$ . At first let us consider the already continuous oscillation. Mass  $m_1$  moves steadily downward beginning with time  $\Delta t$  and then  $t_1$ , mass  $m_2$  (that is the valve) is kept in position by the spring on the seat. The two masses collide centrically in the moment  $t_1$ ;  $m_1$  gives  $m_2$  kinetic energy which puts the latter into motion. Since the natural frequency of oscillatory system 2; characterised by  $(m_2; K_{r2})$  differs from that of oscillatory system 1, the two masses separate necessarily from each other. This has been proved by film tests. Thus, mass 2 carries out a free oscillation after the impact impulse, but since its path is limited and  $x(t)$  cannot have negative values, the impact on the valve seat is carried out with  $x = 0$ , in our figure in  $t_2$ . It is an elastic collision and, therefore, the attenuated oscillation pattern has a small amplitude after  $t_2$ .  $m_2$  cannot come to a standstill at once and without transition. Between time  $t_1$  and  $t_2$  the lower valve is open and lets pulsively supply air into the outlet space below the effective diaphragm surface designated with  $A_2$ , i.e., it delivers an impulse which is opposed to  $m_1$ , the latter moving steadily downward in direction  $+y$ . Subsequently,  $m_1$  moves to the utmost top position ( $t''$ ) where it loses its kinetic energy. Motion of  $t''$  results from the effect of the energy which has been accumulated in the fictitious spring by the spring rigidity characterised with  $K_{r1}$ ; then the process repeats periodically from  $t_3$ .

If we generalise the facts stated up to now, it can be said that two special mechanical oscillatory systems ( $m_1, K_{r1}$  and  $m_2, K_{r2}$ ) are present in the transparent amplifier according to Figure 1. These two systems energize each other in the following way:

- a) Effect of the first on the second: mechanical  
(collision)
- b) Effect of the second on the first: pneumatic  
(opening of the  
supply resistance  
and the pressure  
impulse onto the  
diaphragm).

Energy is required in order to maintain the oscillation. The system must take up this energy from the outside. Therefore, it is possible to maintain permanent oscillations only if the energy taken from the pneumatic supply air is larger between  $t_1$  and  $t_2$  than the energy consumed by the two oscillatory systems in period  $T$ . Unbounded extension of the oscillation amplitude is limited by the non-linear effects of the system.

The beginning of the oscillations is completely similar to the process which occurs with electronic self-oscillating oscilloscopes. One single impulse which, for instance, is unavoidable during energization, is sufficient to unbalance both oscillatory systems; under these oscillatory conditions we have permanent self-excited oscillations.

### 3) Some Problems of Mathematical Approach

Since the size of this paper is limited, we cannot go into detail of explaining the complicated non-linear differential equation system with variable coefficients. We would like to direct the attention of the persons interested in this to [1] and [2]. In case of [1] we have applied version [2] for the revision of the mathematical model. Thereby, we had to modify the original conditions of version [2] very strongly, that is, we based our considerations on an outlet rated with open  $R$  and, in addition to this, have made a few simplifying statements stricter.

We have chosen different ways for solving the above-mentioned differential equation system. For [2], which

divides a period into stages, we use a power series approximation; for [1] we apply the method of harmonic linearisation which results automatically from the corresponding actual oscillogram, because  $y(t)$  or  $P_2(t)$  which cannot be seen in the figure but have been included, too, have only a slightly higher harmonic functional capacity.

[2] is concerned only with theoretical problems and, therefore, the physical contents of the figuring parameters have not been studied in detail. In the course of our studies we have encountered difficulties in defining some parameters. It has, for instance, been difficult to interpret the rigidity of the mentioned fictitious spring  $K_1$ . We intend to consider this phenomenon and a few other questions of minor importance in greater detail in a later publication.

#### 4) Power Amplifier with Pneumatic Attenuation and Stable Functioning

A mechanical method is suggested in order to avoid the mechanical oscillations ([2]) under discussion. In our case the tests could not lead to any realisable result because of differing initial conditions. Therefore, we have studied the pneumatic solution of the problem with which we shall acquaint you in the following.

Let us first look at Figure 3 which demonstrates the approximate causal relationship of the formation of the oscillation pattern which has been physically described under Section 2).

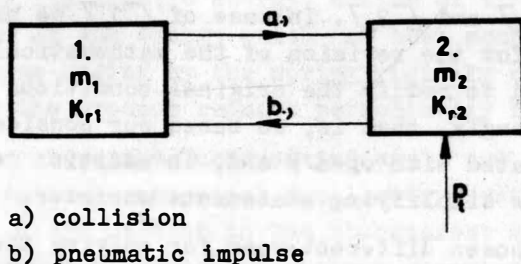


Fig. 3



Both above described oscillatory systems energize each other; the complicated system acquires the energy required for the whole process from the supply air of the active oscillatory system (symbol 2).

Our method consists in separating the blocks with numbers 1. and 2. The active block, marked with 2, is made stable in itself so that it should attenuate the fast excitations occurring along the graph and that it, at the same time, should not affect the slow changings which belong to the plotting strips.

Figure 4, in which the mechanical parts have been neglected, represents active block 2 where electrical analogy has been used to simplify the discussion.

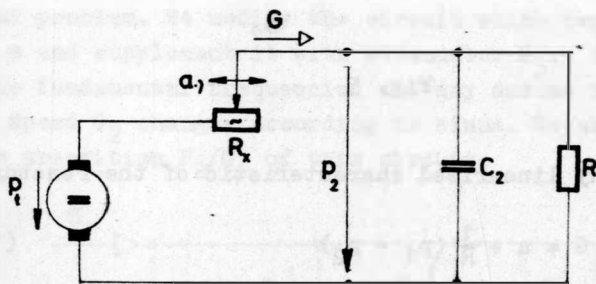


Fig. 4

$R_x$  is the pneumatic resistor which changes with the oscillation rhythm according to coordinate "x". Its range of changing lies in principle between an infinitely and a finitely small value.

In the following we shall take into account only alternating components from the viewpoint of oscillation attenuation. Furthermore, we shall linearise the bent characteristics in a corresponding environment. Those functions which do not consist of a harmonic element are approximated to their Fourier's series by means of the first harmonic function,

Now we derive the characteristics of the two pneumatic basic elements, reactor and storage unit, which have been calculated in alternating components.

a) Reactor

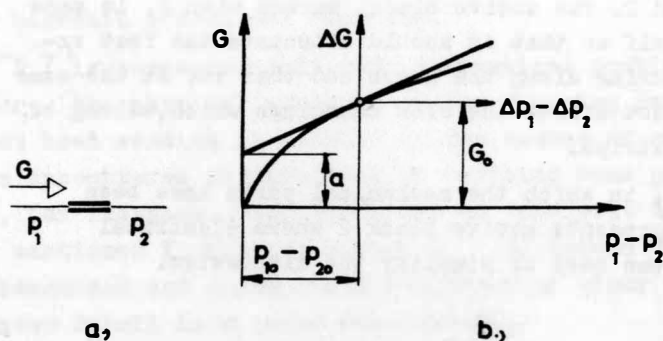


Fig. 5

The already linearised characteristic of the reactor is

$$G = a + \frac{1}{R} (p_1 - p_2) \quad (1)$$

(Equation of the tangential line in Figure 5b).

Let us start with the transform equations

$$G = G_0 + \Delta G \quad (2)$$

$$p_1 = p_{10} + \Delta p_1 \quad (3)$$

$$p_2 = p_{20} + \Delta p_2 \quad (4)$$

Those magnitudes with  $\Delta$  are the new variables.

We get

$$\Delta G = \frac{1}{R} (\Delta p_1 - \Delta p_2) \quad (5)$$

if we take only the alternating components from equations (1) to (4).

b) Storage unit

The basic equation for the storage unit is

$$p - p(0) = \frac{1}{C} \int_0^t G(t) dt \quad (6)$$

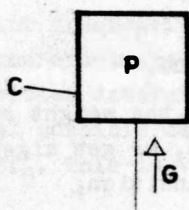


Fig. 6

We get

$$\Delta \dot{P} = \frac{1}{C} \Delta G \quad (7)$$

if we transform (6) into a differential form and express it with new variables marked with  $\Delta$ .

We shall now return after this short deviation to the original problem. We modify the circuit which replaces Figure 4 and supplement it with attenuator  $R_3$ ,  $C_3$ ; we regard only the fundamental frequencies and may assume that the weight speed  $G_2$  changes according to sinus. We shall now examine transition  $P_2/G_2$  of this circuit.

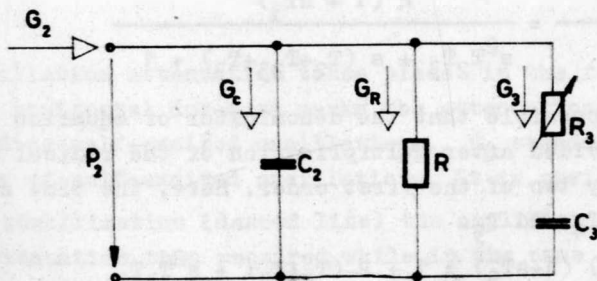


Fig. 7

The equation for the individual basic elements are

Storage unit  $C_2$ :  $\Delta G_C = P_2 C_2 \quad (8)$

Load  $R$ :  $\Delta G_R = \frac{1}{R} \Delta P_2 \quad (9)$

Resistance  $R_3$ :  $\Delta G_3 = \frac{1}{R_3} (\Delta P_2 - \Delta P_3) \quad (10)$

Storage unit  $C_3$ :  $\Delta G_3 = \Delta P_3 C_3 \quad (11)$

thereby applying the above-mentioned equations.

Nodal-point equation

$$\Delta G_2 = \Delta G_C + \Delta G_R + \Delta G_3$$

expresses the distribution of the weight speeds.

If we transform this equation, we get algebraic equations which express the desired transition,

$$\frac{\overline{\Delta p_2}}{\overline{\Delta G_2}} = \frac{R (1 + s R_3 C_3)}{s^2 R C_2 R_3 C_3 + s(RC_2 + RC_3 + R_3 C_3) + 1} \quad (13)$$

where the transformed functions are indicated by a dash-dot line and the complex operator of the transformation is "s".

The following expressions are valid for the individual time constants:

$$RC_2 = T_2; \quad RC_3 = T_{23}; \quad R_3 C_3 = T_3 \quad (14 \text{ a, b, c})$$

Thus we get

$$\frac{\overline{\Delta p_2}}{\overline{\Delta G_2}} = \frac{R (1 + s T_3)}{s^2 T_2 T_3 + s (T_2 + T_{23} + T_3) + 1} \quad (15)$$

It is possible that the denominator of equation (15) is being divided after multiplication of the radical coefficient by two of the first order. Here, the time constants are  $T_4$  and  $T_5$ .

$$(1 + s T_4) (1 + s T_5) = 1 + 2 (T_4 + T_5) + s^2 T_4 T_5 \quad (16)$$

We compare this equation with the denominator of equation (15) and get two equations for the determination of  $T_4$  and  $T_5$ :

$$T_4 T_5 = T_2 T_3 \quad (17)$$

$$T_4 + T_5 = T_2 + T_{23} + T_3 \quad (18)$$

Then we have the transform function

$$\frac{\overline{\Delta p_2}}{\overline{\Delta G_2}} = \frac{R (1 + s T_3)}{(1 + s T_4) (1 + s T_5)} \quad (19).$$

The braking-point frequencies which have been determined by the individual time constants are positioned opposite each other, this position determining the shape of the Bode diagram among several possible cases. Stabilisation occurs if we have  $f_4 < f_3 < f_2 < f_5$ . This is visible in Figure 8.

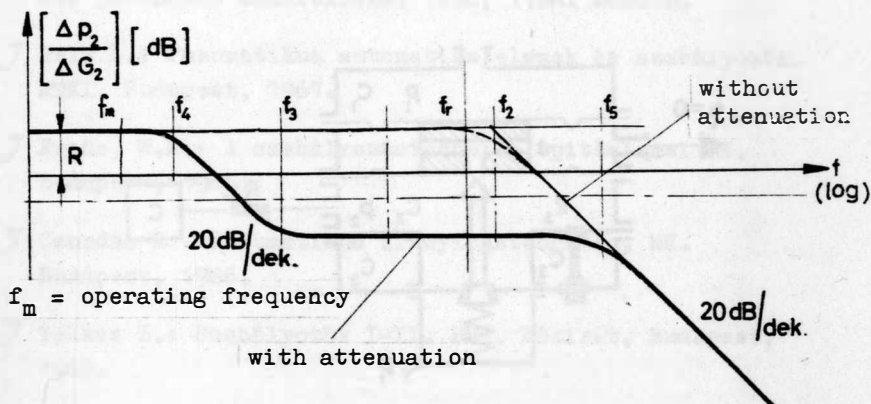


Fig. 8

Oscillation attenuation takes place in the following way: the horizontal dot-dash marks the attenuation required for avoiding self-excited oscillations.  $f_r$  stands for frequency of self-excited oscillations. It is obvious that without stabilisation (dashed line) the amplifier has a lower attenuation than required while in the case of stabilisation (continuous line) it has a larger attenuation. Subsequently, no oscillations may occur. We found  $f_r = 300$  to  $600$  c/s for the amplifiers examined. Adjustment and coupling of the attenuator is correct if  $f_4 > f_m$ , because in this case the effective range remains undisturbed by low frequencies. We would like to point out that the described conditions have only approximate character; their purpose is rather to give a qualitative image since the validity of our approximations is substantially limited because of the strong non-linear effects. Design and adjustment always require tests to be carried out.



We have developed a design for the RC element which is connected to the amplifier and shown in Figure 9.  $R_3$  may be provided with external adjusting facilities to make it possible that changes of parameters and deviations caused by the tolerances can be adjusted separately.

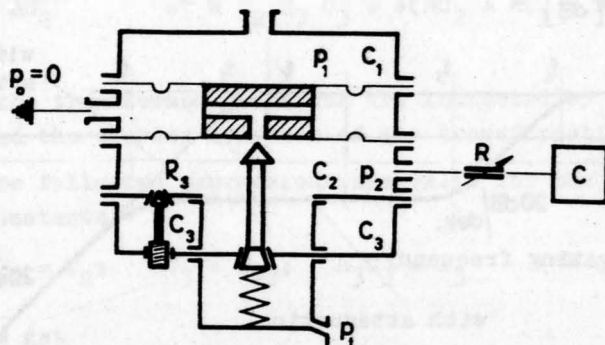


Fig. 9

### Literature

- [1] Pneumatikus teljesítményerősítők vizsgálata MTA-AKI.  
Témajelentés. Budapest, 1967, Kiadatlan kézirat.
- [2] H. Bader: Self sustained oscillations in amplifiers  
for pneumatic controllers. IFAC, 1966. London.
- [3] Helm L.: Pneumatikus automatika elemek és szabályozók.  
MTKI. Budapest, 1961.
- [4] Frede, W.E.: A szabályozástechnika építőelemei MK.  
Budapest, 1966.
- [5] Csordás Z.: Pneumatikus irányítástechnika. MK.  
Budapest, 1966.
- [6] Telkes Z.: Szabályozók I-II. BME. Kézirat, Budapest,  
1963.
- [7] Magyar Találmányi bejelentés MA-1713 szám. Budapest,  
1967.



# THE DYNAMIC BEHAVIOUR OF HYDRAULIC COMPONENTS

J. J. Hunter  
National Engineering Laboratory  
East Kilbride, Glasgow, Scotland

## 1. INTRODUCTION

The analogy of fluid pressure and flow to voltage and current is often used to introduce electrical concepts to students. It is therefore rather surprising to find that circuit theory does not occupy a central position in the study of fluid mechanics. The main reason for this is to be found in the non-linear relation between pressure and flow in most hydraulic machines and systems, even for the simplest case of incompressible flow.

It is now possible to solve the circuit equations by computer, more particularly by digital computer. There already exist some comprehensive programs for circuit analysis<sup>1,2</sup>, which are capable of initial value, steady state and transient analysis of circuits with passive and active circuit components which may be linear or non-linear. What is required to make use of such programs is to characterize hydraulic components such that the resulting mathematical models may be interconnected to form systems. Very little experimental investigation of hydraulic components, in order to make realistic models, has been carried out. This paper describes a dynamic response test rig and associated instrumentation for investigating the dynamic behaviour of water hydraulic components. The results of some preliminary investigations are given.

### 1.1 Background

In order to appreciate what is required from a system theory point of view the following axiom and postulate as proposed by Koenig<sup>3</sup> are useful.

Axiom: A mathematical model of a component characterizes the behaviour of that component of the system as an entity and independently of how the component is interconnected with other components to form a system.

The necessary conditions are given as the first postulate.

Postulate 1: The pertinent performance (behavioural) characteristics of each  $n$ -terminal component in an identified system structure are completely specified by a set of  $n-1$  equations in  $n-1$  pairs of oriented complementary variables  $x_i(t)$  and  $y_i(t)$  identified by an arbitrarily chosen terminal graph.

A useful choice of complementary variables for water hydraulic components is volumetric flowrate  $Q$  ( $\text{m}^3/\text{s}$ ) and pressure  $P$  ( $\text{N}/\text{m}^2$ ). As their product is power ( $W$ ), which is invariant, this facilitates modelling of complex components involving transformations from hydraulic to mechanical

and electrical variables.

To obtain sufficient information to model the component it is necessary to subject it to a known or measurable time-varying input (or inputs) and measure the response of the output variable (or variables). For example, for a simple two-terminal component such as a valve, the pressure difference across the valve can be measured for a known flow input, conversely the flowrate through the valve can be measured for a known pressure input. Whether a variable should be regarded as dependent or independent depends on the excitation source.

There remains the question of what kind of time-varying input to the components should be used. The method adopted in the dynamic response rig to be described is to carry out frequency response tests by superimposing a small sinusoidal perturbation on the mean flowrate. The phase and amplitude response of the output variables can be measured over the frequency range from 0.01 to 100 Hz. By varying the mean flowrate, transfer functions at different operating points can be obtained. From these measurements and by making some assumptions about the physical processes involved, non-linear mathematical models can be constructed. These models can now be further investigated by subjecting them in the computer to other forms of time-varying inputs, e.g. square wave, ramp, bandwidth limited random inputs etc. and comparing their response to that of the actual component subjected to the same input on the experimental rig.

In this paper the design of a dynamic response test rig will be described as well as a transient flowmeter for use on that rig. The results of some initial tests are also given. The problem of dynamic pressure measurement will not be discussed as there are a number of papers available on this subject.

## 2. DYNAMIC RESPONSE TEST RIG

In the dynamic response rig developed at NEL the steady flow is provided by a centrifugal pump (Fig. 1) with an output pressure of  $3.3 \text{ MN/m}^2$  at a flowrate of  $9 \times 10^{-3} \text{ m}^3/\text{s}$ . In order to make the pump into a constant flow generator, most of the output pressure is lost across a series of multi-hole orifice plates before the test section. The line pressure at the test section is  $1 \text{ MN/m}^2$ , which is set by adjusting the back pressure valve. The total flow from the pump is kept approximately constant by adjusting the flow in the bypass and test sections. A small percentage of the total flow is bypassed through a linear modulating valve controlled by a moving-coil force generator. With this arrangement different types of modulation can be generated in the electrical circuits driving the moving-

coil force generator.

A schematic diagram of the modulating valve control system is shown in Fig. 2. Two difficulties encountered were that a power amplifier operating at low frequencies was not commercially available, neither were there any suitable hydraulic control valves. An amplifier and control valve suitable for use with an existing moving-coil force generator were designed. The moving-coil force generator was a Goodmans type V390A with a maximum stroke of  $\pm 8$  mm, a thrust of 20 N/A, a total thrust (naturally cooled) of 100 N, a moving system mass of 0.08 kg, an unloaded fundamental resonance of 35 Hz and a d.c. resistance of 6.6  $\Omega$ .

### 2.1 Power Amplifier Design

The current limitation of the force generator is 2.5 A with natural cooling and 5 A with forced air cooling. At the upper rig operating frequency of 100 Hz these currents correspond to peak voltages of  $\pm 17$  and  $\pm 35$  V respectively. These output power requirements can be easily satisfied with power transistors in a bridge configuration (Fig. 3) with differential input and output.

The input points A and B are driven with equal voltages but of opposite phase. Transistors  $T_1$  and  $T_3$  act as emitter followers on one-half cycle during which  $T_2$  and  $T_4$  are reverse biased, on the next half cycle  $T_2$  and  $T_4$  conduct while  $T_1$  and  $T_3$  are off. The input diodes and resistors add a bias voltage to overcome the transistor base to emitter voltage gaps. These resistors must be low enough in value to supply the input current required at the peak signal voltage. The collector resistors are safety resistors to limit the transistor current in the event of a short circuit on the output terminals. Because the force generator was being used with natural cooling it was convenient to use commercially available operational amplifiers, with an output voltage of  $\pm 10$  V to drive the output stage. As the output stage is being driven by anti-phase inputs this is equivalent to maximum output swings of  $\pm 20$  V across the load. The anti-phase voltages are developed in a differential input, differential output operational amplifier. This is preceded by a differential input, single output operational amplifier, which provides a summing junction for the displacement transducer signal and the input from the signal generator. This ensures that the valve displacement follows the signal generator input within the limits set by the available force and dynamic response of the system. It was found possible to maintain a constant valve stroke of 5 mm up to a frequency of 100 Hz.



## 2.2 Flow Control Valve

The most useful characteristic for a flow control valve is to have a linear flow to valve displacement relation at any given pressure. This can be done either by making the flow path resistance proportional to displacement (viscous friction) or by making the valve area proportional to displacement (velocity energy dissipation). An assessment of a valve design based on viscous friction soon showed that this was impractical because of the large physical dimensions required.

A flow control valve, based on velocity energy dissipation, was then designed consisting of two opposed slots in a cylinder, whose length could be varied by a piston moving inside the cylinder (Fig. 4).

For a slot width of 0.812 mm, a pressure difference  $P$  of 1 MN/m<sup>2</sup> and a specific mass  $\rho$  of  $1 \times 10^3$  kg/m<sup>3</sup>

$$\begin{aligned}\text{flow velocity} &= \sqrt{\frac{2P}{\rho}} \\ &= \sqrt{\frac{2 \times 10^6}{1 \times 10^3}} = 44.6 \text{ m/s}\end{aligned}$$

and volumetric flow  $Q$  for a slot 10 mm long by 0.812 wide is

$$\begin{aligned}Q &= vA = 44.6 \times 10 \times 0.812 \times 10^{-6} \\ &= 0.362 \times 10^{-3} \text{ m}^3/\text{s}.\end{aligned}$$

From results of a test on this valve (Fig. 5) for a 10 mm slot

$$\begin{aligned}Q &= Q_{20} - Q_{10} = (0.664 - 0.319) \times 10^{-3} \text{ m}^3/\text{s} \\ &= 0.345 \times 10^{-3} \text{ m}^3/\text{s}\end{aligned}$$

which is in reasonable agreement with the predicted flow. In addition, because the flow path is small, 2.5 mm, and the pressure difference is high, the flow response time of the valve is good. For example, assuming the valve piston was instantaneously moved, then

$$\text{initial acceleration of fluid} = \frac{\text{force}}{\text{mass}} \quad (2)$$

$$\begin{aligned}&= \frac{\text{pressure}}{\text{specific density} \times \text{flow path length}} \quad (3) \\ &= \frac{1 \times 10^6}{1 \times 10^3 \times 2.5 \times 10^{-3}} \\ &= 4 \times 10^5 \text{ m/s}^2.\end{aligned}$$

## 3. TRANSIENT FLOWMETER

In many reports of experiments involving fluid dynamics, only pressure measurements are made and the flow is inferred from these measurements. This is because of a lack of suitable measuring instruments. The only type of flowmeter in common use for measuring unsteady flows is the hot wire anemometer, which is mainly used for turbulence measurements in air flow, i.e. velocity measurements at a point. Because of its fragility

this is a difficult instrument to use in air so that it did not appear promising for use in water. There is conflicting evidence regarding the transient performance of the electromagnetic flowmeter<sup>4,5</sup>; apart from this it was unsuitable for some of our applications which were with fluids of low conductivity. The ultrasonic flowmeter, exploiting the Doppler effect, might be suitable but has not really come into use for normal flowmetering, so that there is a lack of information on it. In addition, the measuring path length in the fluid tends to be long. The turbine flowmeter has a rather poor transient response<sup>6</sup> particularly at low flowrates. Of the other flowmeters that depend on a change in momentum, only the drag plate flowmeter had any evidence of success for transient use<sup>7</sup> so that it was decided to design a flowmeter of this type.

### 3.1 Drag Plate Flowmeter

The earliest drag flowmeters, used in the seventeenth century, consisted of a pendulum freely suspended in a stream. The drag force due to the water velocity deflected the pendulum. The magnitude of this deflection provided a measure of water velocity. The drag plate flowmeter described here differs mainly in the use of an electrical displacement transducer and the processing by electronic circuits of the resulting signal into the desired form. By making the plate deflection very small, the resonant frequency of the mechanical assembly can be in the range of a few hundred Hertz. This fast response can easily be maintained by electronic signal processing.

The mechanical arrangement can be envisaged from Fig. 6. The drag plate is a thin disc mounted on a rod set normal to the flow. The restoring force is provided by a torsion hinge which also acts as a pivot. Movement of the plate is sensed by a displacement transducer formed by a fixed E-core and an armature mounted on the opposite end of the drag rod from the plate.

The use of a thin sharp-edged plate as the sensing element ensures that the mass and effective length are minimized. In addition, because the flow separates from the plate edge at a low Reynolds number, the drag coefficient is constant over a wide range of flows. For example, the drag coefficient for a 30 mm disc in water at 20°C attains a steady value for a free stream velocity of 0.1 m/s.

The drag coefficient  $C_d$  is defined from

$$\text{drag force} = C_d \frac{1}{2} \rho v^2 A \quad (4)$$

where  $\rho$  is the specific mass of the fluid,  $v$  is the fluid velocity, and  $A$  is the plate area.

In the region where the drag coefficient is constant the drag force is caused by the change in momentum of the fluid in flowing past the plate. For streamlined bodies where the flow phenomena are more complicated the drag coefficient may be linear only over small ranges and may be affected by the turbulence level of the flow.

It was found convenient to start the design study from a restriction set by the pressure drop across the flowmeter in a given pipe not exceeding a certain magnitude. This results in an upper limit on plate area. From the plate area and maximum flow the drag force can be estimated. From this force the plate and rod thickness can be calculated and thus the moment of inertia for a given material. If the full-scale deflection required to operate the displacement transducer is known, the spring rate and resonant frequency can be calculated. It is not very useful to start out from a consideration of the natural frequency because this is not greatly affected by the plate area, for although the force increases with plate area so does the mass. The plate area is probably best kept large for this application in order to obtain a better average of the flow.

This type of flowmeter is very similar to the annular orifice plate. The main difference is that the force on the plate rather than the pressure difference is being measured. It would thus be expected that it would share the advantages claimed for the annular orifice plate relative to the normal orifice plate, namely that it is less sensitive to upstream conditions.

### 3.2 Flowmeter System

A block diagram of the flowmeter system is shown in Fig. 6. The E-core inductive displacement transducer is energized from a 10 kHz oscillator. The resulting a.c. signal is amplified and then converted to a d.c. signal proportional to the plate displacement in a phase-sensitive demodulator. This d.c. signal is passed through a frequency response compensation circuit which corrects for the underdamped second order response of the mechanical system. (It is not practical to arrange damping in the mechanical system.) The compensated signal, which is proportional to the square of flow, is linearized in a square-rooting circuit which allows for two-quadrant operation. In order to find the mean flow with unsteady flow conditions the linearized flow signal is averaged in an operational amplifier circuit of long time constant (8 seconds).

### 3.3 Steady and Pulsating Flow Tests

One model of flowmeter for use in a 6 cm diameter pipe had a 1 cm diameter drag plate, a pressure loss of  $250 \text{ N/m}^2$  and a resonant frequency

of 360 Hz in water.

Steady flow tests were carried out. A comparison of the indicated flow against that found by diverting the flow into a weigh-tank over a measured period of time is shown in Fig. 7.

A square-wave modulated flow waveform (Fig. 8) was then produced by a quick-acting valve. The average flow signal, under these conditions, against the average found by weighing and timing, is also shown in Fig. 7.

This type of test has provided one of the few checks on the transient performance of the drag plate flowmeter. The assumption has been that, if the average flow indication is correct under unsteady flow conditions, then the non-linear transformation from flow to force is the inverse of that in the electronic function generator circuit. That is, the non-linearity is not frequency dependent within the frequency spectrum covered by the tests.

#### 4. TESTS ON DYNAMIC RESPONSE RIG

Some initial tests have been carried out on the rig and the results are given. These results do not, in general, give enough information to construct complete models and this has not been attempted in this paper.

##### 4.1 Equivalent Circuit of Flow Line

Choosing pressure  $P$  and volumetric flow  $Q$  as the 'across' and 'through' variables respectively leads to the circuit parameters volumetric flow resistance  $R$  and an inertia term  $I$ , which are defined by

$$P = RQ \quad (5)$$

$$P = I \frac{dQ}{dt} \quad (6)$$

In general,  $R$  is non-linear. For small signal operation the linearized value  $r = dP/dQ$  can be used.

For resistances which operate by dissipation of velocity energy the pressure difference  $P$  across the resistor can be equated to the destruction of velocity energy, i.e. where  $v$  is the fluid velocity and  $A$  is the cross-sectional area of the resistor, and assuming the exit velocity is much lower

$$\begin{aligned} P &= \frac{1}{2} \rho v^2 \\ &= \frac{1}{2} \rho \frac{Q^2}{A^2} \end{aligned} \quad (7)$$

$$\begin{aligned} \text{and} \quad r = \frac{dP}{dQ} &= \rho \frac{Q}{A^2} = \rho \frac{v^2}{Q} \\ &= 2 \frac{P}{Q} \end{aligned} \quad (8)$$

The multi-hole orifices and control valves in the rig are of the above form. The line resistance is negligible. The inertial components are due to the inertia of the fluid in the pipe and pump.

For a pipe of constant diameter, cross-sectional area  $A$  and length  $L$ ,  
as

$$\text{force} = \text{mass} \times \text{acceleration}$$

then 
$$PA = \rho AL \frac{dv}{dt}$$

$$P = \frac{\rho L}{A} \frac{dQ}{dt} \quad (9)$$

where  $v$  is the fluid velocity and  $P$  is acceleration pressure,

i.e. 
$$I = \frac{\rho L}{A}. \quad (10)$$

An equivalent circuit for the dynamic response rig, ignoring compressibility, (Fig. 9(a)) consists of

$r_p$  = pump resistance + multi-hole orifice resistance

$r_b$  = bypass valve resistance

$r_c$  = modulating valve resistance

$r_o$  = back pressure valve resistance

$I_p$  = pipe inertia component, and

$I_s$  = pump inertia component.

At low frequencies where  $I_p$  is negligible, the equivalent circuit, seen from the modulating valve, can be simplified to Fig. 9(b) and (c). The small signal resistance of the pump found by measuring the slope of the pump characteristic at its operating point is  $3.1 \times 10^8 \text{ Ns/m}^5$ .

For a pressure drop of  $2.2 \text{ MN/m}^2$  and a flow of  $9 \times 10^{-3} \text{ m}^3/\text{s}$ , from equation (8),

$$\text{the orifice plate resistance} = \frac{2 \times 2.2 \times 10^6}{9 \times 10^{-3}} = 4.9 \times 10^8 \text{ Ns/m}^5,$$

therefore

$$r_p = (3.1 + 4.9) \times 10^8 = 8 \times 10^8 \text{ Ns/m}^5$$

$$r_f = r_b \text{ in parallel with } r_o \text{ at } 1 \text{ MN/m}^2 \text{ and } 9 \times 10^{-3} \text{ m}^3/\text{s}$$

$$= \frac{2 \times 1 \times 10^6}{9 \times 10^{-3}} = 2.2 \times 10^8 \text{ Ns/m}^5.$$

The equivalent output resistance  $r_e$  to the modulating valve is  $r_f$  in parallel with  $r_p$ .

$$r_e = \frac{8 \times 2.2}{8 + 2.2}$$

$$= 1.73 \times 10^8 \text{ Ns/m}^5.$$

Experimental values, found from sinusoidal frequency response tests, are shown in Fig. 10. There is reasonable agreement with the calculated value considering the approximations involved.

The inertial term  $I_p$  for a pipe 1 metre long and 60 mm diameter is

$$I_p = \frac{\rho L}{A}$$



$$= \frac{1000 \times 1}{28.3 \times 10^{-4}} = 3.54 \times 10^5 \text{ kg/m}^4.$$

Values found from frequency response tests were of the order of  $2 \times 10^5 \text{ kg/m}^4$ . The measurement proved to be very difficult at low frequencies because the acceleration pressure component is small and flow is normally 'noisy'.

#### 4.2 Turbine Flowmeter

The small signal transfer function, rotor angular velocity/volumetric flowrate, has been found for a turbine flowmeter of 50 mm nominal bore over a frequency range of 0.01 to 20 Hz. The portion from 0.1 to 10 Hz is shown in Fig. 11 in terms of amplitude and phase lag. The rotor angular velocity is shown in dB relative to the value at 0.02 Hz. The steady flow calibration factor for this meter is given by the manufacturer as 233 pulses/gallon which, as it has ten blades, is equivalent to a rotor rotation of  $32.2 \times 10^3 \text{ radians/m}^3$ . The value found at 0.02 Hz was in reasonable agreement with this (note that radians per second/cubic metre per second gives radians per cubic metre). The mean flowrate for this test was  $8 \times 10^{-3} \text{ m}^3/\text{s}$  with a superimposed sinusoidal flow of  $\pm 0.25 \times 10^{-3} \text{ m}^3/\text{s}$  (peak values). From Fig. 11 it can be seen that the response of this meter is relatively slow, the amplitude is almost 20 dB down at 10 Hz with a  $147^\circ$  phase lag which reaches  $180^\circ$  at 20 Hz.

#### 5. CONCLUSIONS

An account has been given of an initial investigation into hydraulic components from the point of view of system theory. There still remain many difficulties, both theoretical and practical, to be overcome. For example, there are difficulties in measurement arising from the noisy character of normal flow. There are problems in deciding what should be regarded as the component terminals. There is a lack of information on the behaviour (waveform) of flow encountered in normal practice - it is certain that flow is rarely steady.

The incentive, of course, is that once component models have been established then use can be made of modern system theory and, in particular, of computer circuit analysis programs for the analysis of problems arising from the dynamic behaviour of hydraulic systems and for the design of new systems.

#### ACKNOWLEDGEMENTS

The investigation described in this paper forms part of the work carried out for a Ph.D. study at the University of Salford, under the supervision of Mr. W. L. Green. His valuable assistance and guidance is gratefully acknowledged.

This paper is published by permission of the Director, National Engineering Laboratory, Ministry of Technology. It is British Crown copyright and is reproduced with the permission of the Controller, Her Britannic Majesty's Stationery Office.

#### REFERENCES

1. SEDORE, S. R. SCEPTRE: A program for automatic network analysis. IBM J1 Res. Dev., 1967, 11(11), 627-637.
2. KATZNELSON, J. AEDNET: A simulator for non-linear networks. Proc. IEEE, 1966, 54(11), 1536.
3. KOENIG, H. E., TOKAD, Y., KESAVAN, H. K. and HEDGES, H. G. Analysis of discrete physical systems. London: McGraw-Hill, 1967.
4. McDONALD, D. A. Blood flow in arteries, p 123. London: Edward Arnold, 1960.
5. BALLING, N. R. and CONNOR, B. V. An electromagnetic flowmeter for low conductivity fluids. Tech. Report No 32-329. Pasadena, Calif: Jet Propulsion Laboratory, California Institute of Technology, 1962.
6. HIGSON, D. J. The transient performance of a turbine flowmeter in water. J. Scient. Instrum., 1964, 41(5), 317-320.
7. LI, Y. T. New schemes for pulsating flow measurement with head-type meters. ASME Paper No 55-SA-79. New York: American Society of Mechanical Engineers, 1955.



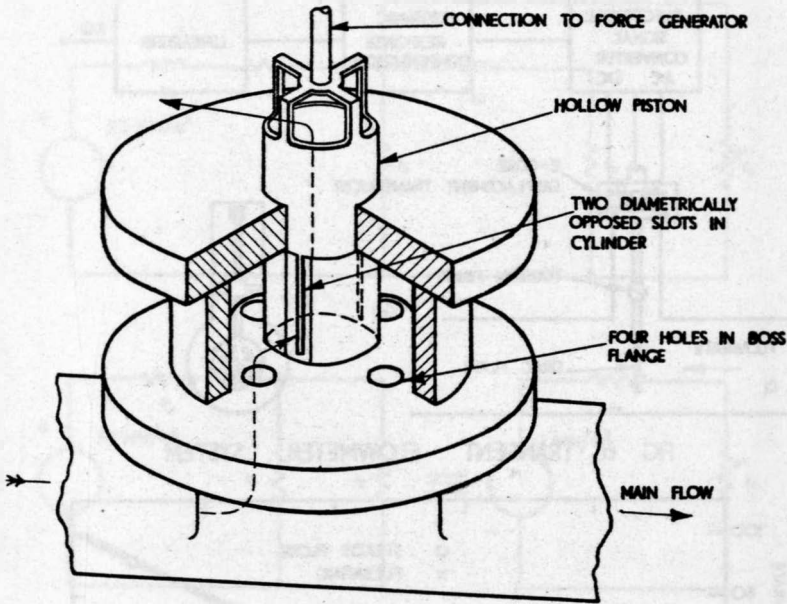


FIG 4 FLOW CONTROL VALVE

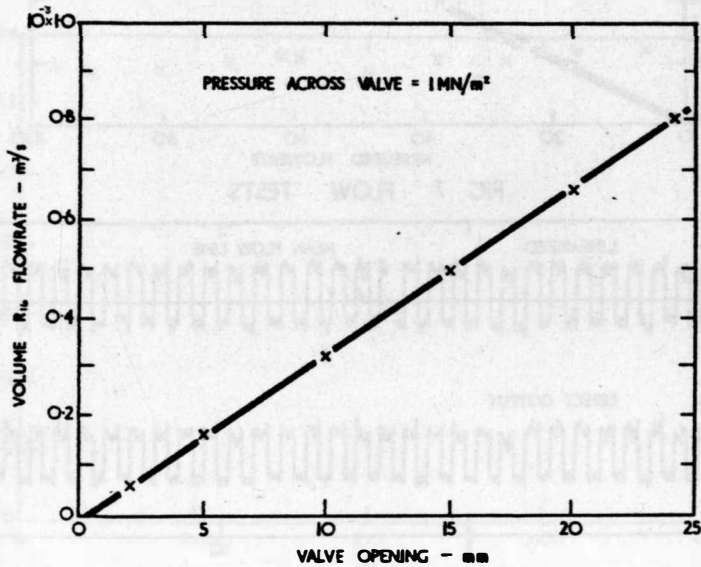


FIG 5 FLOW RATE / VALVE OPENING FOR MODULATING VALVE

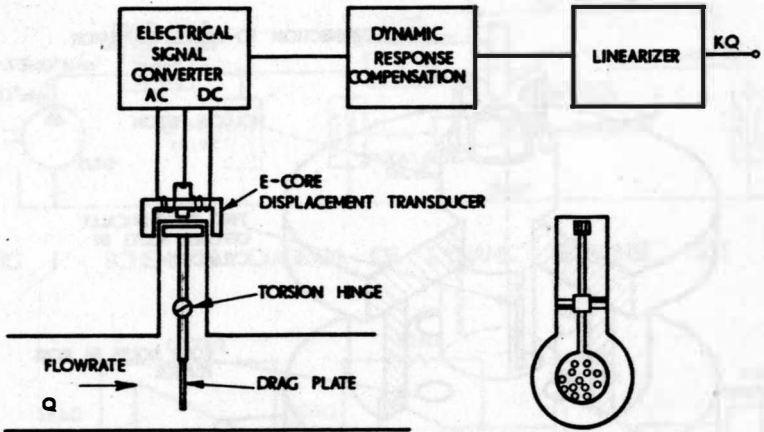


FIG 6 TRANSIENT FLOWMETER SYSTEM

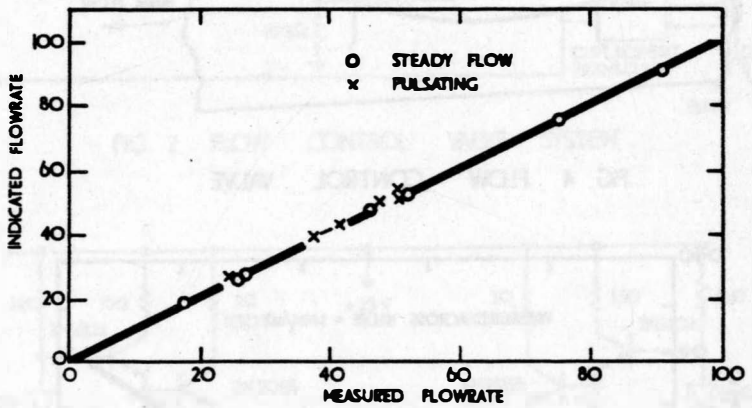


FIG 7 FLOW TESTS

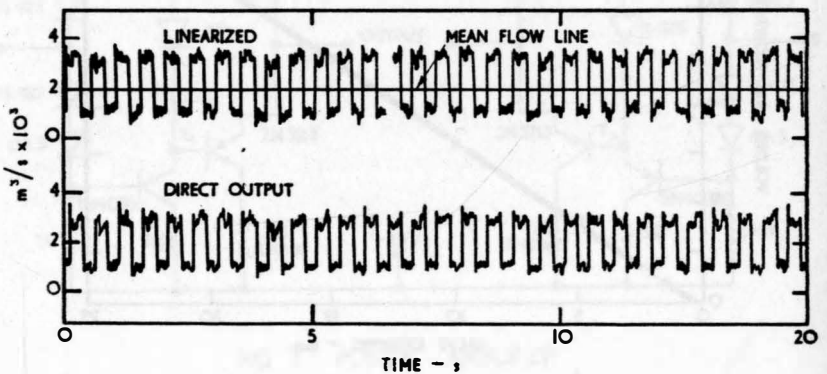


FIG 8 TYPICAL PULSATING FLOW RECORD

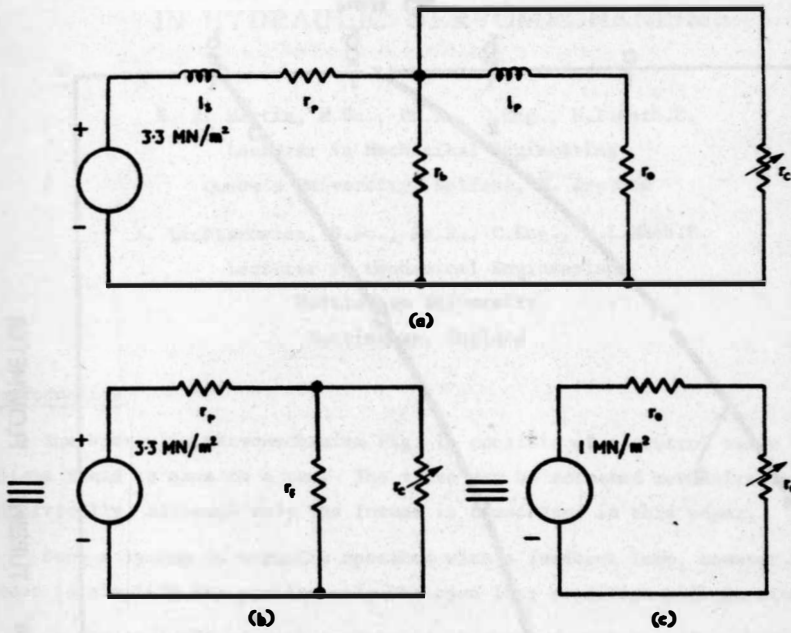


FIG 9 EQUIVALENT CIRCUITS FOR DYNAMIC RESPONSE RIG

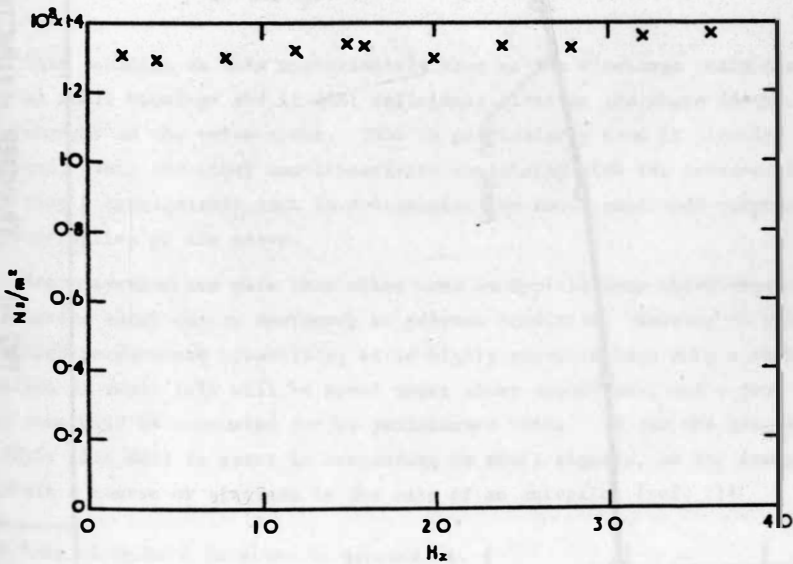


FIG 10 VOLUMETRIC FLOW RESISTANCE AGAINST FREQUENCY

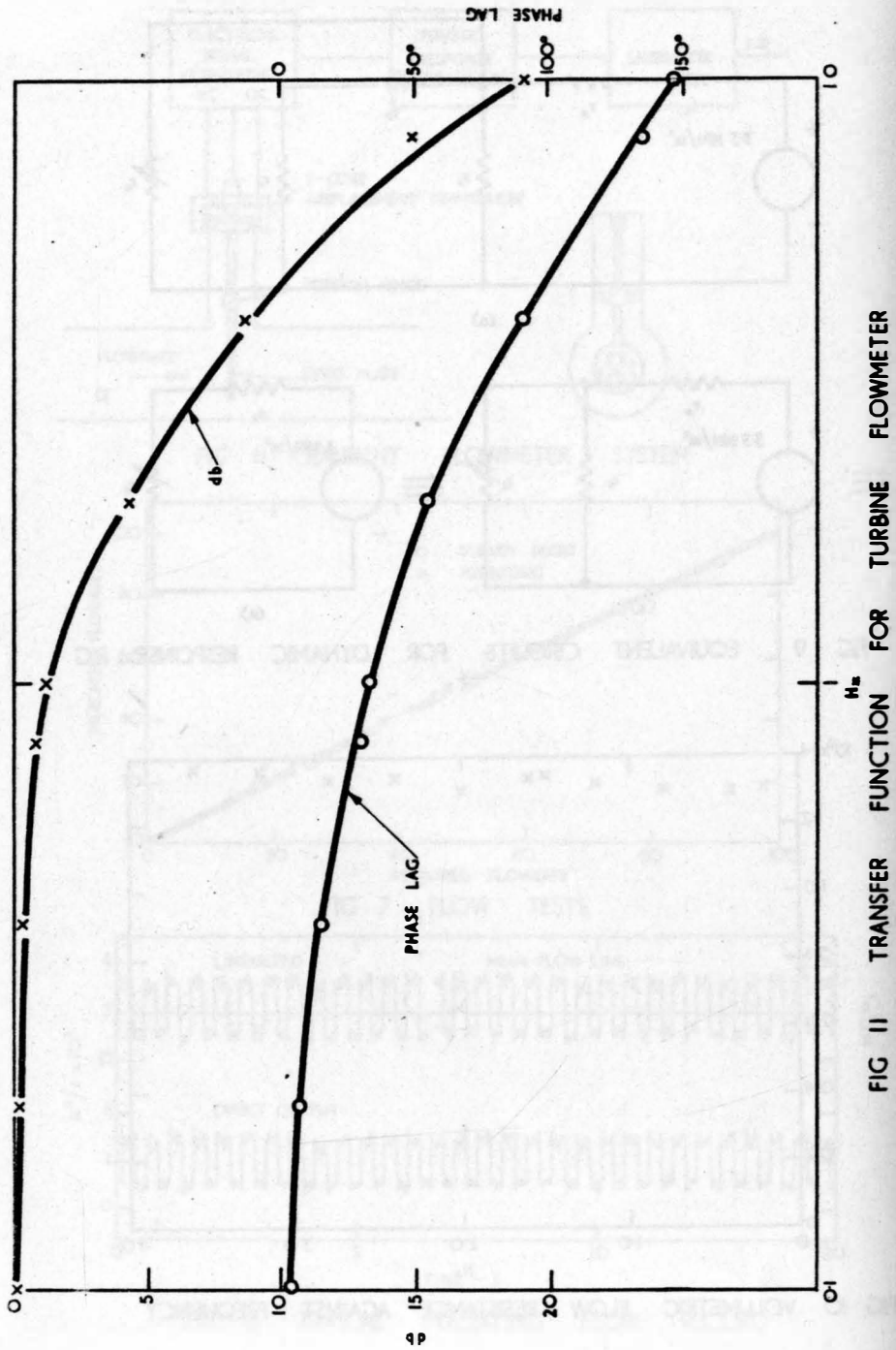


FIG II TRANSFER FUNCTION FOR TURBINE FLOWMETER

# SMALL AMPLITUDE RESPONSE CHARACTERISTICS IN HYDRAULIC SERVOMECHANISMS

by

H. R. Martin, M.Sc., Ph.D., C.Eng., M.I.Mech.E.

Lecturer in Mechanical Engineering

Queen's University, Belfast, N. Ireland

A. Lichtarowicz, B.Sc., Ph.D., C.Eng., M.I.Mech.E.

Lecturer in Mechanical Engineering

Nottingham University

Nottingham, England

## Introduction

The hydraulic servomechanism Fig. 1, consists of a control valve which allows fluid to pass to a ram. The valve may be actuated mechanically or electrically, although only the former is considered in this paper.

Such a system is normally operated with a feedback loop, however in order to simplify the problem only the open loop condition will be studied.

In the analysis of such systems it is assumed that the flow through the control ports of the valve is given by

$$Q = K_a \sqrt{P} \quad (1)^\dagger$$

This equation is only approximately true as the discharge coefficient will vary at small openings and it will definitely alter as the shape of the valve port changes as the valve opens. This is particularly true if circular ports are used. This and other non-linearities associated with the actuator and load will play a considerable part in determining the small amplitude response characteristics of the servo.

Servo-systems are more than often used in applications which require a fast response to cater for an emergency or extreme condition. However in spite of this high performance capability, it is highly probable that only a small fraction of their life will be spent under these conditions, and a good deal of this time will be accounted for by performance tests. By far the greater part of their life will be spent in responding to small signals, as for example to maintain a course or altitude in the case of an autopilot (ref. 1)\*

<sup>†</sup> A list of symbols is given in Appendix 1.

\* A list of references are given at the end of this paper.



It is the purpose of this paper to consider the effects of various non-linearities on the performance of the servomechanism when subjected to small disturbances.

### System Equations

With respect to Fig. 1, the flow into and out of the ram has three components that due to the movement of the piston, that due to the compressibility of the fluid, and that due to leakage.

In this analysis it is assumed that,

- (a) The flow through the valve is determined by equation 1.
- (b) The flow due to compressibility is determined for equal volumes on either side of the piston.
- (c) The leakage flow is laminar and can be represented by

$$Q_l = \ell(P_1 - P_2)$$

where  $\ell$  is a constant depending on the shape of the leakage path and on the fluid properties.

Equating the flow through the valve to the flow through the ram gives,

$$Q_1 = K_a \sqrt{P_s - P_1} = A \frac{dy}{dt} + \frac{1}{N} \frac{V}{2} \frac{dP_1}{dt} + \ell(P_1 - P_2) \quad \dots\dots\dots (2)$$

$$Q_2 = K_a \sqrt{P_2 - P_T} = A \frac{dy}{dt} - \frac{1}{N} \frac{V}{2} \frac{dP_2}{dt} + \ell(P_1 - P_2) \quad \dots\dots\dots (3)$$

The pressure force on the ram piston is reacted against forces due to the inertia of the load, viscous damping, and by Coulomb friction of the seals. The seal friction force  $F$  is taken to be constant in magnitude for simplicity. Its direction is such as to oppose the motion. Hence the loading equation is given by,

$$P_1 - P_2 = \frac{M}{A} \frac{d^2 y}{dt^2} + \frac{f}{A} \frac{dy}{dt} + \frac{F}{A} \left( \frac{dy}{dt} / \left| \frac{dy}{dt} \right| \right) \quad \dots\dots\dots (4)$$

In order to generalise the analysis (ref. 2) the equations are non-dimensionalised; each term being divided by some reference quantity of the system. The definitions of all the dimensionless coefficients used, are given in Appendix 2.

Since the investigation deals with small amplitudes and a low excitation frequency, cavitation will not occur; equations (2) and (3) can be combined since flows in and out of the actuator are equal. The equations after rearrangement give,

$$a^* \sqrt{1 - \left( \alpha \omega^* \frac{du^*}{d\tau} + \gamma u^* + \eta \frac{u^*}{\sqrt{u^*}} \right)}$$

$$= \omega^{*2} \frac{d^2 u^*}{d\tau^2} + \left( \frac{\gamma}{\alpha} + \phi \right) \omega^* \frac{du^*}{d\tau} + \left( 1 + \frac{\phi \gamma}{\alpha} \right) u^* + \frac{\phi}{\alpha} \eta \frac{u^*}{\sqrt{u^*}} \dots\dots\dots (5)$$

where  $\alpha$ ,  $\gamma$ ,  $\eta$ ,  $\phi$ , are respectively the load, viscous damping, seal friction, and leakage factors;  $\omega^*$  is the frequency ratio and  $\tau$  is the non-dimensionalised time.

Fig. 2 shows the variation of the valve area with displacement for a spool valve with circular ports. Normally assumed linear area characteristics will give correct results only for square valve ports. With circular ports however, the considerable change in gain for small valve displacements must affect the behaviour of the system. To investigate the response of the system to small amplitude signals it is important to work with a more realistic area representation. The nearest reasonable approximation to the true displacement-orifice area relationship is given by, (ref. 4)

$$a = K_1 x^n \quad \text{where } n = 3/2 \text{ for circular ports and} \\ n = 1 \text{ for square ports.}$$

For a sinusoidal input, let

$$x = T \hat{x} \sin \tau$$

where  $T$  is some factor by which the input is altered, and describes the input amplitude selected. The maximum value of  $T$  is unity.

Hence,

$$a^* = \frac{K_1 x^n}{\hat{a}}$$

$$= \frac{K_1 (T \hat{x} \sin \tau)^n}{K_1 (\hat{x})^n} = (T \sin \tau)^n \dots\dots\dots (6)$$

which can be substituted in equation 5. Any valve displacement area law can then be investigated.

### Method of Solution

The solution of the system equation could be carried out on an analogue computer, however equipment available at the time of this investigation was not accurate enough, hence the digital machine was more suitable.

Rearrangement of equations 5 and 6 will give two first order non-linear differential equations which can then be solved by a numerical method. In this case the fourth order Runge-Kutta numerical method was used, and the equations programmed for solution on an I.C.T. 1907.

The method of solution is to assume some initial values for the velocity and acceleration terms. Then by dividing a half cycle of operation into 50 increments obtain, by the Runge-Kutta method, final values for velocity and acceleration. If the initial and final values of velocity and acceleration are within 0.01 of each other respectively, the solution is assumed satisfactory. If not, new values of the initial conditions are estimated and the process repeated.

This process is repeated for reducing values of  $T$  until  $T < .003$ , which is chosen as the minimum amplitude value.

### Small Amplitude Limit

The threshold condition of a servomotor can be defined as the minimum input giving a controllable output. The problem is complicated by the fact that a system will exhibit a different threshold, depending on whether the measurement is taken under static or dynamic conditions (ref. 1). Experimental work shows that the dynamic threshold is about 30% of the measured static threshold. The threshold is due to the combined effects of valve overlap, backlash, friction, leakage, hysteresis and resolution of the various components in the system.

Predictions of the magnitude of the threshold are difficult, because so many factors contribute to the condition and the final gain of the system may not be known. An attempt is made by this investigation to evaluate trends towards the threshold condition, under rather idealised conditions.

The minimum requirement to achieve a threshold condition is that a leakage path must be present. Without a leakage path any opening of the valve will allow full system pressure to act on the ram, and hence overcome the resistance. This is not the case in a real system where a leakage path is always present. Before the ram can move, flow must take place across the leakage path to establish a pressure sufficient to overcome the load.

The theoretical absolute threshold value can be obtained from equation 5, if it is assumed that all output motion ceases, giving  $u^*$ ,  $du^*/dt$ , and  $d^2u^*/dt^2$  zero value, then

$$T = \left( \frac{\phi\eta}{\alpha\sqrt{1-\eta}} \right)^{1/n} \dots\dots\dots (7)$$

From this relationship it is seen that only leakage and seal friction affect the final steady state condition. This assumes that  $\alpha$  (see appendix 3) and  $n$  are fixed for the system and that no other system components contribute to the condition.

The results from equation (7) are plotted in Figs. 3 and 4. It is clear that the true orifice area relationship ( $n = 1.5$ ) has a marked effect on the achievable threshold value, making it considerably worse.

In the case of seal friction, it is interesting to note that the threshold value is infinite when there is 100% seal friction ( $n = 1.0$ ).

This means simply that the seal friction becomes equal to the available pressure force on the ram.

#### Small amplitude oscillation

Computer results, an example of which is shown in Fig. 5, indicate that at the smaller amplitude values,  $T = 0.0173$  (1.7%) for example, the motion of the system becomes oscillatory.

It was first thought that this alteration in the waveform pattern was due to breakdown in the numerical method. Further tests showed that this was not the case.

It was then noticed that the number of oscillations in the half cycle ( $2\frac{1}{2}$ ) were related to the natural frequency since,

$$\omega^* = \omega/\omega_n = 0.2$$

therefore

$$\omega_n = 5\omega$$

This result was checked by repeating the excitation at a different frequency. In each case a similar relationship resulted.

It would appear therefore that a stage is reached when a small input will cause the system to oscillate at its natural frequency. It seems likely that at these small amplitudes, conditions can be such that the inherent damping contribution from the servo valve is not able to keep the

system stable. This, no doubt, is part of the explanation of the small amplitude oscillations referred to in ref. 1.

It is interesting to note that Rolye, (Ref. 3) shows a similar occurrence, when at low velocity the viscous damping of the load is insufficient to maintain a satisfactory response.

#### Effect of Seal friction on the response

To investigate this condition it is necessary to have a leakage path for realistic results. This is simulated by introducing a leakage factor of  $\phi = 0.05$ , which corresponds to a leakage factor ( $\ell$ ) of  $4.79 \times 10^{-5}$  in<sup>5</sup>/lbfs for a small hydraulic servomotor.

The results in Figs. 6 and 7 show the pattern of the small amplitude response for different values of seal friction.

The case of  $\phi = 0.05$  and  $\eta = 0.15$ , can be taken as the normal condition existing in many systems. In the case of  $n = 1.0$ , this condition shows remarkable linearity. When these results are repeated for  $n = 1.5$ , there is a noticeable change in the characteristics.

#### Effects of viscous damping and leakage

The results shown in Fig. 8 show the pattern of small amplitude response for different values of viscous damping coefficient ( $\gamma$ ). The conditions of  $\phi = 0.05$  and  $\eta = 0.15$  are imposed.

Deviation from the ideal condition is not as great as that in the case of seal friction.

The condition for  $n = 1.5$  is shown in Fig. 9.

In the case of leakage, shown in Figs. 10 and 11, deviation from the ideal is greater than either of the previous cases, but it is interesting to note in Fig. 10 that there is a value of  $\phi$  between 0.01 and 0.1 which can make the results correspond to the ideal condition. The condition for  $n = 1$  is shown in Fig. 11.

#### Conclusions

An elementary analysis of a servo system shows that an increase of forward path gain helps to reduce the effects of threshold and improves the small amplitude responses. Its action could however introduce stability problems in the closed loop configurations, for larger input signals. This infers that gain adjustment should be confined to a limited region. This however may be impractical.

A more detailed investigation of the small amplitude response shows that a true representation of the valve area gain, alters the characteristics to a noticeable extent.

Viscous damping has the least effect in deviating the small amplitude response from the ideal, while leakage appears to worsen the characteristics. The effect of seal friction lies somewhere between the two.

The absolute threshold can be estimated from equation 7, the results showing once more that the valve area characteristic has a considerable effect. The absolute threshold is essentially a static measurement. Since no account is taken of stiction in equation 7, (which builds up with time), the results are optimistic. It must be remembered however, that at very small valve openings the flow through the valve may be laminar so that the pressure drop will be smaller and thus some compensation for the increase in stiction will be provided.

Very small amplitude responses indicate a loss of damping in the valve, which results in the system oscillating at its natural frequency.

When considered in relation to the other aspects of performance, there is no straightforward answer. The optimum system can only be achieved by compromise with respect to other parameters. It is hoped that the graphs presented in this paper give an indication of trends and help in some small way, the designer to reach his compromise more efficiently.

#### Acknowledgements

The work published here is based on the thesis (5) submitted by the first author for a doctorate degree at Nottingham University.

Facilities provided by the University and digital computing facilities provided by the Queen's University of Belfast are therefore acknowledged.

#### References

1. Carrington, J. F. and Martin, H. R. "Threshold problems in electro-hydraulic servomotors". Proc. Instn. Mech. Engrs., London, 1966, Vol. 180, pt. 1, No. 37.
2. Martin, H. R. and Lichtarowicz, A. "Theoretical investigation into the prevention of cavitation in hydraulic actuators". Proc. Instn. Mech. Engrs., London, 1967, Vol. 181, Pt. 1, No. 18.
3. Royle, J. K. "Hydraulic damping techniques at low velocity". Conf. Oil Hyd. Power transmission and Control 1961, Instn. Mech. Engrs., London.

4. Davies, R. M. "Generalised solutions for the transient response of Hydraulic Servomechanisms, with non-linear valve flow characteristics". Quart. Jourl. Mech. and App. Maths., Vol. XVII, Pt. 4, 1964.
5. Martin, H. R. "A Theoretical study into peaking pressure reduction and its effects on hydraulic servo performance". Ph.D Thesis, University of Nottingham, 1968.

## Appendix 1

### Notation

$A$	Area of ram piston
$a$	Orifice area
$\hat{a}$	Reference orifice area
$a^*$	Dimensionless orifice area
$F$	Seal friction
$K$	Flow constant
$K_1$	Orifice area constant
$\ell$	Leakage constant
$M$	Mass
$n$	Valve area index
$N$	Bulk modulus of fluid
$P$	Pressure drop across the valve
$P_S$	Supply pressure
$P_T$	Tank pressure (normally zero)
$P_1$	Pressure on one side of ram
$P_2$	Pressure on other side of ram
$P_1, P_2$	Dimensionless pressures
$Q_1$	Flow one side of actuator
$Q_2$	Flow other side of actuator

T	Output amplitude adjustment factor
t	Time
u	Piston velocity
$\hat{u}$	Reference velocity
$u^*$	Dimensionless velocity
V	Cylinder volume
x	Valve Displacement
$\hat{x}$	Reference valve displacement
$x^*$	Dimensionless valve displacement
y	Piston displacement
$\alpha$	Dimensionless load factor
$\gamma$	Dimensionless viscous damping factor
$\eta$	Dimensionless seal friction
$\tau$	Dimensionless time
$\phi$	Dimensionless leakage factor
$\omega$	Driving angular frequency
$\omega_n$	Natural frequency
$\omega^*$	Frequency ratio ( $\omega/\omega_n$ )

## Appendix 2

### Notes on the system equations

The non-dimensional factors used in the equations are defined as follows:-

$$a^* = a/\hat{a}$$

$$x^* = x/\hat{x}$$

$$P_1 = P_1/P_S$$

$$\tau = \omega t$$

$$\omega^* = \omega/\omega_n$$

$$P_2 = P_2/P_S$$

$$\omega_n = \frac{4NA^2}{MV}$$



Reference valve displacement =  $x$

Reference velocity =  $\hat{u} = \frac{K_a}{A} \sqrt{\frac{P_S}{2}}$

Load factor =  $\alpha = \frac{MK_a}{P_S A^2} \sqrt{\frac{P_S}{2}}$       $\omega_n = \frac{\text{maximum inertia load at } \omega_n}{\text{stall force}}$

Viscous damping factor =  $\gamma = \frac{f}{P_S A} \hat{u} = \frac{\text{maximum viscous damping force}}{\text{stall force}}$

Seal friction factor =  $\eta = \frac{F}{P_S A} = \frac{\text{seal friction force}}{\text{stall force}}$

Leakage factor =  $\phi = \frac{Ml\omega}{A^2} n$

### Appendix 3

In order to give real meaning to the non-dimensionalised terms, the following parameters refer to a small 5 H.P. servomotor.

Supply Pressure  $P_S = 1800 \text{ lbf/in}^2$

Maximum valve displacement  $x = 0.01 \text{ in.}$

Valve area gain  $K_1 = 0.16 \times 10^3 \text{ in}^2/\text{in}$  (assume  $n = 1.0$ )

Piston area  $A = 1.0 \text{ in}^2$

Mass at output  $M = 2.47 \text{ lbs}^2/\text{in}$  (960 lb)

Structure and oil stiffness  $N = 0.53 \times 10^5 \text{ lbf/in.}$

If the system is excited at the natural frequency,  $\alpha = 1.0$ , for the above conditions, but this figure drops to  $\alpha = 0.2$  if  $x$  is reduced to  $0.002 \text{ in.}$

A viscous damping coefficient of  $f = 365 \text{ lbfs/in}$  results in  $\gamma = 1.0$  for the above conditions, while a leakage of  $4.79 \times 10^5 \text{ in}^5/\text{lbfs}$  will give  $\phi = 0.05$

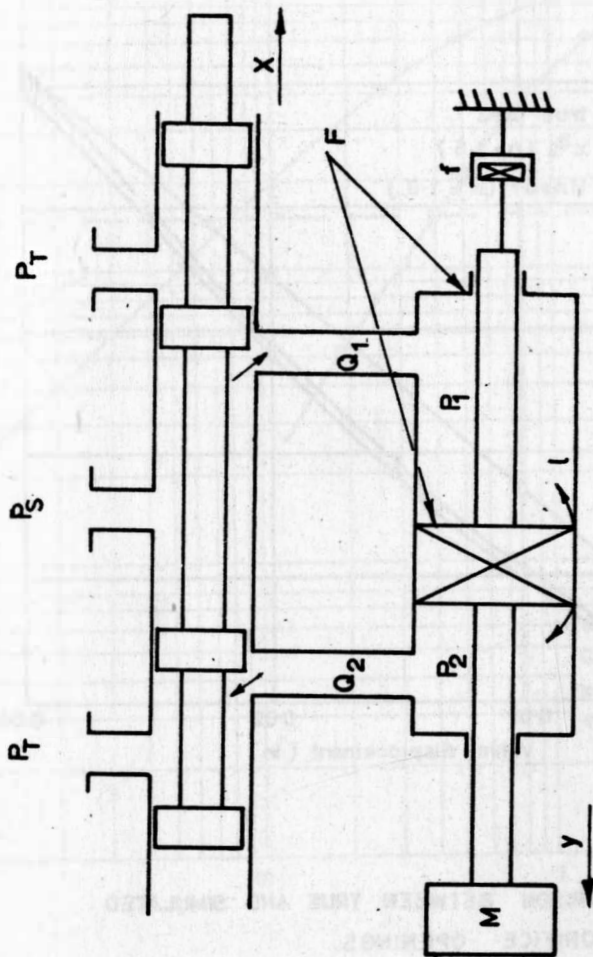


FIG. 1. HYDRAULIC SERVOMECHANISIM

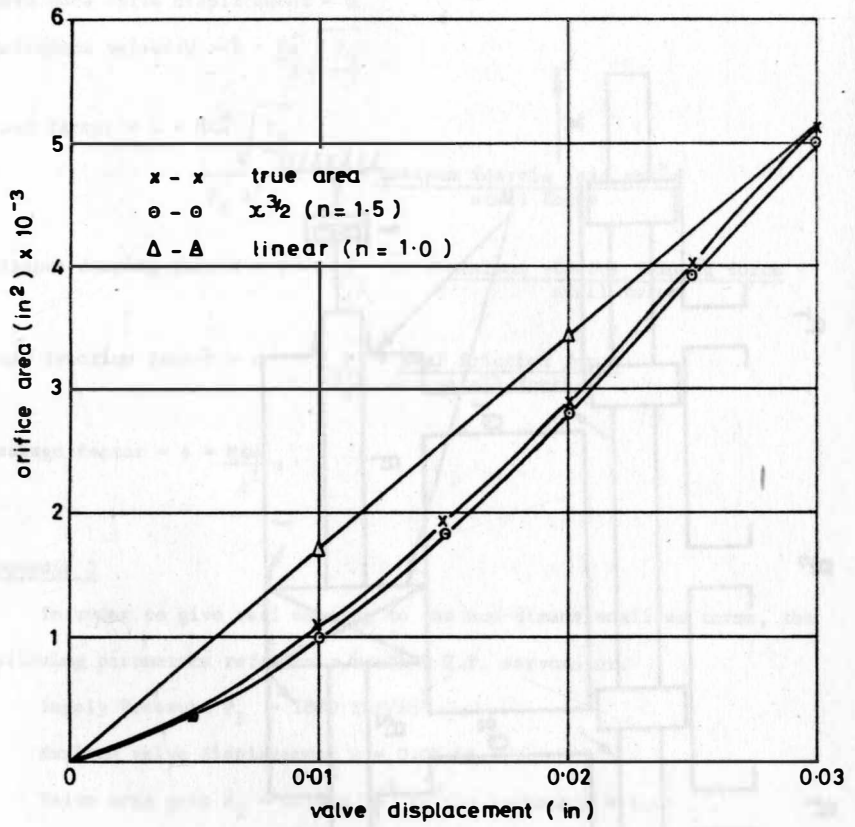


Fig.2. COMPARISON BETWEEN TRUE AND SIMULATED ORIFICE OPENINGS.

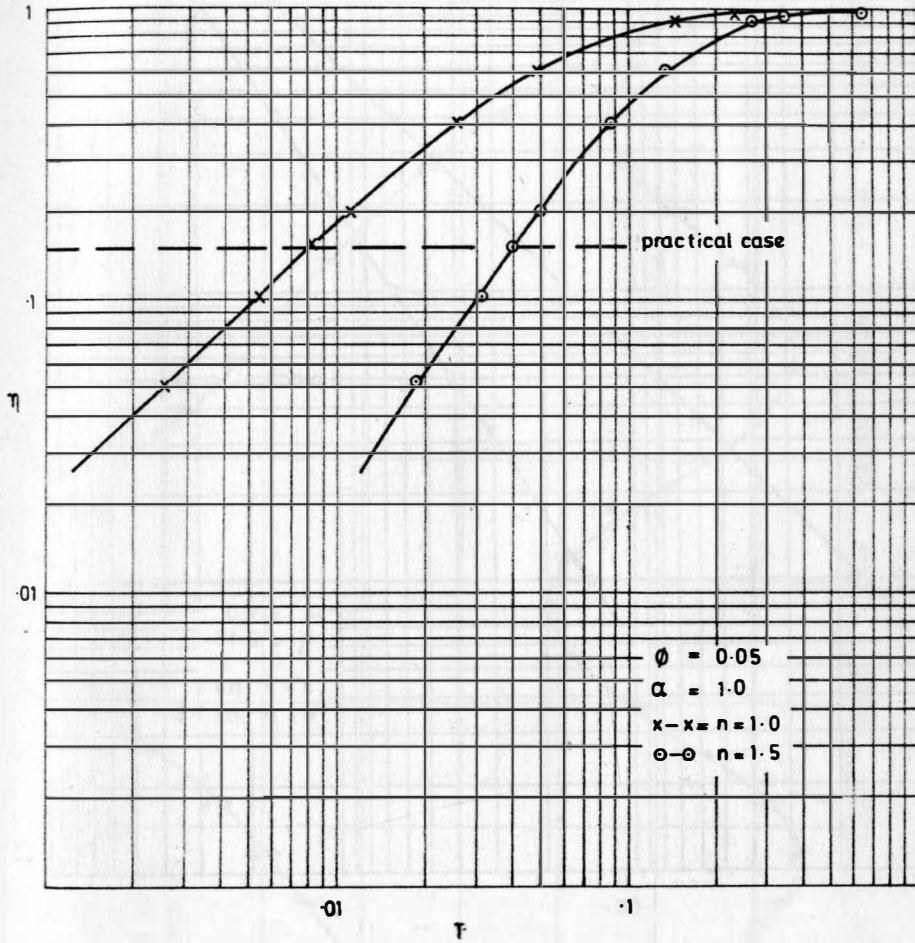


Fig. 3. THEORETICAL VARIATION OF ABSOLUTE THRESHOLD  
WITH SEAL FRICTION

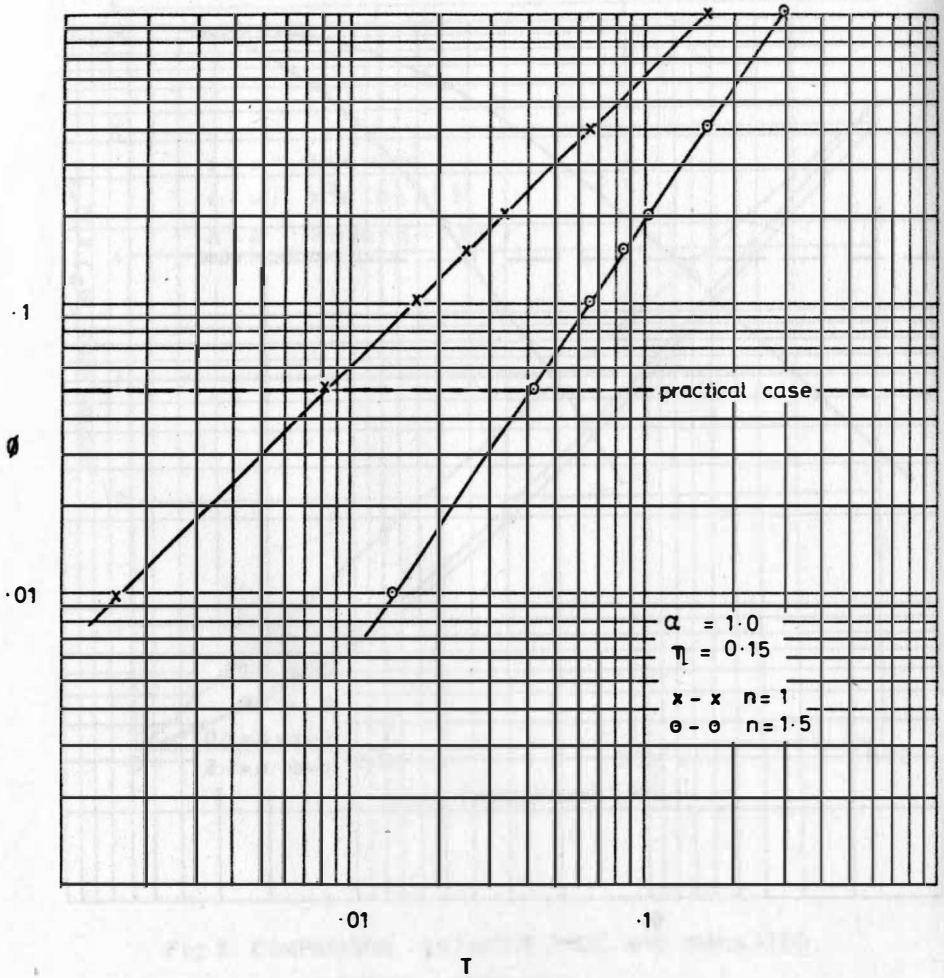


Fig. 4. THEORETICAL VARIATION OF ABSOLUTE THRESHOLD WITH LEAKAGE.

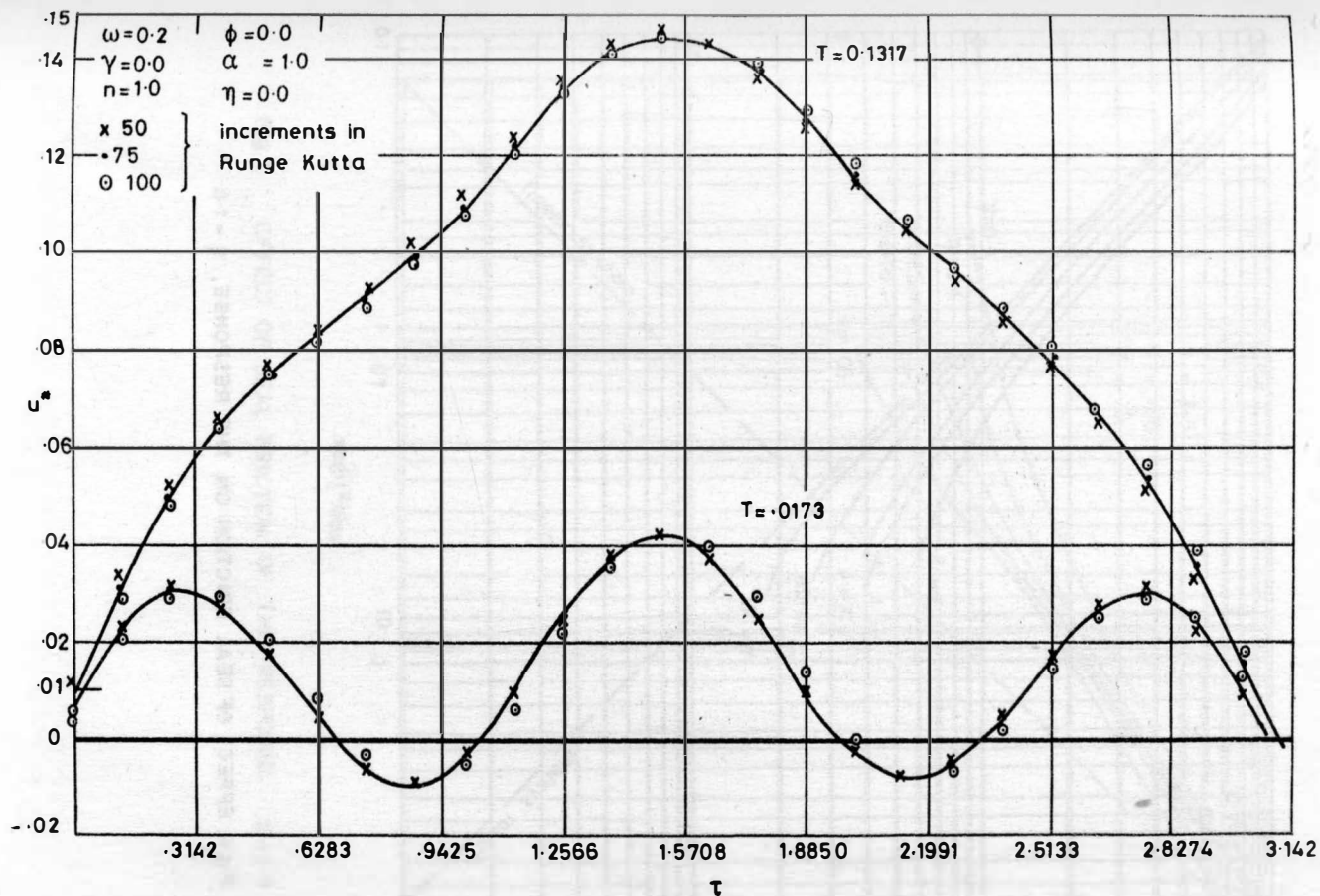


Fig. 5. EFFECT OF INCREMENT CHANGE IN PROGRAM

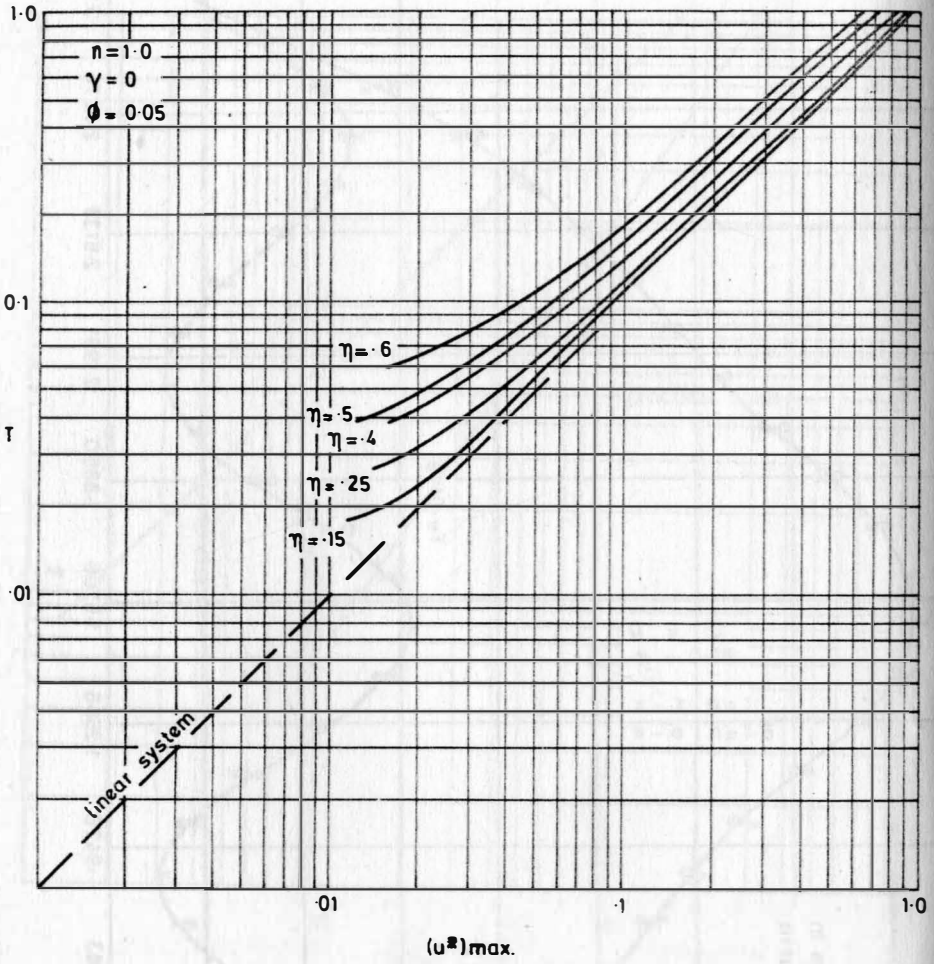


Fig. 6. EFFECT OF SEAL FRICTION ON THE RESPONSE,  $\eta = 1.0$

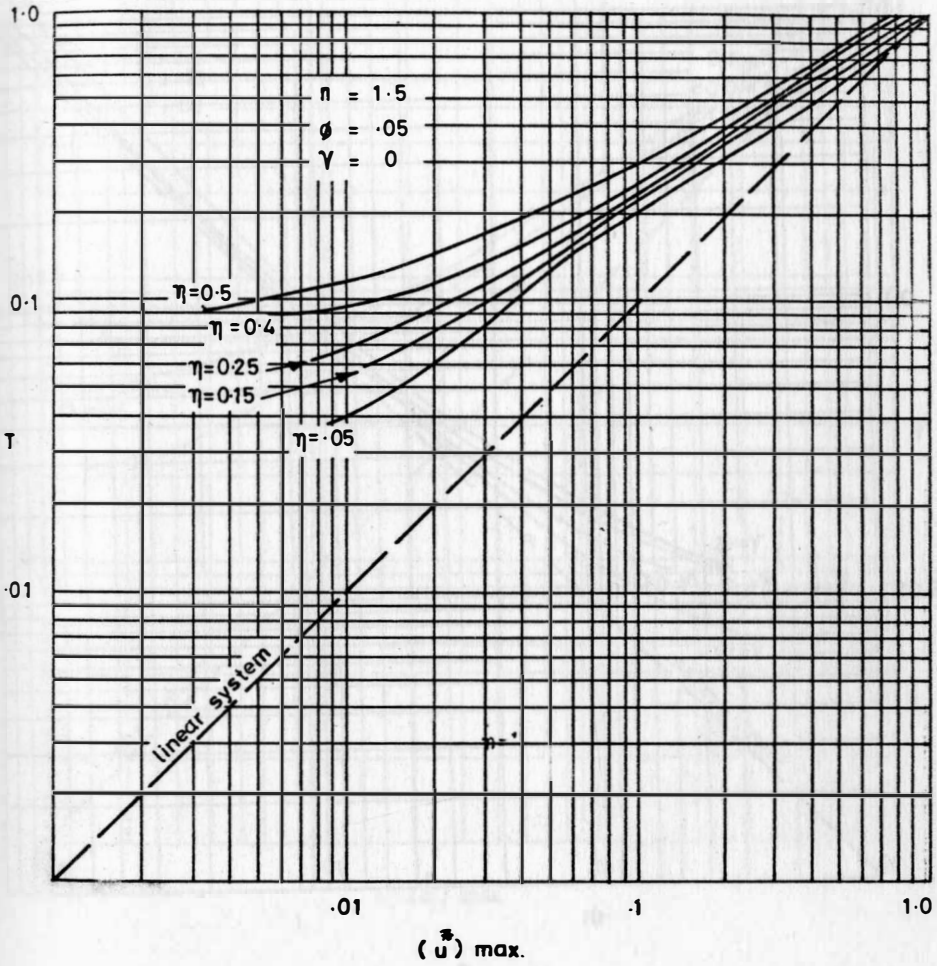


Fig 7. EFFECT OF SEAL FRICTION OF THE RESPONSE  $\eta = 1.5$



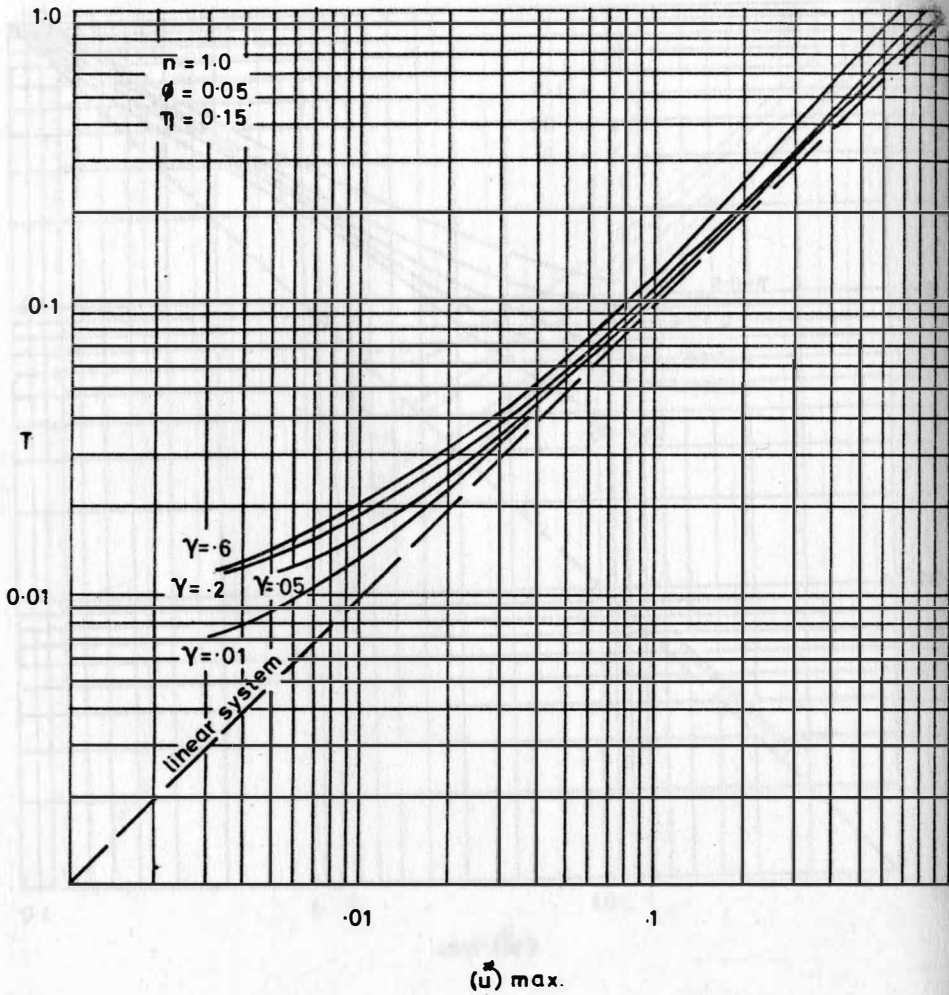


Fig.8. EFFECT OF VISCOUS DAMPING ON THE RESPONSE.  
 $n = 1.0$

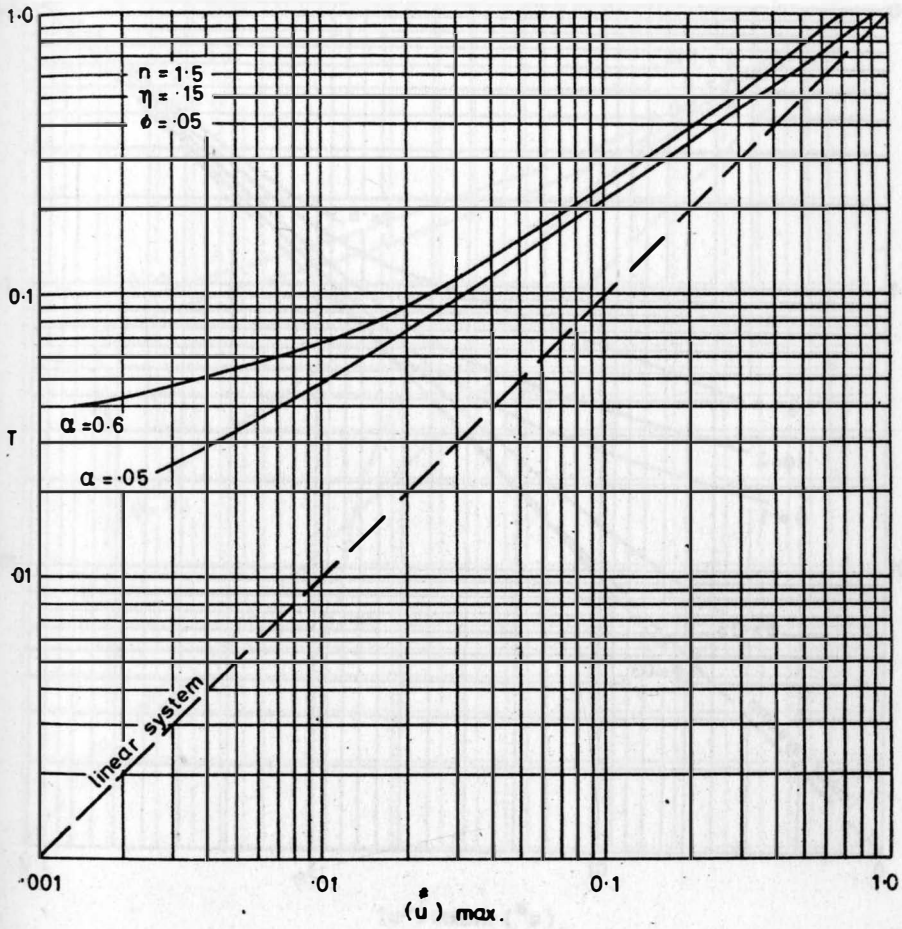


Fig.9. EFFECT OF VISCOUS DAMPING ON THE RESPONSE,  $n=1.5$

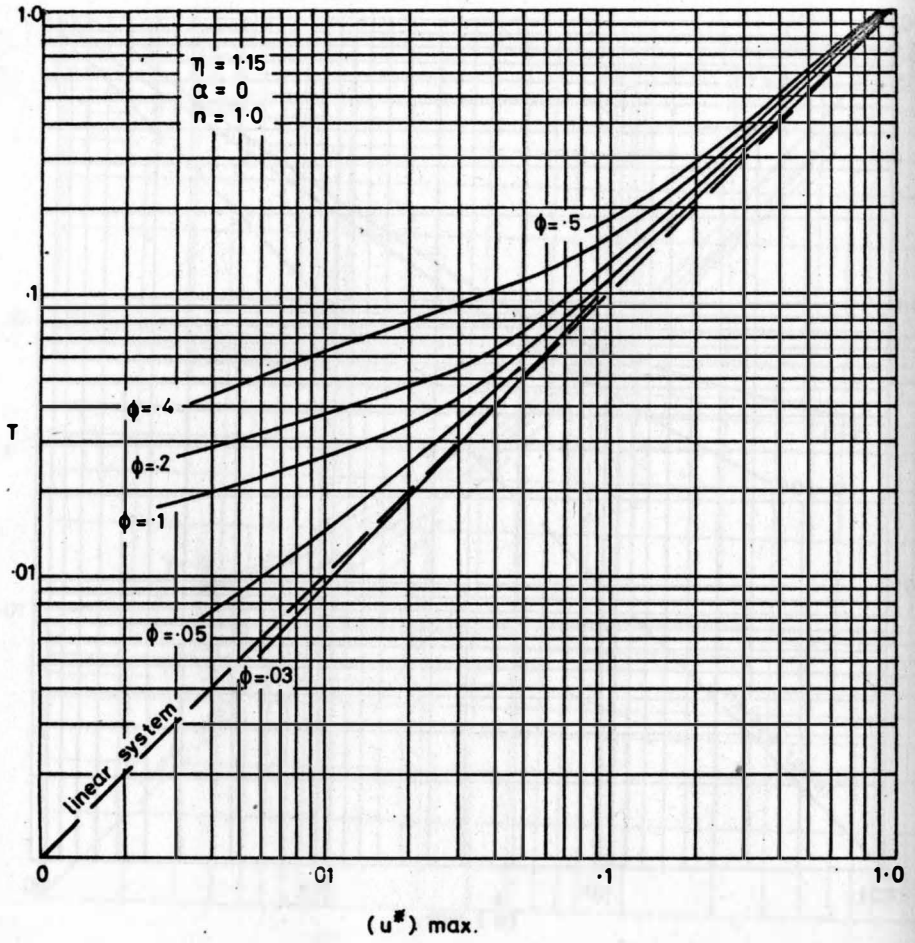


Fig. 10. EFFECT OF LEAKAGE ON THE RESPONSE.  $n=1.0$

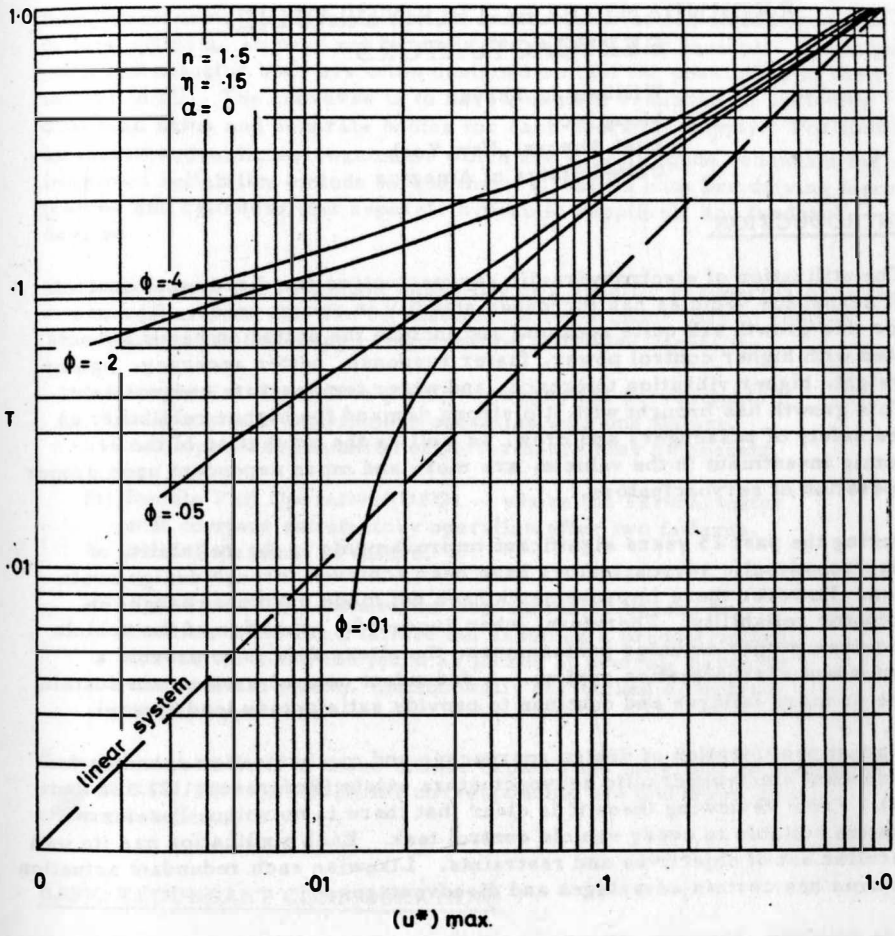


Fig.11. EFFECT OF LEAKAGE ON THE RESPONSE  $n = 1.5$

## REDUNDANT ELECTROHYDRAULIC SERVOACTUATORS

William J. Thayer  
Moog Inc.  
East Aurora, New York  
United States of America

### INTRODUCTION

The utilization of electrohydraulic servoactuators for directional control of aerospace vehicles has increased steadily in recent years. Reasons for this growth are quite apparent and include the actuation needs associated with higher control power, faster response, better accuracy, lighter weight, higher vibration tolerance, and wider temperature environment. This growth has brought with it a strong demand for higher reliability as the safety of passengers and crew, as well as the protection of the economic investment in the vehicle, are more and more dependent upon proper operation of servoactuators.

During the past 15 years significant improvements in the reliability of electrohydraulic servoactuators have been achieved through design evolution. However these improvements have not made quantum changes in actuator reliability. Therefore, when successful operation of the vehicle requires proper actuator performance, the alternative is to provide a redundant servoactuation system. A redundant control system can sustain one or more failures and continue to provide satisfactory load control.

A great proliferation of design approaches and mechanization schemes for redundant electrohydraulic servoactuators exists (References 12, 13, and 14). From reviewing these it is clear that there is no unique "preferred" system suitable to every vehicle control task. Each application has its own peculiar set of objectives and restraints. Likewise each redundant actuation scheme has certain advantages and disadvantages.

It is possible, however, to categorize the various redundant servoactuation schemes into a few classes and make general observations about these. This is one objective of this paper. From this summary, and from the illustrative designs described, a better prospective on the current "state of the art" should be achieved.

### SERVOACTUATION FAILURES

It is important first to define the scope of failures to be accommodated by a redundant servoactuator. This scope generally includes

- (a) Loss of function of any element within the servoactuator
- (b) Loss of supply power (fluid pressure) to the servoactuator
- (c) An erroneous hardover electrical command or loss of command signal to the servoactuator

Sometimes certain components of a servoactuator are excluded from the failure criteria, so need not be made redundant. For example, the output shaft and actuator body are often designed so that the possibility of their failure is nil. The converse is to have complete redundancy, including dual load paths and separate bodies for each hydraulic supply. Portions of an electrohydraulic servoactuator which are usually made redundant for improved reliability include torque motors, valves with low driving force, pistons and cylinders (for separate hydraulic supplies), and feedback devices.

One measure of the redundant capability of a specific servoactuator is the number of failures that can be sustained without undue loss of control. This leads to the following categorization of failure capability.

- (a) Single Fail Operative (SFO) -- where the servoactuator will continue satisfactory operation with one failure. Anticipated degradation of performance may be present.
- (b) Double Fail Operative (DFO) -- where the servoactuator will continue satisfactory operation after two failures, even if identical in nature.
- (c) Fail Safe (FS) -- where the servoactuator ceases to function following a failure but assumes a predetermined, non-active condition (such as locked at neutral, hardover at maximum stroke, mechanically declutched or hydraulically bypassed).

Certain combinations of these failure capabilities may also be provided, such as SFO/FS or DFO/FS for corresponding two and three failure characteristics.

### BASIC REDUNDANT CONFIGURATIONS

Servoactuators are active devices in that power is available and, in event of failure, an uncontrolled load disturbance may result. Therefore the redundant servoactuator configuration must either detect the failure condition and correct for it (usually by shutting off the failed portions), or it must overpower the failure.

For certain components within a servoactuator it is possible to provide redundant failure protection by simple paralleling of parts. Examples include springs, screws, seals, filters, and sometimes coils, valves and pistons. The individual component failure in these cases must be passive. When passive paralleling is used for redundancy, special care must be directed towards preflight checkout or inflight indication of failure status.

The various approaches for contending with active servoactuator failures are (1) averaging systems, (2) majority voting systems, (3) mid-value systems, and (4) detection-correction systems. Often the principle of

switching-out a failure embodied in the fourth category is used with one of the three preceding categories to extend the failure capability of the system. These are, then, hybrid systems.

### Averaging Systems

Three or more control channels may be used to perform one task so that failure of one channel will be partially offset by the presence of at least two good channels (see Figure 1). It is necessary to limit the authority or range of each channel and the channel outputs must be summed without interaction. Examples of averaging flight control systems are airplanes with multiple control surfaces and space launch vehicles with multiple engines for thrust vector control. Averaging can also be used with servoactuators by output force summation or by output position summation.

Averaging systems suffer significant performance degradation following a failure. A hardover failure leaves only one-third of the normal control range (for one direction), together with a one-third system null offset. Also with a hardover failure, system sensitivity or gain is reduced to two-thirds normal. With an open failure there is no null offset; however, system range and sensitivity are both two-thirds normal.

If maximum load demands are less than the full output of all three channels working normally, then it is possible to detect a hardover failure condition in an averaging system and switch-off the failed channel. A subsequent hardover failure with just two channels operating will Fail Safe with a stall condition between channels.

### Majority Voting Systems

These systems use three or more active channels in an averaging arrangement, but include feedback to reduce the effects of a failure on system performance (see Figure 2). The multi-engine space launch vehicle mentioned previously is actually a majority voting system when the vehicle guidance loop is considered. However the context of majority voting used in this paper is restricted to the servoactuator.

The degree to which normal actuation performance can be retained following a failure in a majority voting arrangement depends to a great extent upon the loop gain utilized. Output null offset with a single hardover failure can be made very small, and the change in actuator sensitivity can be negligible. However the range of the output will be limited to one-third normal with a hardover failure unless an integration element is included following the channel summation. With a hydraulic actuator this integration may be provided by the summation of flow into a piston, or by force summation on a load having negligible friction and/or spring restraint to ground.



Majority voting servoactuation systems are attractive because of their basic simplicity. No special failure sensing nor switching elements are necessary and, should the failure be transient or temporary, the system reverts to normal operation without special reset. However, most majority voting systems have certain nonredundant elements. Also it is necessary to add provisions for failure indication (as for a pilot display) or for failure shutoff. Another usual limitation of majority voting systems is that special checkout procedures are necessary to ascertain that full operation is being achieved (i. e., that no failures are present). A typical procedure involves a programmed test sequence which successively disables two channels with opposing hardover signals and assesses the performance of the third.

Sometimes more than three channels are used in a majority voting system. One reason is to give protection for multiple failures. Another reason which arises with flight control servoactuators is the availability of either two or four separate power supplies. In these cases a four channel majority voting servoactuator may be attractive.

### Mid-Value Systems

The mid-value redundant system is similar to a three channel majority voting system but rather than average the three channels, the channel having an output between the other two is continuously selected. This selection can be achieved by the arrangement indicated in Figure 3. Here the three channel outputs feed a majority voting loop having near-infinite gain within the saturation region. The outputs from two of the three channels will always be fully opposed to each other.

Two mechanizations which are used to achieve mid-value redundancy are (1) mechanical position detents (which have high force-to-displacement gain within their detent range), and (2) pressure relief valves (which have high pressure-to-flow gain within their relief setting).

An important difference between mid-value and majority voting systems is the change in performance following a failure. This is summarized in Figure 4. Simple failures (i. e., a hardover or an open with no previous channel mismatch) will produce a change in performance of majority voting systems but not with mid-value systems. The significance of this performance change is minimized by the feedback present about all three control channels. This feedback causes some error equalization as the unfailed channels act to partially offset the effects of a failure. In mid-value systems a simple failure is completely discriminated against so causes no change in output performance. However, in the more practical case where there is interchannel mismatch due to drifts or gain differences, a failure may cause significant change in the output of a mid-value system. For example, the null shift following hardover failure may be twice the maximum channel drift, whereas with a majority voting system it can never be more than one-third the maximum channel drift. Concern for such output shifts following a failure leads to the use of null equalization schemes for most mid-value systems.



### Detection-Correction Systems

Each of the systems described previously uses three or more parallel channels operating simultaneously to control the load. A failure in one channel is masked by the continued operation of the remaining channels.

In detection-correction systems the performance of both operating and standby channels is continuously monitored. This monitoring may involve cross-channel comparison, or comparison to a model of the channel. If the comparison exceeds a preset threshold value, a failure is presumed.

Following detection of a failure, subsequent action is taken to remove the failed channel from control of the output. The diagram in Figure 5 illustrates a detection-correction system where one channel is normally active. Failure of this channel will cause transfer of control to the standby channel. In a system where two channels are normally driving the load, failure detection will call for removal of the failed channel from an active status.

Certain inherent advantages and disadvantages exist for detection-correction systems. On the positive side, it is very convenient to provide an external indication of failure as a failure detector is an essential part of the system. Secondly, performance following a failure is usually equal to that before the failure, as the failed channel is removed from the system. Another usual advantage is that multiple failure capability is easier to accomplish by extensions of the detection-correction logic and switching mechanisms. Finally, ground checkout is usually easier with detection-correction systems as performance monitors are an inherent part of these systems.

On the negative side, usual disadvantages of detection-correction systems include

- (a) Separate mechanisms are needed for failure sensing and switching. In hydraulic servoactuators these sensing and switching components usually involve sliding spools, and if the failure logic is provided electrically, then also solenoid valves.
- (b) The failure sensing, logic and switching elements are usually nonredundant.
- (c) The sequential action of failure sensing and switching takes time to accomplish, so a transient occurs during transfer of operation from one channel to another. The magnitude of this transient -- both in duration and amplitude -- can be made very small by judicious location of the failure sensing devices, as discussed later.

- (d) A detection-correction system must be reset following the switching process should the failure be temporary. Likewise a special start-up sequence is usually necessary to prepare the system for first failure.
- (e) If a model is used as the basis for failure detection, the nonlinearities of the operating channel must be closely duplicated in order to achieve accurate failure detection.

It should not be presumed, since the above list is long, that detection-correction systems are undesirable or not preferred. Each item on the list can be sufficiently overcome by proper design such that detection-correction systems are often the best choice.

The switching transient following failure detection is largely dependent upon the location of the failure detector. With electrohydraulic servoactuators (see Figure 6) performance can be monitored at several places, including the position of the output piston ( $x_p$ ), or the position of the valve spool ( $x_s$ ), or perhaps even the position of the torque motor ( $x_a$ ). It is also possible to monitor the differential pressure between the valve and actuator, or the electrical error signal to the torque motor.

Both the valve spool and the actuator piston provide integrations within the actuator servoloop, so failure monitoring preceding these components avoids their integration lag. On the other hand, the difficulty of precise modeling for accurate failure monitoring increases upstream of each integration element.

Electrical modeling of electrohydraulic servoactuators for failure sensing is seldom practical because of significant nonlinearities such as: piston stroke limits, spool stroke limits (velocity saturation), actuator loading effects, torque motor hysteresis, torque motor and valve null shift, acceleration saturation, piston friction and valve friction. Instead, a standby channel or a scaled-down electrohydraulic model are generally used.

Error comparisons and switching logic have been performed both electrically and hydraulically. Hydraulic failure sensing is generally faster (as solenoid valves are avoided) but more complex and costly as many special valves are needed. Also it is usually still necessary to provide electrical failure indication to the pilot.

## REPRESENTATIVE DESIGNS

The references describe an assortment of different redundant electrohydraulic servoactuator designs -- nearly 20 in all. With few exceptions these can all be classified as detection-correction systems. The wide variety of these systems results from differences in (a) location of failure monitors, (b) type of failure monitor (electrical, hydraulic or mechanical),

(c) type of model or reference, and (d) the degree of failure protection. The designs selected for inclusion here represent several redundant classifications; specifically detection-correction, majority voting and mid-value systems. All examples are taken from work carried out at Moog Inc., East Aurora, New York, U. S. A.

#### Gemini Launch Vehicle

An early example of redundant electrohydraulic servoactuation is the engine position actuator used in the booster for the Gemini space vehicle (see photo in Figure 7 and block diagram in Figure 8). This is an active/standby/reference detection-correction configuration. Two hydraulic supplies are used and either of two separate servovalves can be connected by a selector valve to drive the tandem piston and cylinder configuration.

Loss of hydraulic power causes immediate changeover to the opposite channel. Other failures of the servoactuator, or loss of guidance command signal, are sensed by vehicle motion transducers together with an electrical reference. Electrical indication of failure causes changeover to the standby channel through operation of the solenoid selector valve. The standby channel is not monitored for failure during flight, but of course is checked out for proper operation immediately prior to launch.

#### F-111 Airplane

A more sophisticated example of a detection-correction redundant servoactuator is that used for stability augmentation in the F-111 (TFX) airplane<sup>6</sup>. This servoactuator has three signal input commands, two hydraulic supplies, and uses an active/active/reference configuration. All performance monitoring, failure logic, channel shutoff, and position feedback is accomplished with hydromechanical components located within the servoactuator. A photo of the servoactuator appears in Figure 9, block diagram in Figure 10, and schematic in Figure 11.

The two normally active channels each use a two-stage flow control servovalve to drive one-half of the tandem piston and cylinder. Performance differences between these two channels are carefully monitored by a free-floating differential flow sensor. This is equivalent to servovalve spool position monitoring, but avoids attaching a position transducer to the valve spools. The differential flow sensor is also used for interchannel feedbacks to achieve null and gain synchronization between channels.

The third channel contains another servovalve together with a separate piston with position feedback. This piston provides a model reference to simulate operation of the tandem piston. The position of the model piston is continually compared to that of the tandem piston by a sliding

valve and sleeve. Excessive position mismatch, together with excessive flow unbalance between active channels, causes an appropriate shutoff of the discrepant channel and signals a pilot warning. Failure of the model reference causes only a pilot warning.

Separate solenoid controlled startup valves are included in the servo-actuator to reset the failure logic devices upon startup or following self-shutoff. The actuator position transient following failure shutoff may be rather large, depending upon the specific condition of channel mismatch immediately preceding the failure (see Figure 12). However in the F-111 airplane, the authority of the stability augmentation servo-actuators together with the limited dynamic response of the surface position servos, are such that reasonable vehicle transients occur.

#### Saturn S-IV B Stage

The S-IV B upper stage of the Saturn launch vehicle uses just one engine for vehicle thrust and steering control. Lower stages of the Saturn each have five engines and achieve steering redundancy by multiple engine positioning controls. A majority voting servoactuator has been developed to provide redundant actuation for the S-IV B stage. The unit is pictured in Figure 13.

The block diagram in Figure 14, schematic in Figure 15, and valve photograph in Figure 16, show the mechanization of this actuator. Three separate electrical commands (ideally identical) supply three torque motors. Each torque motor drives a double-nozzle hydraulic amplifier. Flow from these hydraulic amplifiers positions a valve spool and spool position is fed back mechanically to form a characteristic majority voting arrangement. The position of the actuator piston is also fed back mechanically to each torque motor, thereby closing an outer position servoloop.

The differential piston pressures caused by load reaction forces are used in another feedback loop to provide load damping. A frequency sensitive hydraulic network allows only higher frequency pressure feedback so that static actuator stiffness is retained.

Representative performance for this majority voting servoactuator is given in Figures 17 to 19. The actuator position transient resulting from a temporary hardover signal on one channel shows the corresponding position null shift effect.

Very similar majority voting servoactuators have been developed for the Titan III-M vehicle which will be used to launch the Manned Orbital Laboratory. The booster stage of this vehicle will use two hydraulic supplies, so a choice for actuation was studied comparing a four channel majority voting configuration (two on each hydraulic supply)<sup>5</sup> with a tandem piston/cylinder, and a three channel majority voting arrangement with a single piston/cylinder. The latter, which was the final

choice, uses an automatic supply pressure selector. This unit is pictured in Figure 20.

### SST Airplane

A different majority voting servoactuator is being evaluated for use as a pilot master servo in the Boeing SST. This unit provides pilot assist for moving the control system linkages. A photo, block diagram, and simplified schematic appear in Figures 21 to 23, respectively.

Rotary mechanical inputs and outputs are provided by a dual load path design. Three hydraulic supplies and three electrohydraulic channels are arranged in individual bodies, sandwiched together. Electrical transducers are used for actuator position feedback.

The three single-stage servovalves control differential pressures at the three push-push rotary actuators. The actuator torque summation and load position feedback form a simple majority voting configuration.

Normal actuator loads are well within the total torque capability of the actuator so that maximum differential pressure is used for failure indication. The individual supply pressure to the failed channel may then be shut off. This leaves the unit with only two active channels, so if a subsequent failure occurs the unit will fail safe.

Another redundant electrohydraulic servoactuator for the SST is the Electric Command Servo. One ECS servo is located at each primary flight surface and is used for normal fly-by-wire control of the surface power boost actuators. A possible configuration for the ECS servo is a mid-value redundant arrangement. Design layouts and laboratory testing are presently underway to investigate this approach.

This redundant actuator configuration is illustrated by the block diagram and schematic in Figures 24 and 25. Three electrical channels are used, each comprising a two-stage servovalve, a push-push piston, a detent mechanism, and a position feedback transducer. A common output shaft sums torques from the three electrical channels, together with torque from linkage to the pilot, to drive the surface power boost input.

Since all three electrical channels will not agree on a unique load position, two detents will be out (in opposite directions) and the third will be controlling the load. The amount of detent displacement is indicative of the interchannel mismatch and is used for failure detection.

However, to avoid a severe output position transient when shutting off a failed channel, it is necessary to maintain normal out-of-detent positions small. So the detent position transducers are used to supply integrating equalizers for each channel. These equalizers provide separate electrical signal inputs to each control channel which offset

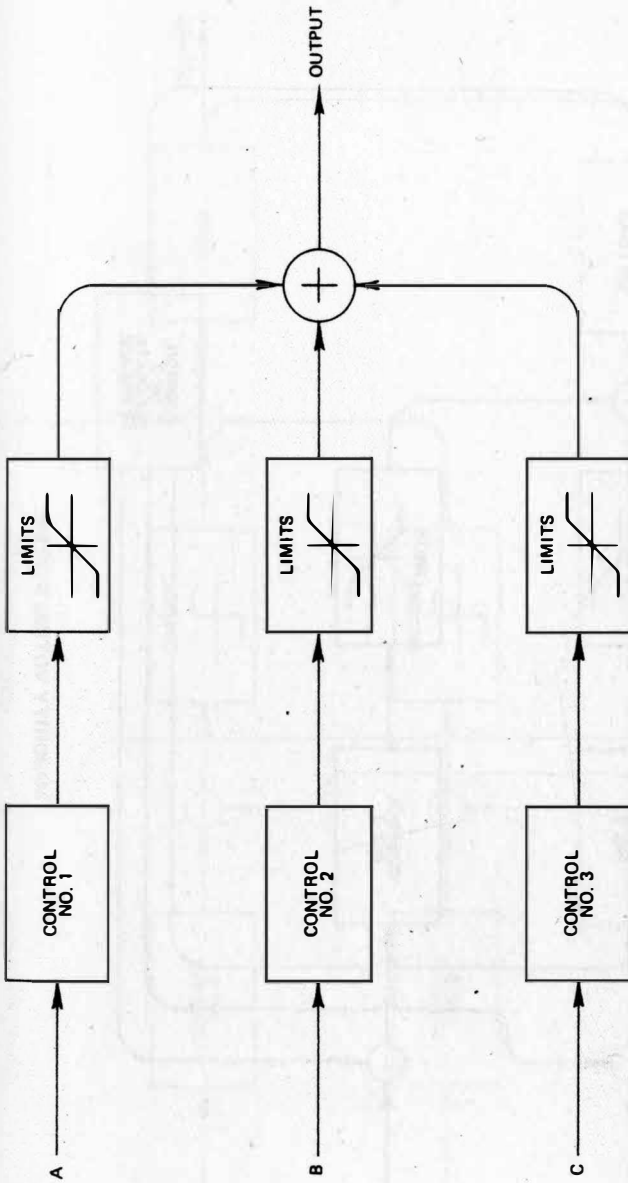
the combined effects of servoactuator drift and command input mismatch.

When integrated equalizer feedback is used, some means must be provided for integrator reset to prevent integrator saturation or cumulative errors between input and output. Generally this means that the integrator for one channel may be reset at any one time, and the remaining channels will then equalize to the null of the channel being reset. With three control channels operating, it is possible to continually select the channel which has an integrated equalizer output between the other two. If the integrator for this channel is then reset, the other two will slave to it. This implementation is indicated by the block diagram of Figure 24.

### REFERENCES

- 1 J. J. Fleck, J. C. Kemp, et al, "Research and Feasibility Study to Achieve Reliability in Automatic Flight Control Systems, " Wright-Patterson Air Force Base Technical Report No. WADD-TDR-61-264, March 1961.
- 2 Vernon R. Schmitt, "A Method to Improve the Reliability of a Dual Flight-Control System, " Wright-Patterson Air Force Base Technical Report No. ASD-TR-61-581, December 1961.
- 3 "Control System Redundancy Mechanization Study, " Wright-Patterson Air Force Base Technical Documentary Report No. ASD-TDR-62-772, February 1963.
- 4 "Demonstration of the Application of Majority Logic for Increased Reliability in Automatic Flight Control Systems, " Wright-Patterson Air Force Base Technical Documentary Report No. ASD-TDR-63-275, July 1963.
- 5 K. D. Garnjost and W. J. Thayer, "New Servovalves for Redundant Electrohydraulic Control, " Second Congress of the International Federation of Automatic Control, Basle, Switzerland, September 1963. Available as Technical Bulletin No. 105, Moog Inc.
- 6 W. J. Thayer, "Redundant Damper Servoactuators for the F-111 Airplane, " Aerospace Fluid Power Systems and Equipment Conference, Los Angeles, California, May 1965. Available as Technical Bulletin No. 107, Moog Inc.
- 7 Vernon C. Sethre, "Status of a Fly-by-Wire System, " SAE Paper No. 650601, Society of Automotive Engineers, Inc., July 1965.

- 8 D. Hogan, W. B. Poteate, and J. R. Shatz, "Research and Investigation of Redundancy Techniques for Nonelectronic Elements," Wright-Patterson Air Force Base Technical Report No. AFFDL-TR-65-80, August 1965.
- 9 H. L. Ehlers, R. D. Bloser, and H. O. Williams, "Trisafe Single Axis Flight Control System," Wright-Patterson Air Force Base Technical Report No. AFFDL-TR-65-89, September 1965.
- 10 D. Wood, "Hydrologic Redundant Systems," Report Number 650575, SAE Transactions Volume 74, 1966, Society of Automotive Engineers, Inc.
- 11 J. Pukite, G. G. Anderson, and K. C. Jones, "Practical Applications of Electromechanical Redundancy for Flight Control Systems," Wright-Patterson Air Force Base Technical Report No. AFFDL-TR-66-31, October 1966.
- 12 J. P. Sutherland, "Fly-by-Wire Flight Control Systems," SAE Aerospace Fluid Power Committee A-6 Meeting, Miami, Florida April 17, 1967.
- 13 F. L. Miller and J. E. Emfinger, "Fly-by-Wire Techniques," Wright-Patterson Air Force Base Technical Report No. AFFDL-TR-67-53, July 1967.
- 14 C. H. Bergquist, C. L. Cohen, and T. G. Lahn, "Investigation and Demonstration of Techniques for Practical Applications of Redundancy for Flight Controls," Wright-Patterson Air Force Base Technical Report No. AFFDL-TR-67-61, October 1967.

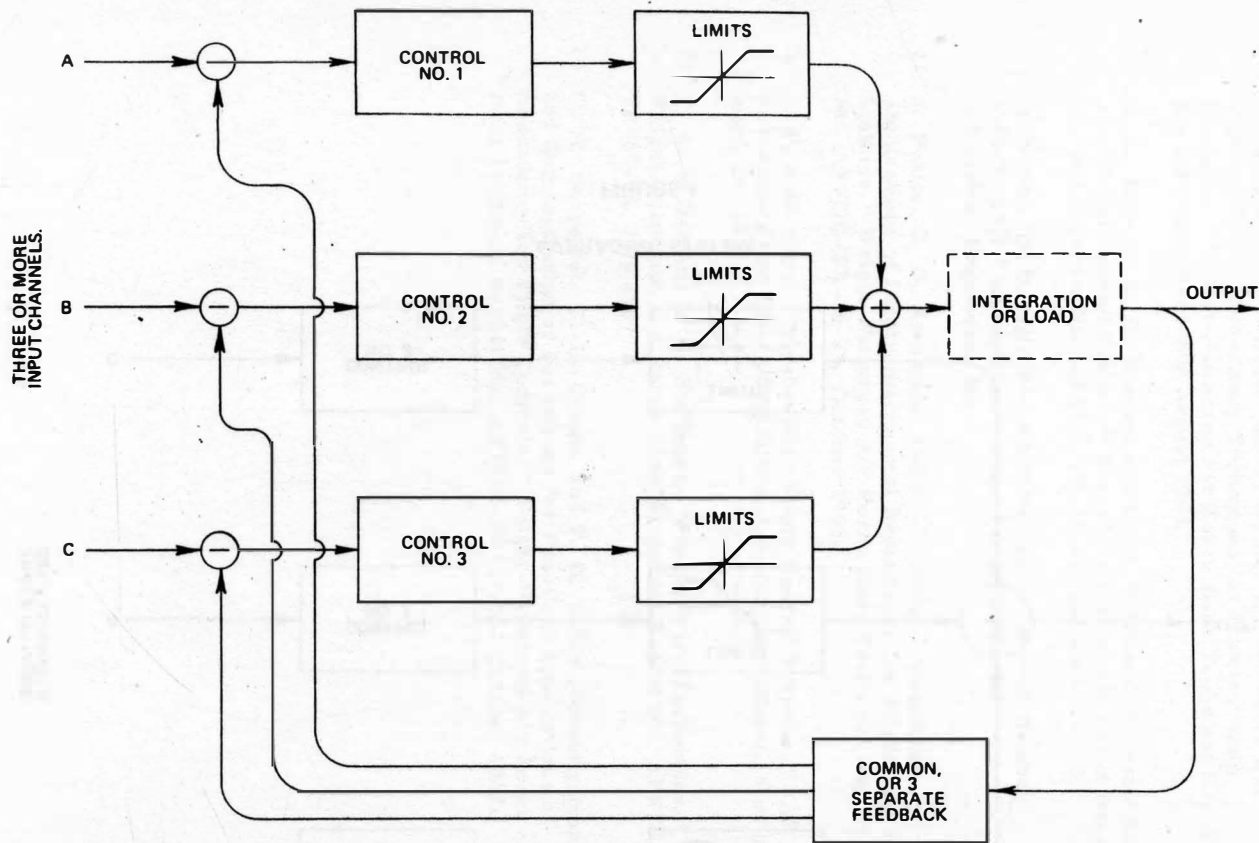


THREE OR MORE  
INPUT CHANNELS.

AVERAGING SYSTEM

FIGURE 1

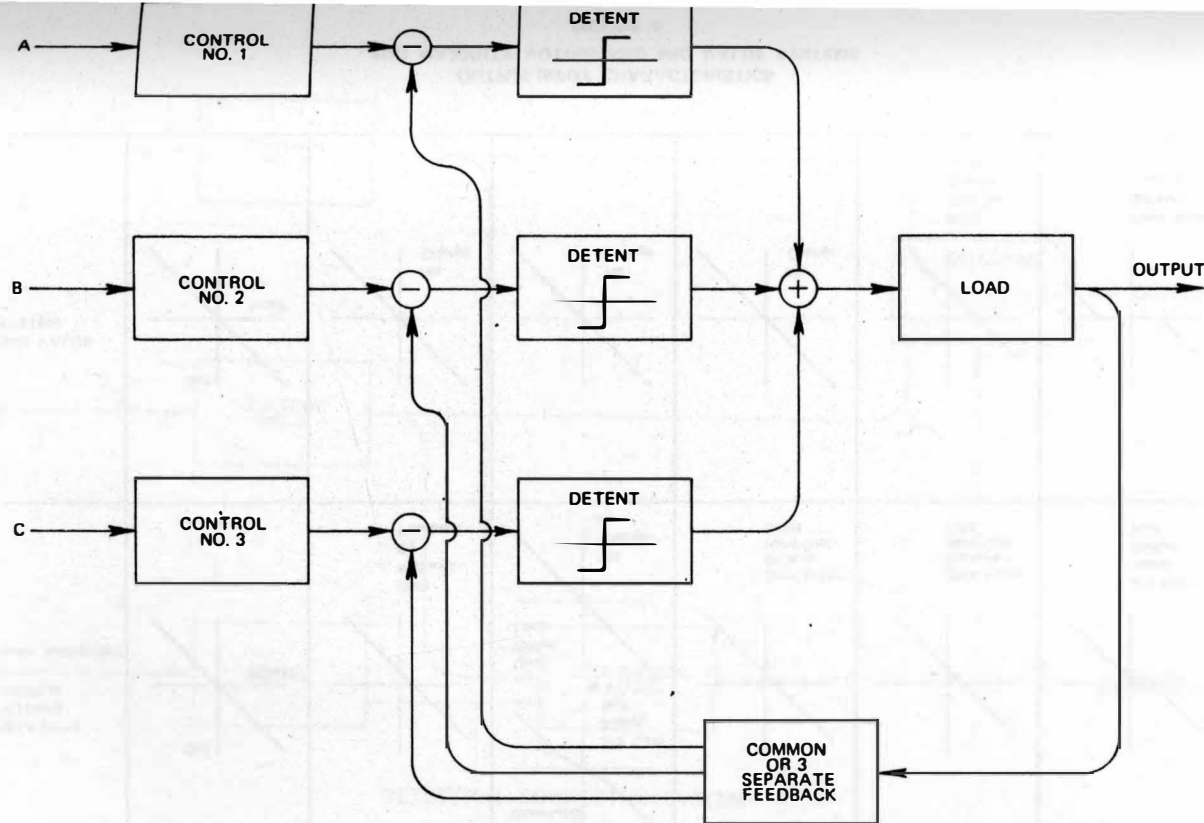




MAJORITY VOTING SYSTEM

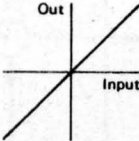
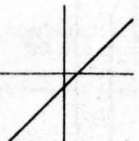
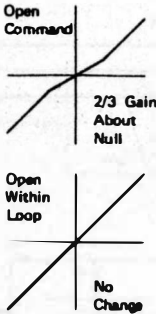
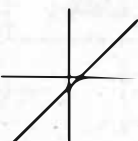
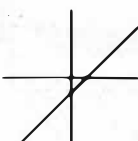
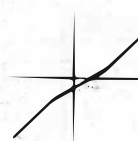
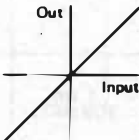
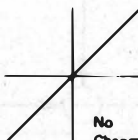
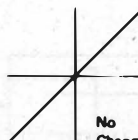
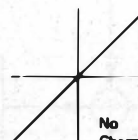
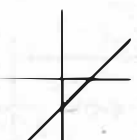
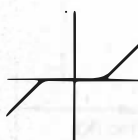
FIGURE 2

THREE OR MORE  
INPUT CHANNELS.

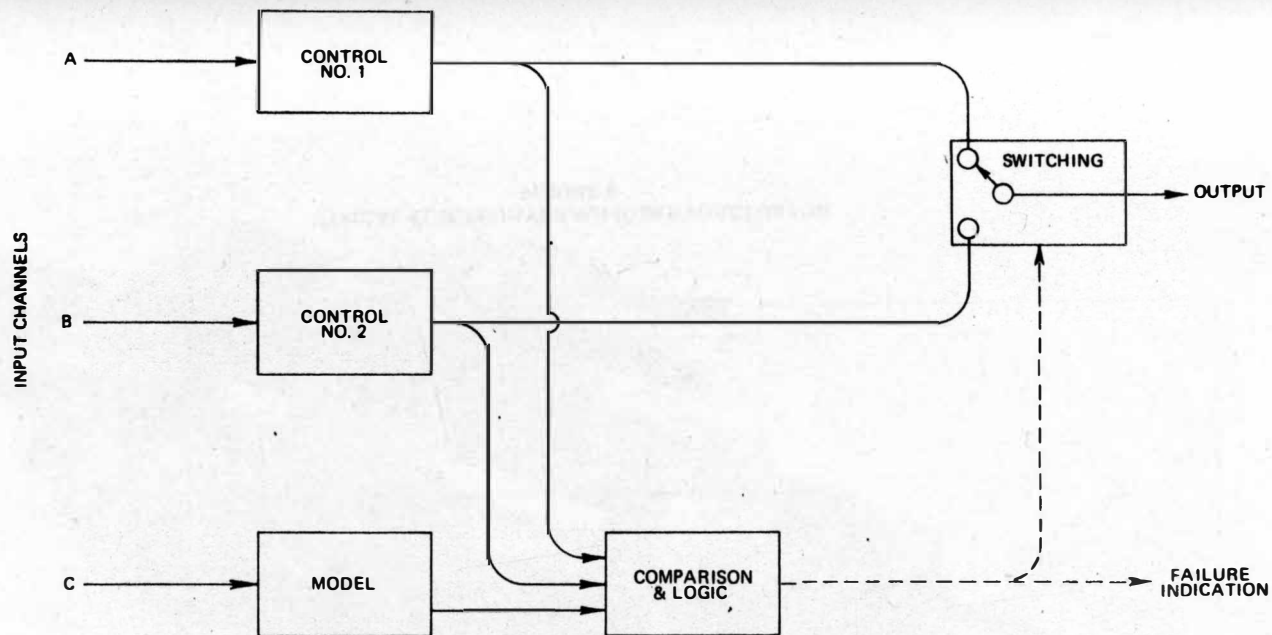


MID-VALUE SYSTEM

FIGURE 3

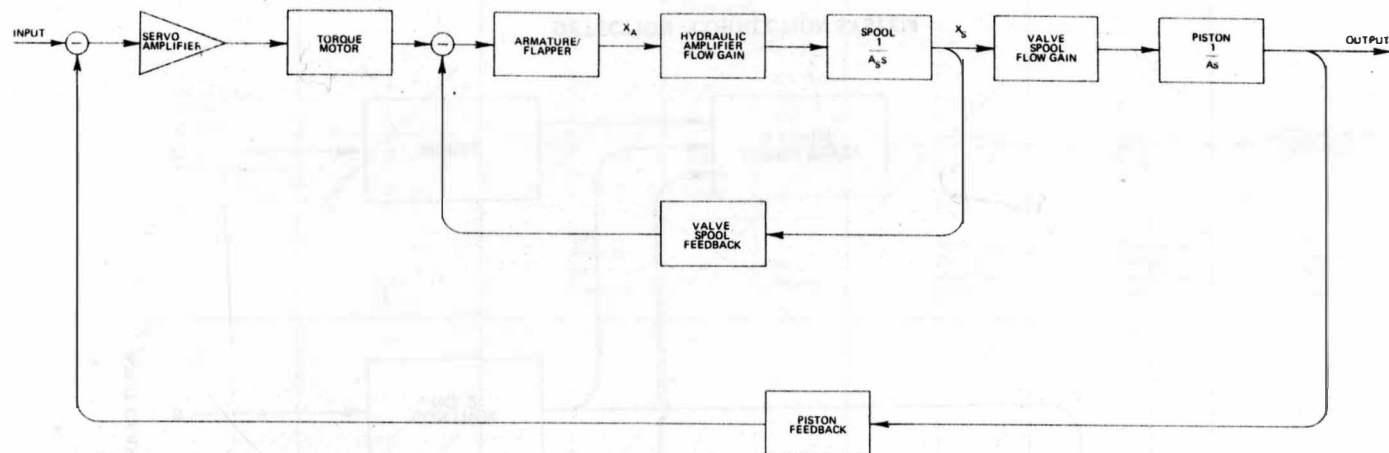
	Normal Operation	One Channel Hardover	One Channel Open	One Channel Drift	Channel Drift + One Hardover	Channel Drift + One Input Open
MAJORITY VOTING SYSTEM (with integration)						
MID VALUE SYSTEM						

OUTPUT-INPUT CHARACTERISTICS  
FOR MAJORITY VOTING AND MID VALUE SYSTEMS

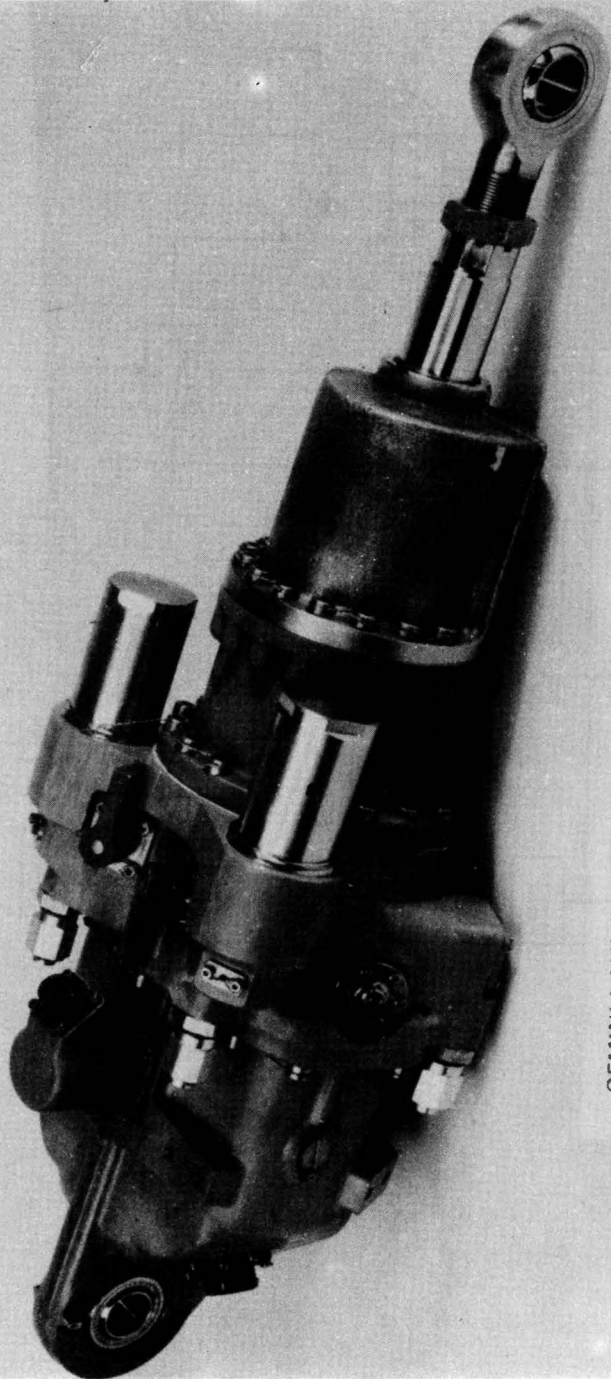


DETECTION - CORRECTION SYSTEM

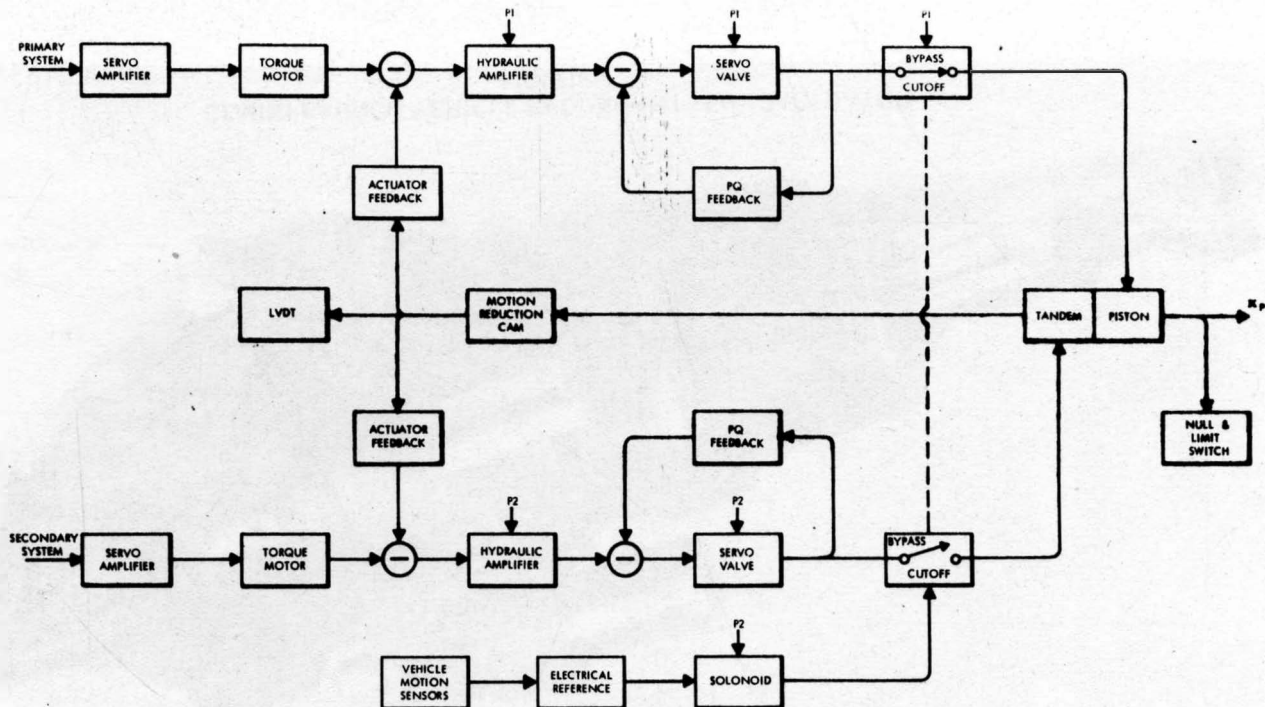
FIGURE 5



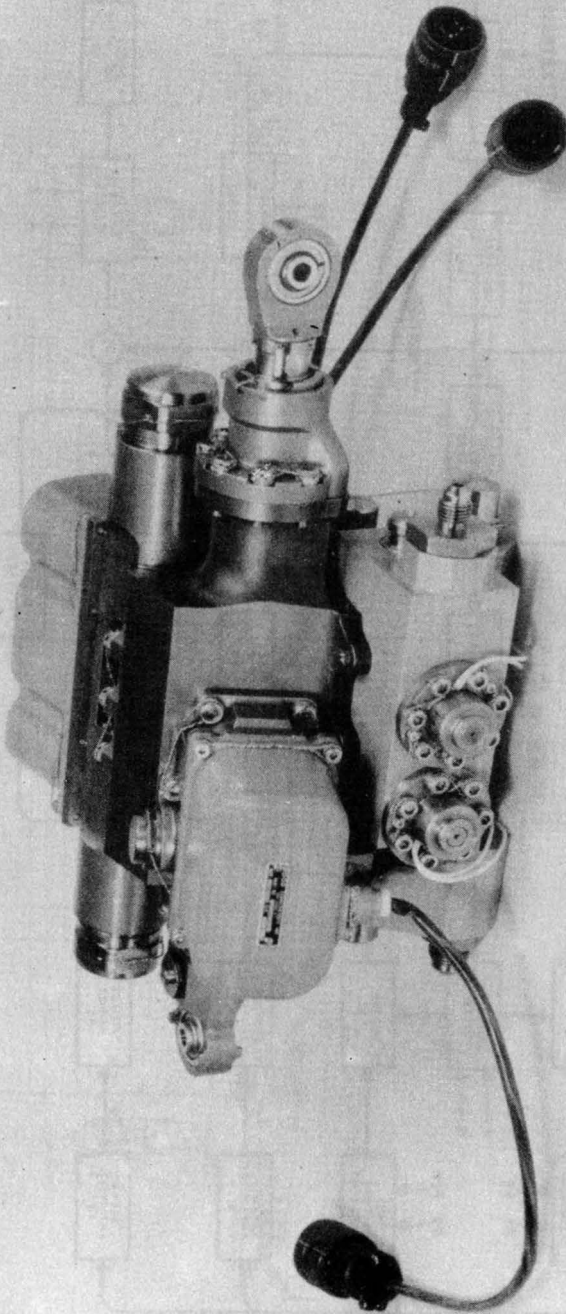
**TYPICAL ELECTROHYDRAULIC SERVOACTUATOR  
FIGURE 6**



GEMINI LAUNCH VEHICLE REDUNDANT SERVOACTUATOR  
FIGURE 7

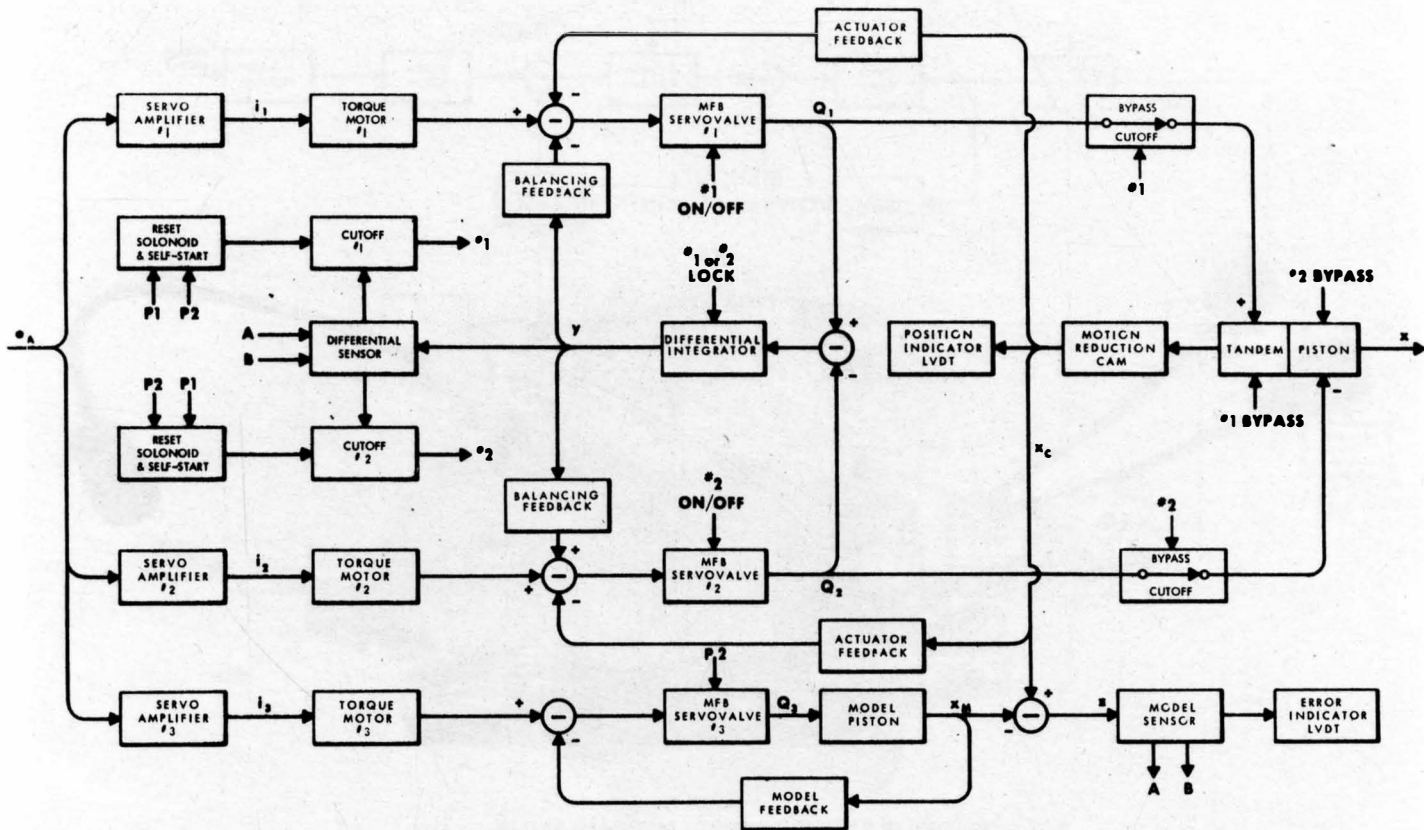


BLOCK DIAGRAM - GEMINI BOOSTER SERVOACTUATOR  
FIGURE 8

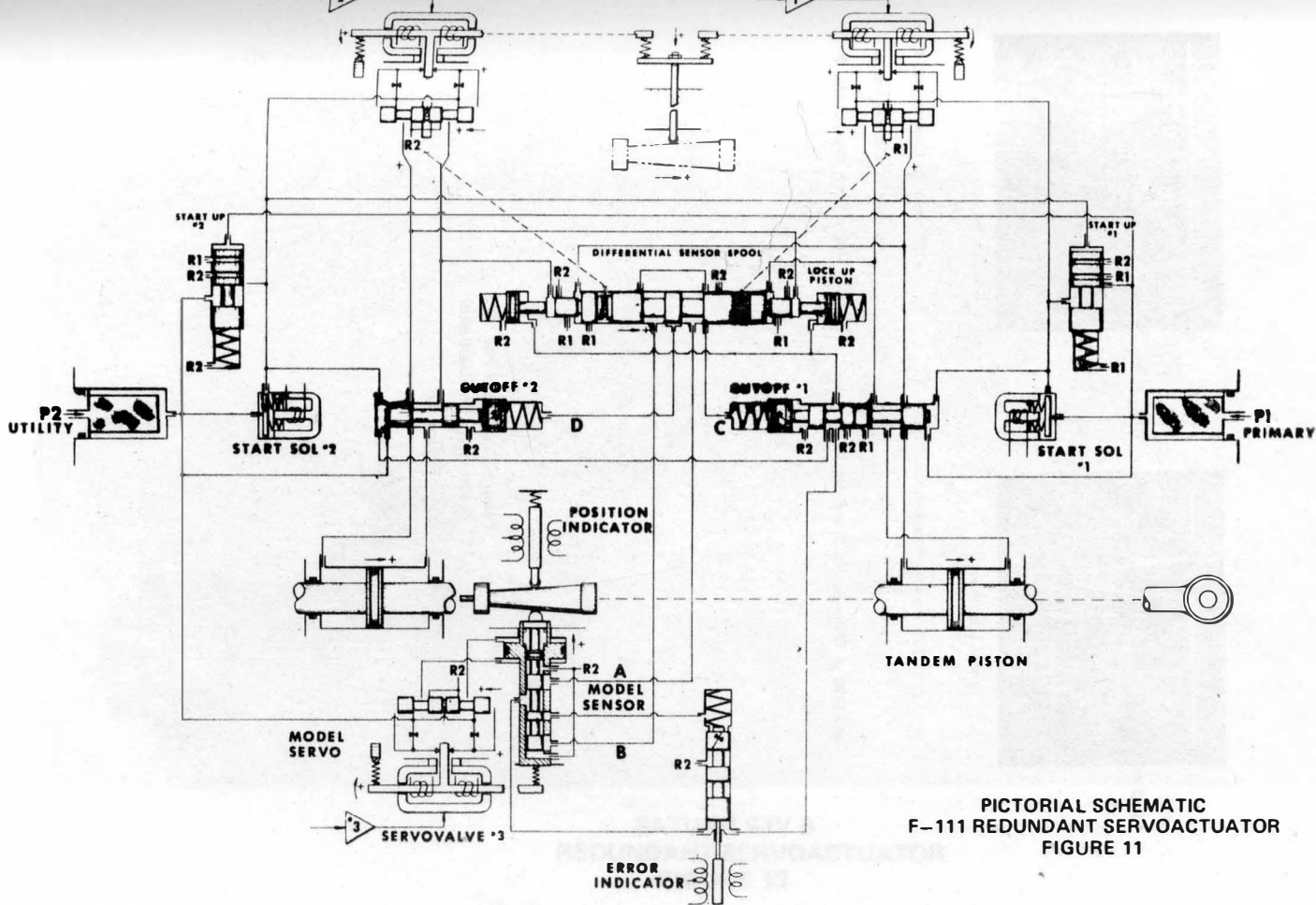


F-111 REDUNDANT SERVOACTUATOR  
FIGURE 9

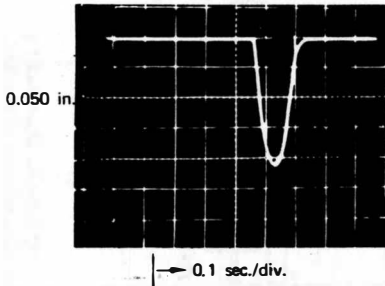




BLOCK DIAGRAM F-111 REDUNDANT SERVOACTUATOR  
FIGURE 10

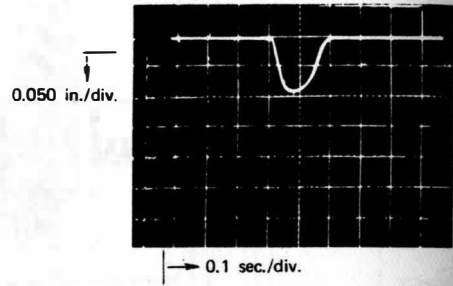


PICTORIAL SCHEMATIC  
F-111 REDUNDANT SERVOACTUATOR  
FIGURE 11



-50% error in Channel No. 1

Zero drift in Channels No. 2 and No. 3

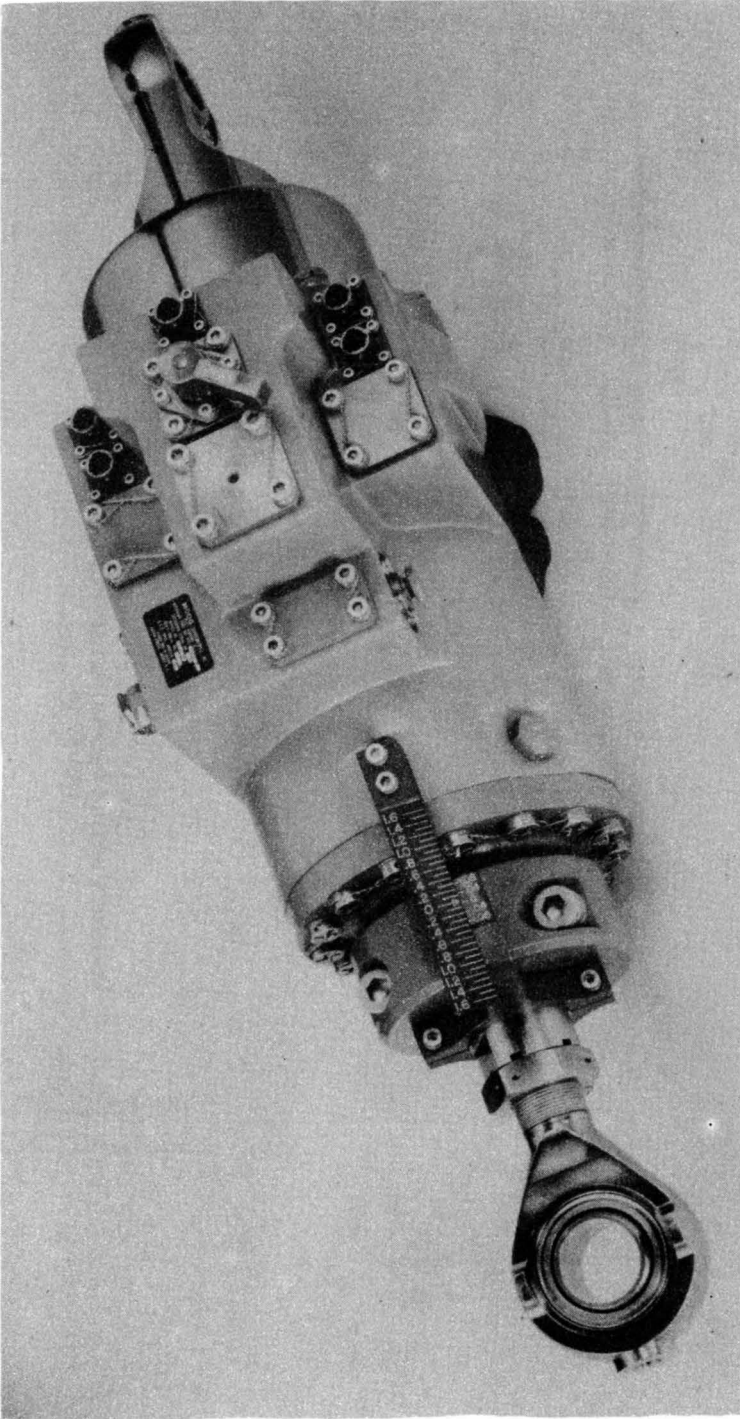


-22% error in Channel No. 1

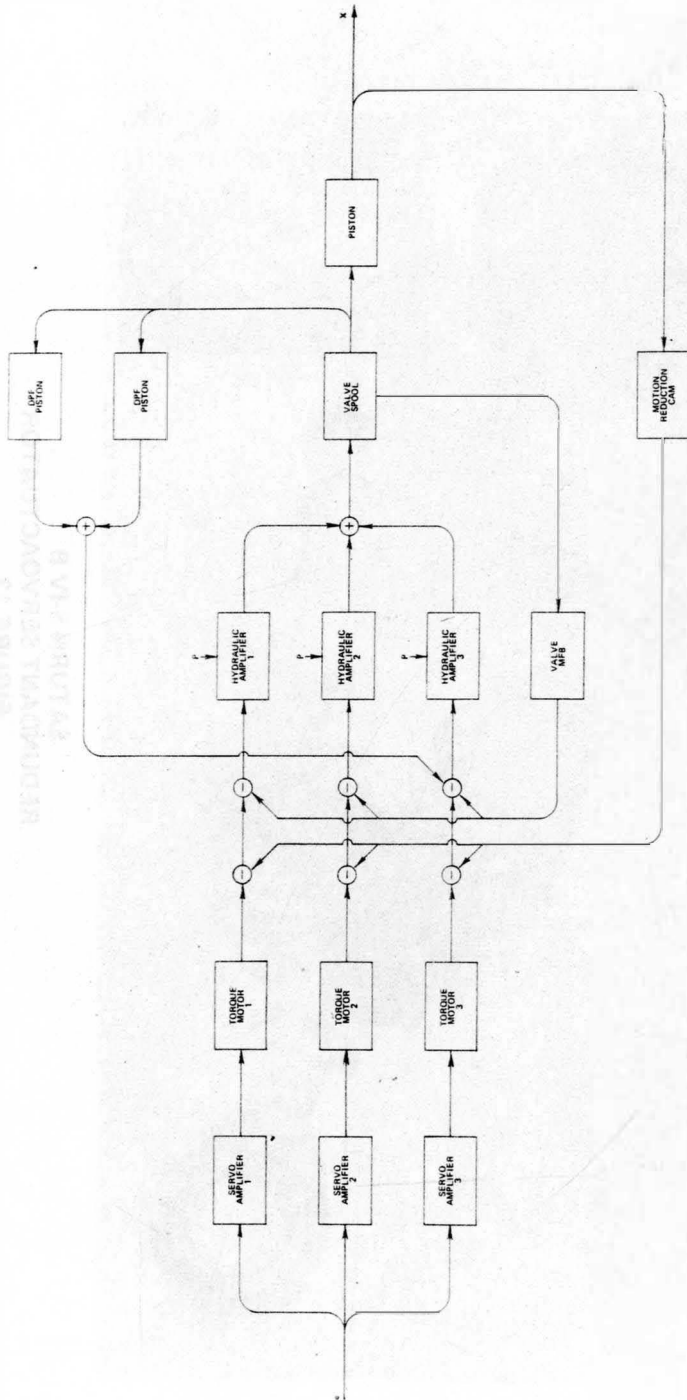
Zero drift in Channel No. 2

10% drift in Channel No. 3

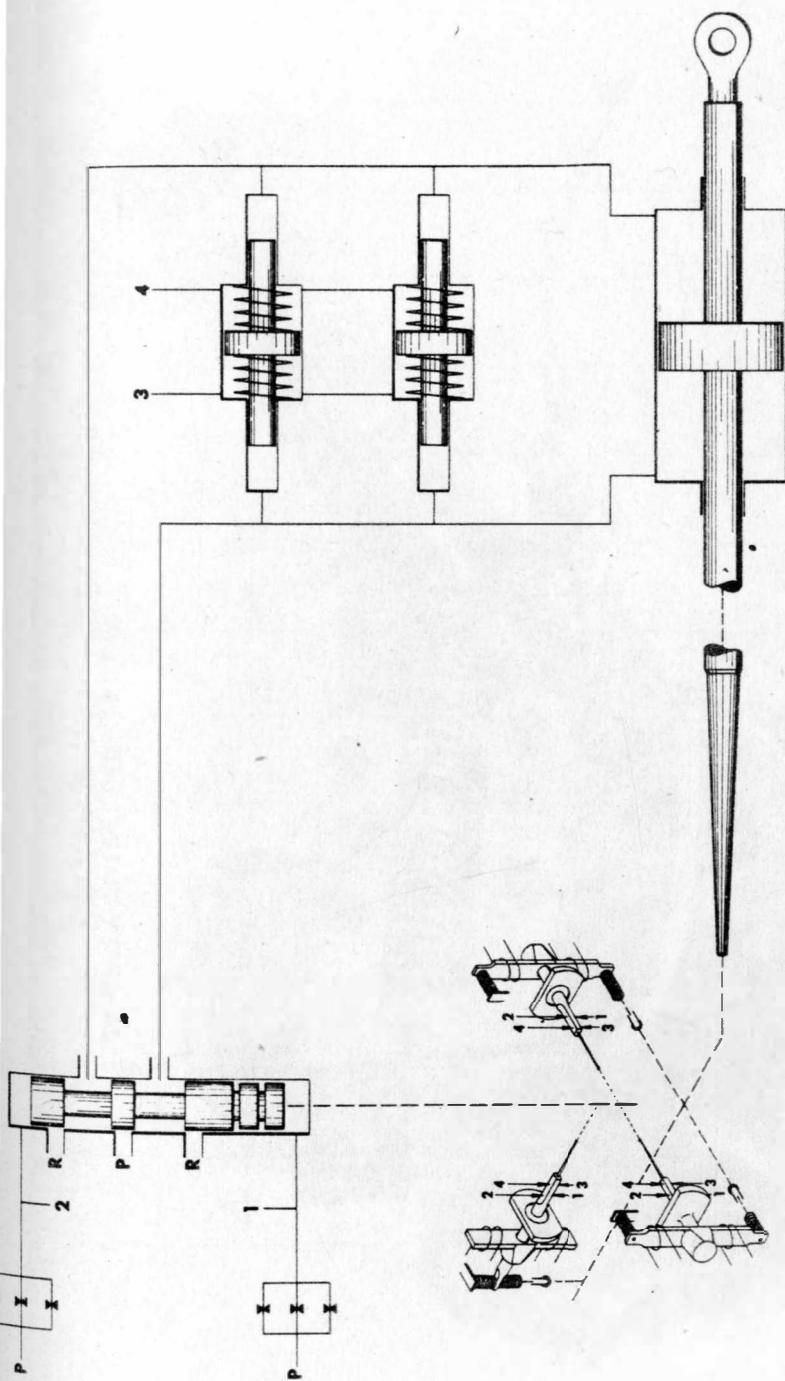
**Failure Transients For  
F-111 Redundant Servoactuator  
Figure 12**



SATURN S-IV B  
REDUNDANT SERVOACTUATOR  
FIGURE 13

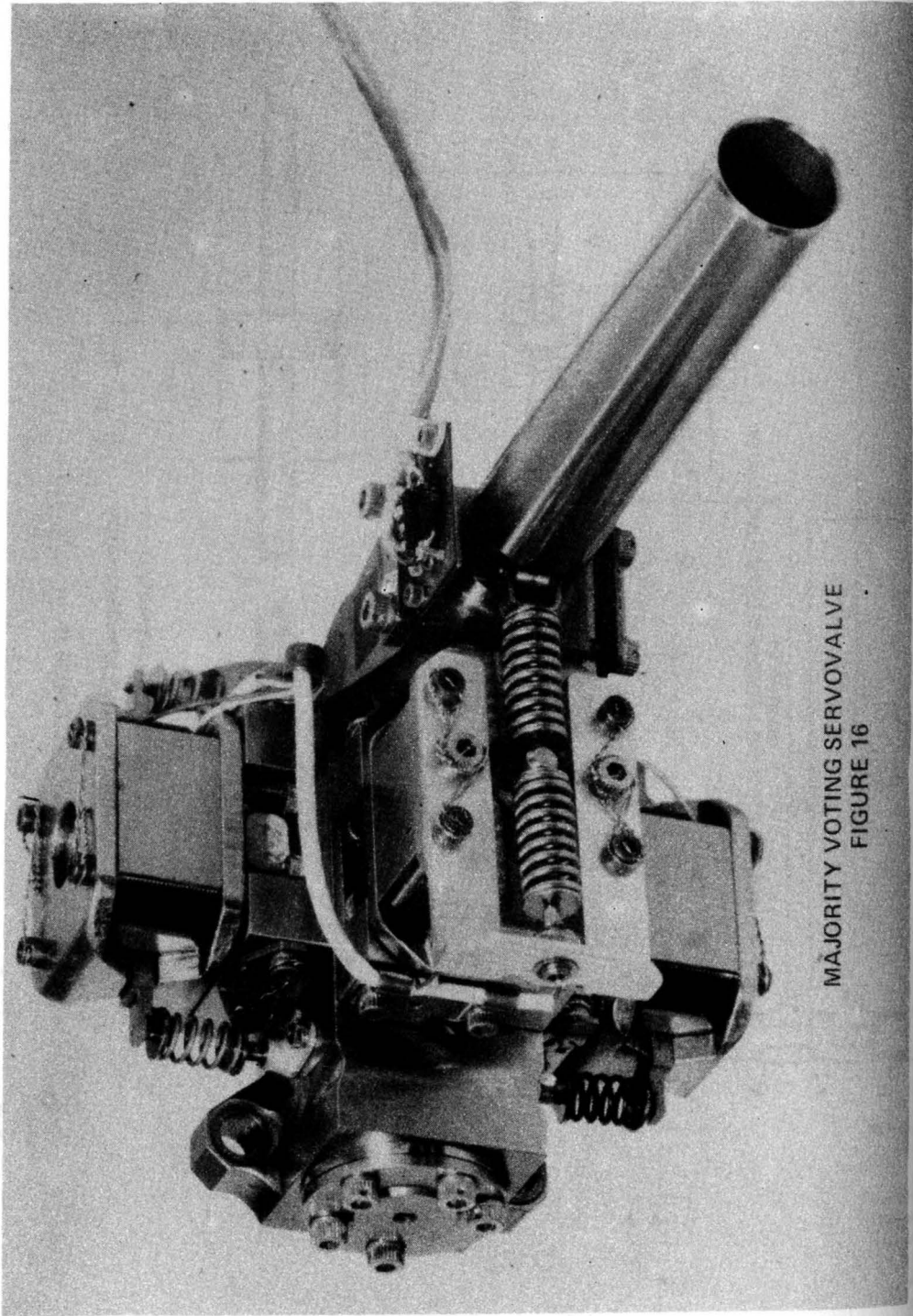


MAJORITY VOTING REDUNDANT SERVOACTUATOR  
FIGURE 14

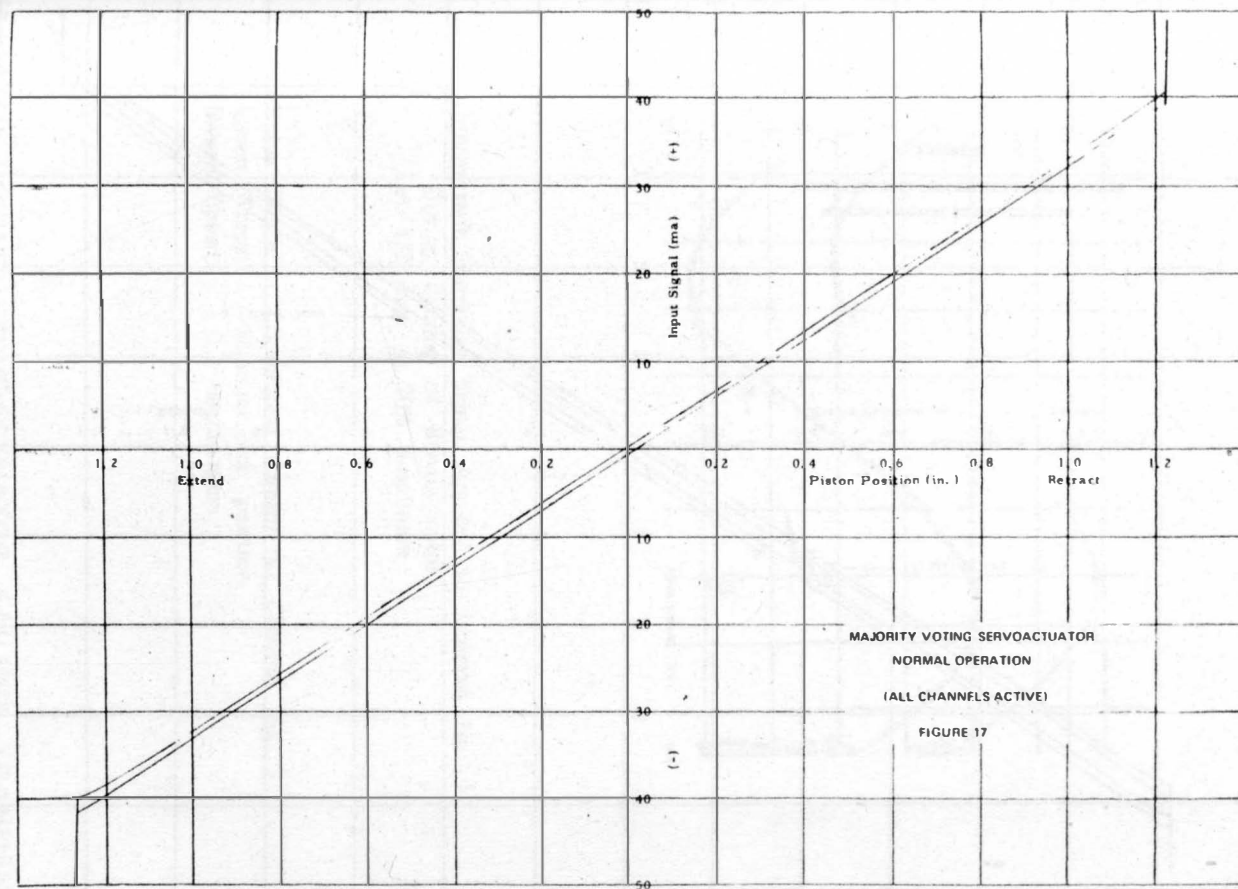


PICTORIAL SCHEMATIC  
MAJORITY VOTING SERVOACTUATOR

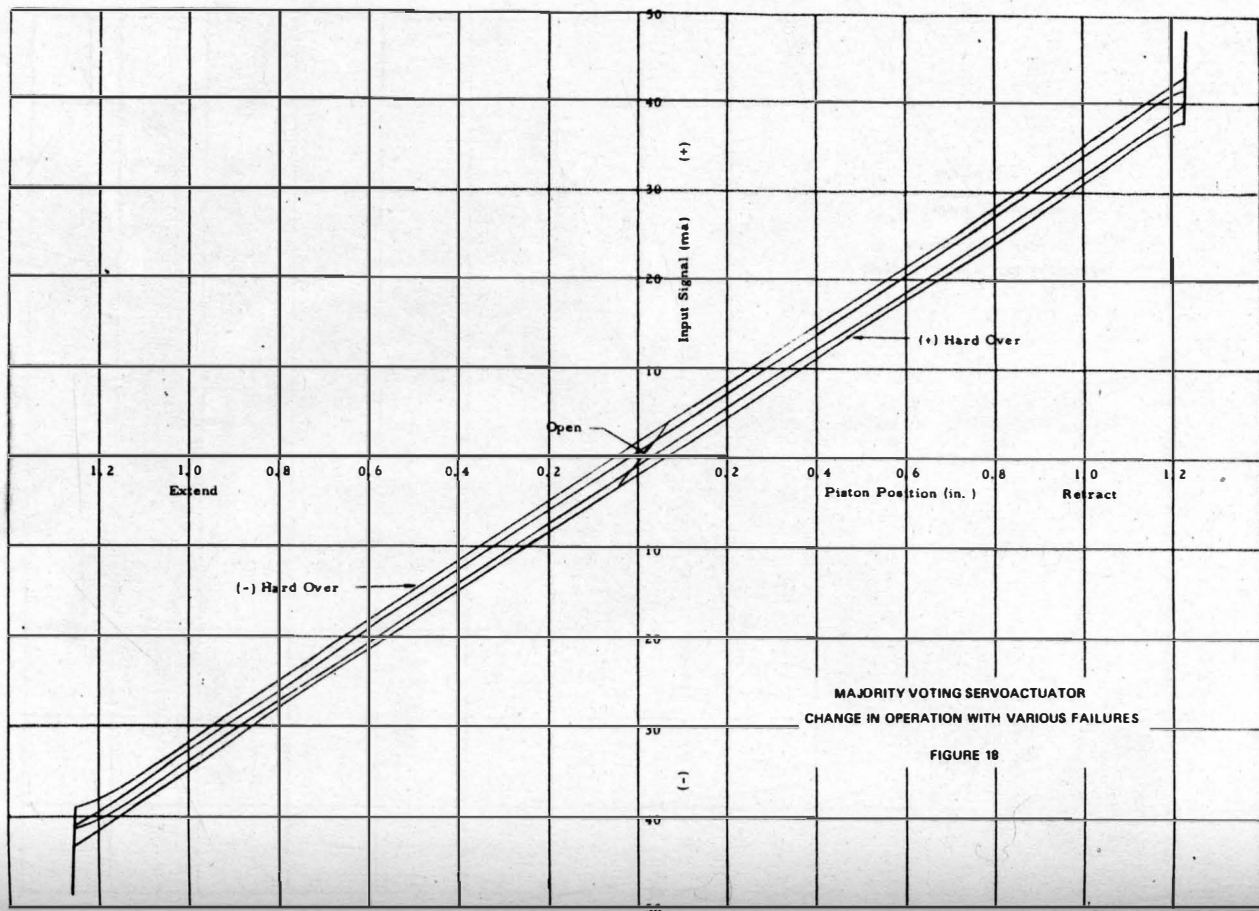
FIGURE 15



MAJORITY VOTING SERVOVALVE  
FIGURE 16

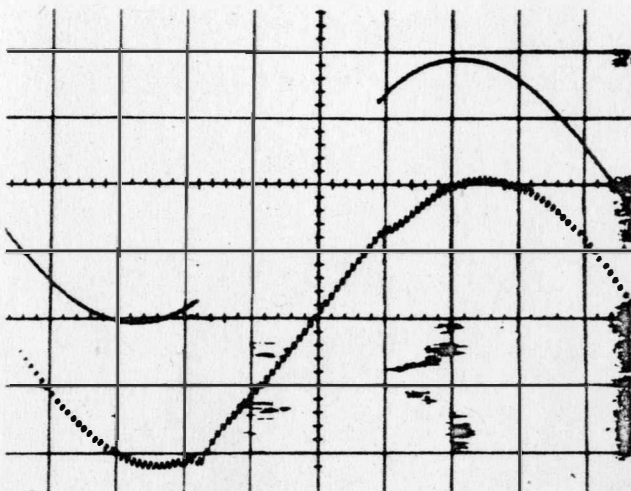






MAJORITY VOTING SERVOACTUATOR  
CHANGE IN OPERATION WITH VARIOUS FAILURES

FIGURE 18

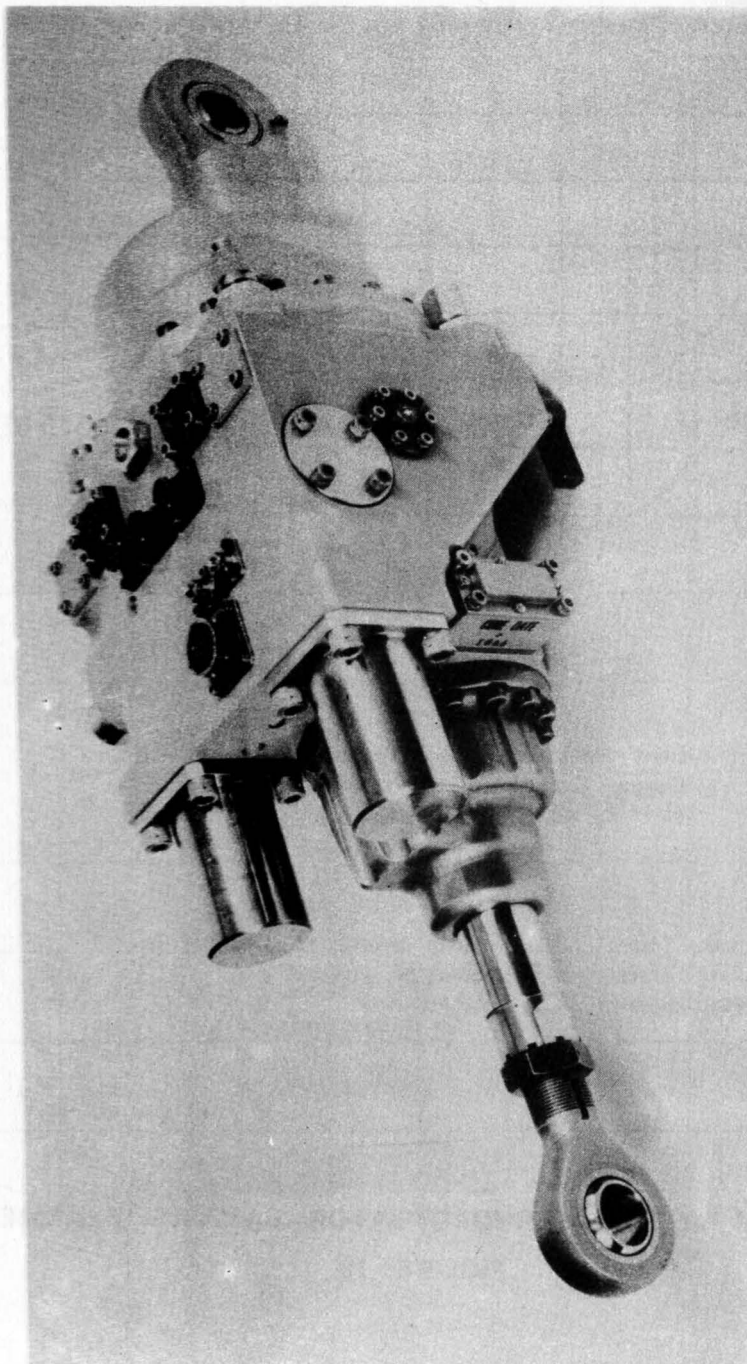


Intermittent Hardover Signal Applied to Channel No. 1  
 During Cycling of Servoactuator  
 at 1/2 cps,  $\pm$  20% amplitude

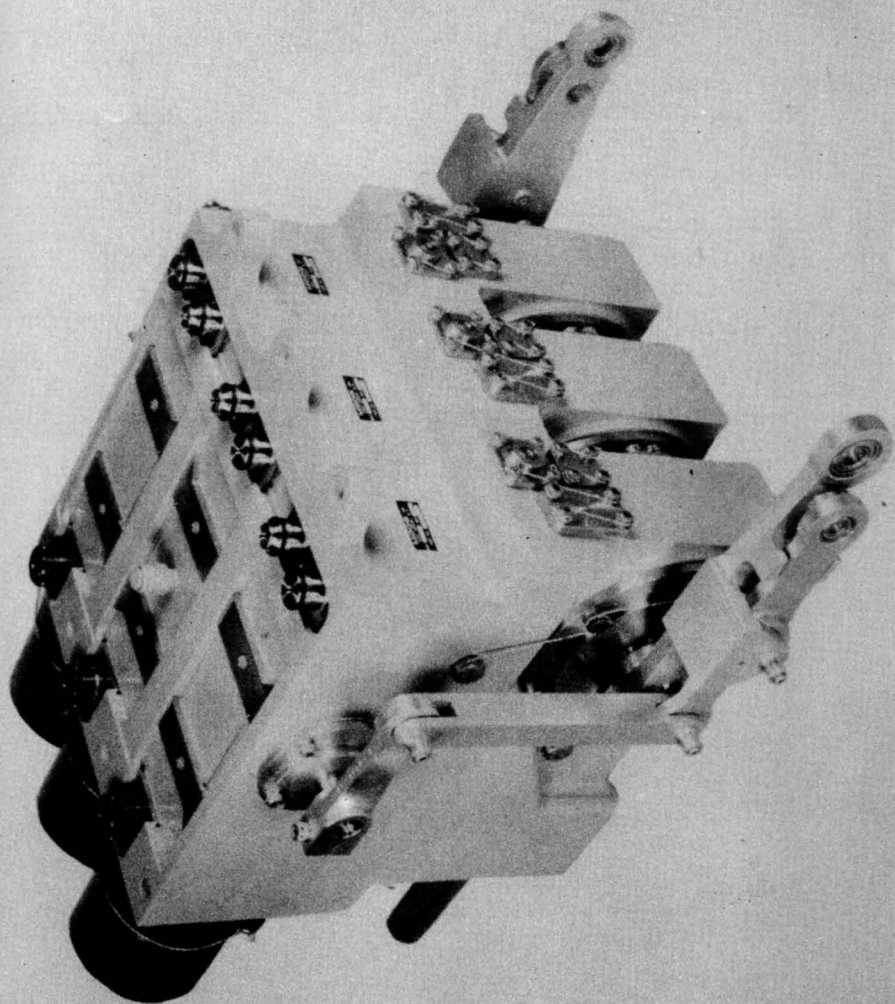
Upper Trace: Command current to Channel No. 1  
 Lower Trace: Servoactuator position  
 Sweep Speed: 0.2 sec/division

## MAJORITY VOTING SERVOACTUATOR FAILURE TRANSIENT

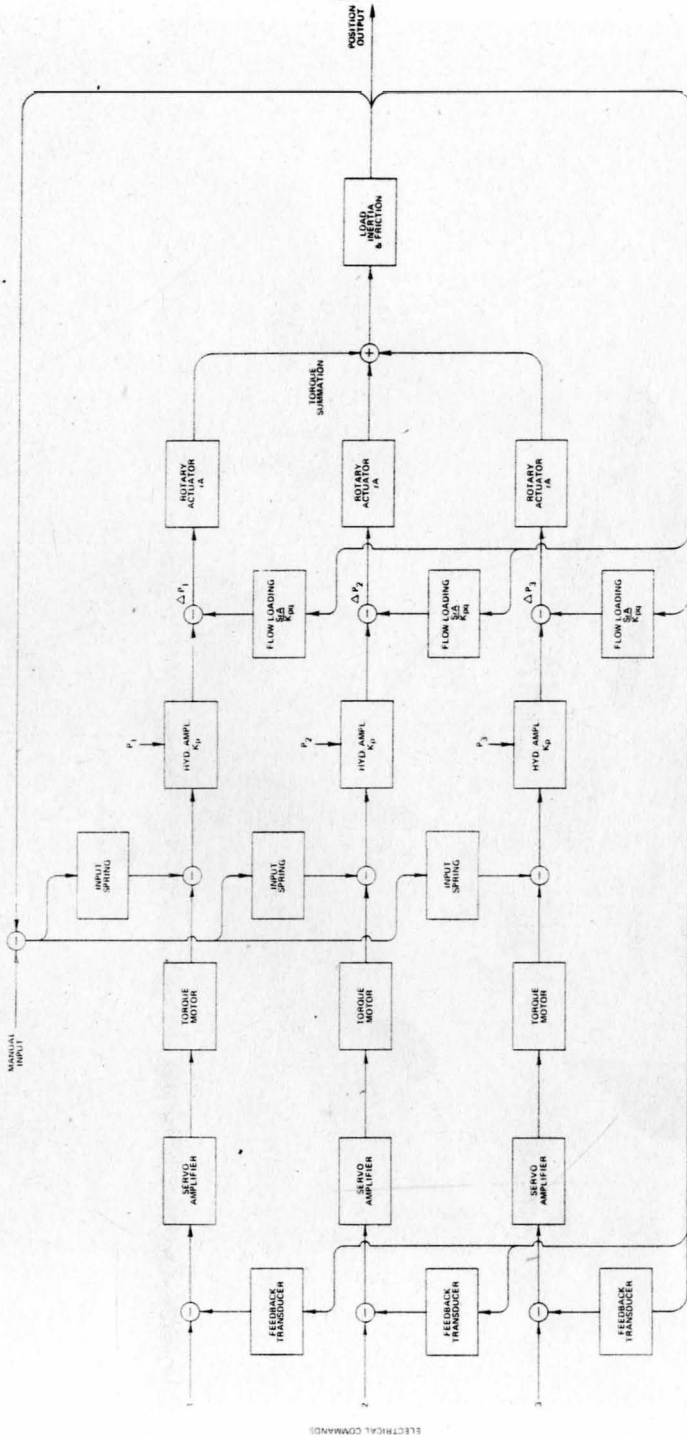
### FIGURE 19



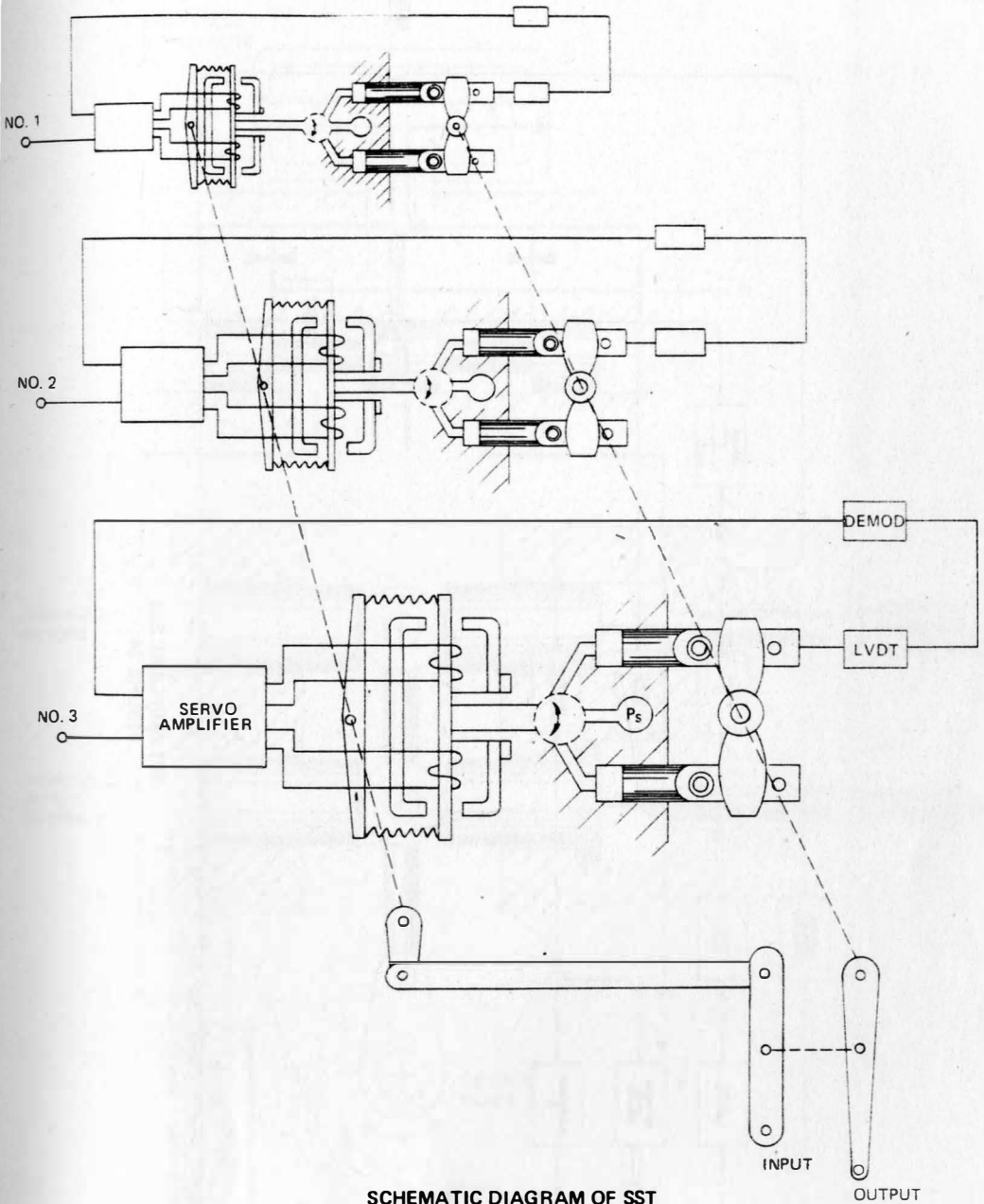
TITAN III-M BOOSTER REDUNDANT SERVOACTUATOR  
FIGURE 20



PROTOTYPE MSU FOR THE SST AIRPLANE  
FIGURE 21

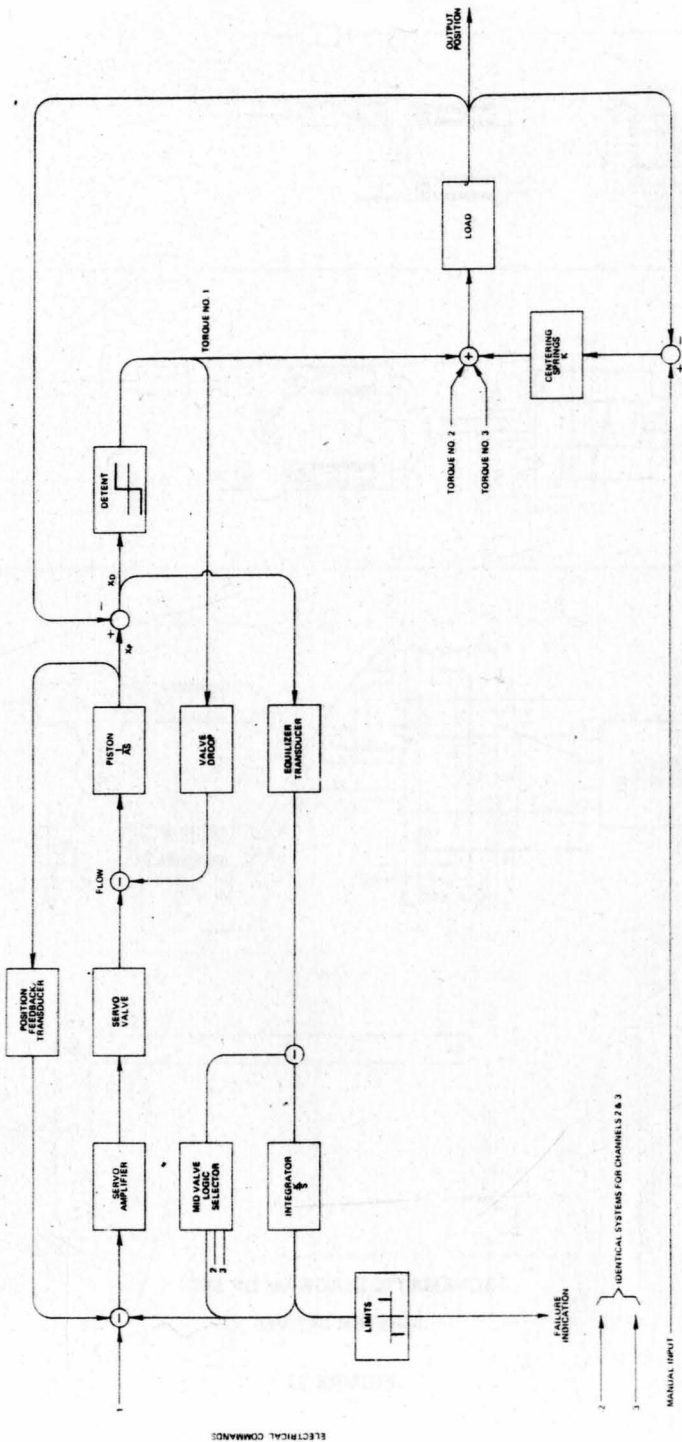


SST AIRPLANE MSU  
FIGURE 22



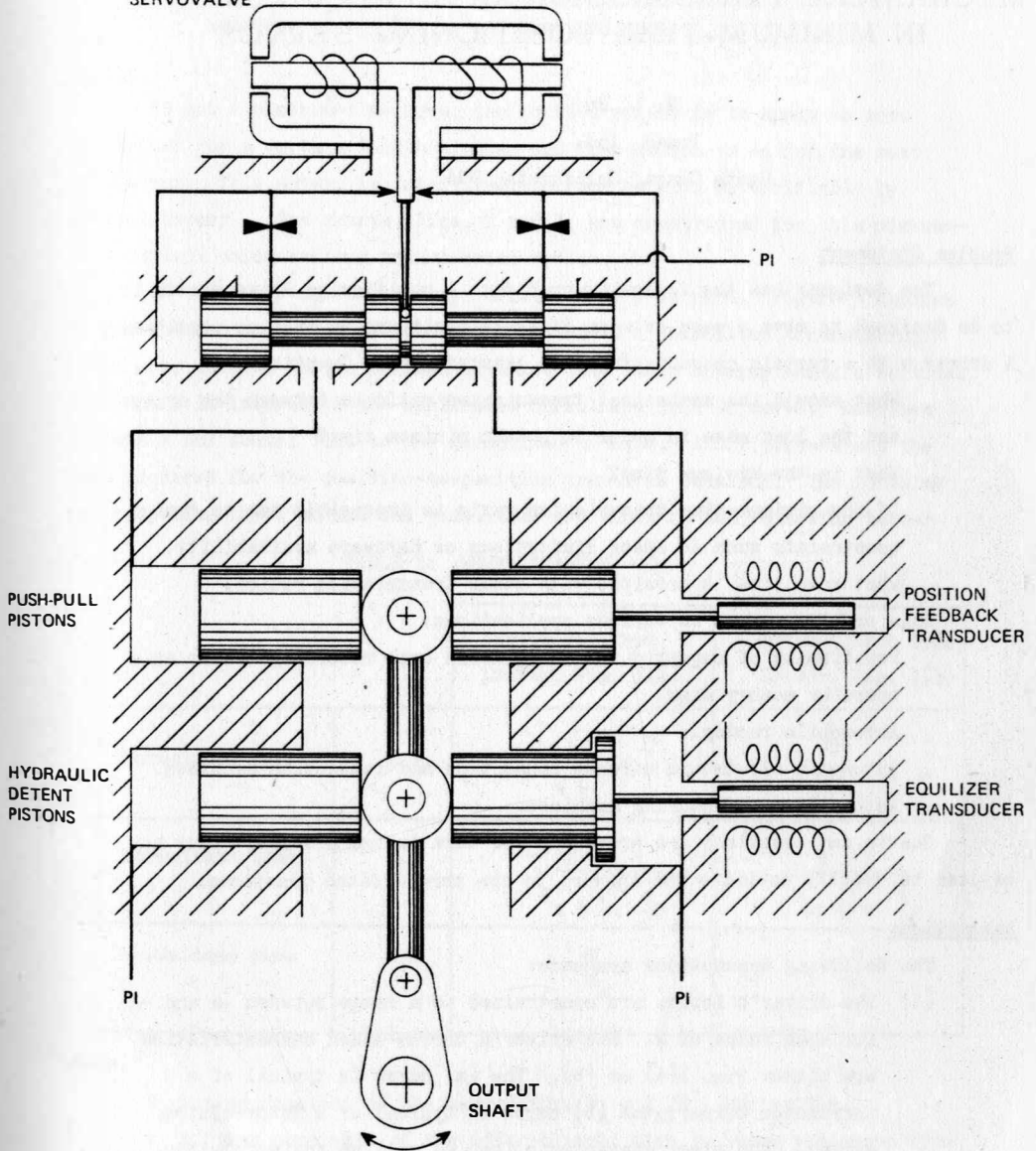
**SCHEMATIC DIAGRAM OF SST  
MASTER SERVO**

**FIGURE 23**



SST AIRPLANE ECS  
FIGURE 24



TWO STAGE  
SERVOVALVE

PICTORIAL SCHEMATIC  
ONE CHANNEL OF ECS SERVO  
FIGURE 25



# MECHANICAL TRANSMISSION RATIO REQUIREMENTS IN MINIMUM-TIME POSITIONING SERVOS

B. L. Ho

Iomec Inc.

Santa Clara, California, USA

## Problem Statement

The designer has the following problem: A positioning drive system is to be designed to move a mass between discrete positions as fast as possible.

A driver with a certain characteristic is assumed given. Questions:

- \* What should the mechanical transmission ratio be between the driver and the load mass in order to obtain minimum time?
- \* What is the minimum time?
- \* If the minimum-time transmission ratio is impossible due to design constraints such as space limitations or hardware availability, what move time is possible with other transmission ratios?

This problem arises in various applications:

- \* Positioning of magnetic recording heads over recording tracks on a computer memory disk.
- \* Automobile racing.
- \* Automatic electronic circuit connection and inspection machines.
- \* Automatic manufacturing machines.

Charts and equations are presented for this design problem. They may be used to quickly estimate the answers to the three stated questions.

## Assumptions

The following assumptions are made:

- (1) The driver's inputs are constrained to a range between  $+a$  and  $-a$  for some value of  $a$ . The driver's torque-speed characteristics are either Fig. 1(a) or (b). The (a) curve is typical of a servomotor driver; the (b) curve is typical of a motor-clutch driver. For other characteristics, we will approximate with (a) or (b).
- (2) As the load mass is moved from a point A to point B, velocities of the mass at points A and B are both zero.
- (3) All forces on the load mass other than the acceleration forces have negligible effect on the travel time.

- (4) Inertia of the transmission is negligible or may be added to the inertias of the driver and the load mass.

### Charts

To get a minimum-time move, the correct scheme is to apply  $+a$  into the driver for a certain length of time and then switch to  $-a$  for the rest of the way. This scheme is intuitively correct as well as verifiable by control theory<sup>1</sup>. The charts, Figs. 2 and 3, are constructed for this minimum-time control using various transmission ratios.

If one has a servomotor-type driver, Fig. 2 is used. Figure 3 applies to the motor-clutch type driver. In both charts a normalized transmission ratio  $\mu$  is entered in the horizontal axis. One reads upwards along a vertical line until it intersects the applicable normalized load  $\lambda$  curve. One then follows a horizontal line to the normalized  $\tau$  axis. After conversion, the time required for the position-to-position travel is obtained. The formulas for computing these normalized quantities are shown in the following table.

TABLE 1: NORMALIZATION

		Servomotor Type Driver, Fig. 1(a)	Motor-Clutch Type Driver, Fig. 1(b)
Normalized ratio	$\mu =$	$\sqrt{\frac{J_m}{I}} m$	$\sqrt{\frac{J_m}{I}} m$
Normalized load	$\lambda =$	$\frac{X \sqrt{I}}{V_s \sqrt{J_m} t_s}$	$\frac{X \sqrt{I}}{V_s \sqrt{J_m} t_c}$
Normalized time	$\tau =$	$\frac{T}{t_s}$	$\frac{T}{t_c}$

where

$t_s$  = time constant of the servomotor;  $t_s = J_m/D$ . Units: Sec.

$t_c$  = "time constant" of the motor-clutch; time to reach top speed from standing still;  $t_c = V_s J_m / T_q$ . See Fig. 1(b). Units: Sec.

$J_m$  = driver inertia. Units:  $\text{lb}_f\text{-in-sec}^2$  for rotary drivers and  $\text{lb}_f\text{-sec}^2/\text{in}$  for linear drivers.

$I$  = load inertia. Units:  $\text{lb}_f\text{-in-sec}^2$  for rotary load and  $\text{lb}_f\text{-sec}^2/\text{in}$  for linear loads.

$m$  = transmission ratio.  $m = (\text{motion in driver})/(\text{motion in load})$ .

Units: rad/rad for rotary to rotary, in/in for linear to linear, rad/in for rotary to linear, in/rad for linear to rotary.

$X$  = distance of load travel for the position-to-position travel.

Units: rad for a rotary load and in for a linear load.

$D$  = electrical or mechanical viscous damping in the driver, see Eq. (1).

Units:  $\text{lb}_f\text{-in-sec}$  for rotary driver,  $\text{lb}_f\text{-sec}^2/\text{in}$  for linear drivers.

$V_s$  = top speed of the driver. Units: rad/sec for a rotary driver, and in/sec for a linear driver.

$T$  = time required to travel the  $x$  distance in a manner described in assumption (2). Units: sec.

$T_q$  = the motor-clutch driver's drive force. Units: in- $\text{lb}_f$  for a rotary driver and  $\text{lb}_f$  for a linear driver.

Note that we may change the units in the above definitions as long as the changes are consistent, for example, all  $\text{lb}_f$  are changed to oz.

Example: The servomotor has the following characteristics:

Inertia:  $1.33 \text{ oz-in}^2$

Top Speed: 3600 rpm

Time constant: .0215 sec.

This motor is to drive a  $40 \text{ lb}_f$  mass for 30 in, standing still to standing still. What is the minimum time one may achieve and what is the required gear-rack ratio?

We have the following values:

$$J_m = .000215 \text{ lb}_f\text{-in-sec}^2$$

$$V_s = 376 \text{ rad/sec}$$

$$t_s = .0215 \text{ sec}$$

$$X = 30 \text{ in}$$

$$I = .104 \text{ lb}_f\text{-sec}^2/\text{in}$$

from which the normalized load is computed to be

$$\lambda = 81.5$$

selecting a  $\lambda$  curve corresponding to 81.5 (interpolation is required in this case), we see the lowest point has coordinates  $\mu = 0.3$ ,  $\tau = 42$ . Converting back from the normalized quantities, we have

$$T = (.000215/.01)42 = 0.9 \text{ sec}$$

$$m = \sqrt{.104/.000215} \cdot 0.3 = 6.6 \text{ rad/in} \approx 1 \text{ rev/in.}$$

The minimum travel time for this application is 0.9 sec, and a gear-rack ratio of one revolution per inch is required. Using any other ratio

(with the switching time appropriately readjusted) will result in more travel time.

#### Derivations:

##### 1. Servomotor Type Driver

The equation of motion of the motor-load system is

$$(I + J_m^2) \ddot{x} + Dm^2 \dot{x} = K u \quad (1)$$

where  $K$  is the motor torque constant, and  $u$  is the motor input which for minimum-time must have the form shown in Fig. 4. The load mass displacement is  $x$ , and other symbols are defined after Table 1.

The following notations are introduced

$$W = (I + J_m^2)/(m^2 D) = t_s (1 + \mu^2)/\mu^2 \quad (2)$$

$$V_s = K a / D \quad (3)$$

Solution to the stated differential equation for  $\alpha T \leq t \leq T$  is

$$x(t) = \frac{V_s}{m} \left[ 2\alpha T - t + W + W e^{-t/W} - 2W e^{-(t-\alpha T)/W} \right] \quad (4)$$

$$m\dot{x}(t) = V_s (1 - e^{-t/W}) - 2V_s \left[ 1 - e^{-(t-\alpha T)/W} \right] \quad (5)$$

where  $\alpha$ , the switching time ratio (see Fig. 4), and  $T$ , the total time for travel, are obtained by applying the following terminal conditions:

$$x(T) = X, \quad \dot{x}(T) = 0. \quad (6)$$

The solutions are

$$\alpha = \frac{1}{2} \left( 1 + \frac{mX}{V_s T} \right) \quad (7)$$

and

$$T/W = 2 \log_e \left( e^{mX/2V_s W} + \sqrt{e^{mX/V_s W} - 1} \right) \quad (8)$$

This equation is transformed into the following normalized form using the definitions given in Table 1:

$$\tau = 2 \left( 1 + \frac{1}{\mu^2} \right) \log_e \left[ e^{\lambda \mu^3 / 2(1+\mu^2)} + \sqrt{e^{\lambda \mu^3 / (1+\mu^2)} - 1} \right] \quad (9)$$

The last equation is plotted in Fig. 2.

##### 2. Motor-Clutch Type Driver

For this case the driver may or may not reach the saturation speed as depicted in Fig. 5. Two sets of equations are required.

When the travel distance  $X$  is long enough for the saturation speed to be reached, we have the situation in Fig. 5 curve (b). The equations are easily written as

$$X = 2(V_s t_c / 2m) + V_s (T - 2t_c) / m \quad (10)$$

obtaining

$$T = v_s(I + m^2 J_m)/(T_q m^2) + (x_m/v_s) \quad (11)$$

for  $x \geq v_s^2(I + m^2 J_m)/(T_q m^3)$

where the following relationship was used.

$$t_c = v_s J_m / T_q \quad (12)$$

Figure 5 curve (a) shows the velocity curve for shorter travel where saturation speed is not reached. The applicable equations are

$$x = v_s(T/2)^2/t_c \quad (13)$$

so that

$$T = 2\sqrt{x(I + m^2 J_m)/(T_q m)} \quad (14)$$

for  $x \leq v_s^2(I + m^2 J_m)/(T_q m^2)$

Normalizing as shown in Table 1, we have

$$\tau = 1 + \frac{1}{\mu^2} + \lambda\mu \quad \text{for} \quad \lambda \geq \frac{1 + \mu^2}{\mu^3} \quad (15)$$

$$\tau = 2\sqrt{(\mu + \frac{1}{\mu})\lambda} \quad \text{for} \quad \lambda \leq \frac{1 + \mu^2}{\mu^3} \quad (16)$$

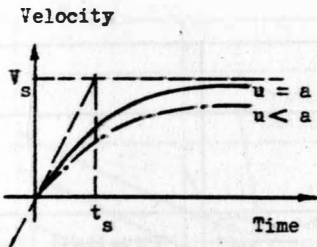
These two equations are plotted in Fig. 3.

### Discussions

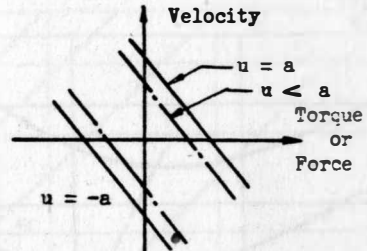
- (1) In conventional load-matching procedure the transmission ratio  $m$  is selected such that  $\mu = 1$ . This gives maximum load acceleration but in general not minimum-time because of the saturation speed. This may be seen in Figs. 2 and 3 where all minimum-time ratios,  $\mu$ , are less than 1.
- (2) The transmission ratio is not very critical to travel times as long as they are close to optimum. As a specific example, in Fig. 2 for  $\lambda = 2.5$ , a 30 percent change in transmission ratio from optimum causes only a 4 percent change in travel time.
- (3) For the motor-clutch type driver, saturation speeds are reached in a minimum-time travel when the load  $\lambda$  is larger than 2. For  $\lambda$  smaller than 2, saturation speeds are not reached, and the transmission ratio required is the conventional  $\mu = 1$ . See Fig. 3.

### Reference

1. La Salle, J.P., "Time Optimal Control Systems," Proc. National Academy of Sciences, USA, Vol. 45, pp. 573-577 (1959).

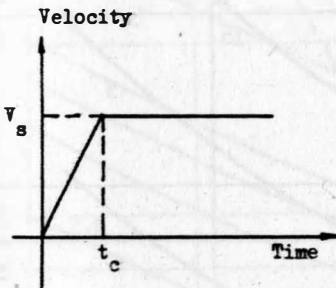


Velocity Response, Step Input.

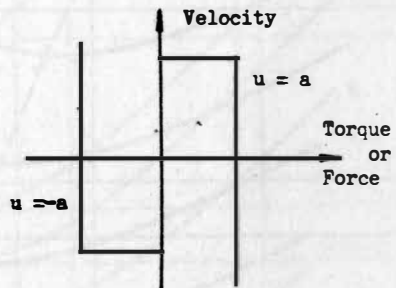


Torque-Velocity Characteristics.

(a) Servomotor Type Driver.



Velocity Response, Step Input.



Torque-Velocity Characteristics.

(b) Motor-Clutch Type Driver.

Fig. 1. Characteristics of Drivers.

Normalized Time

$$\tau = \frac{t}{t_s}$$

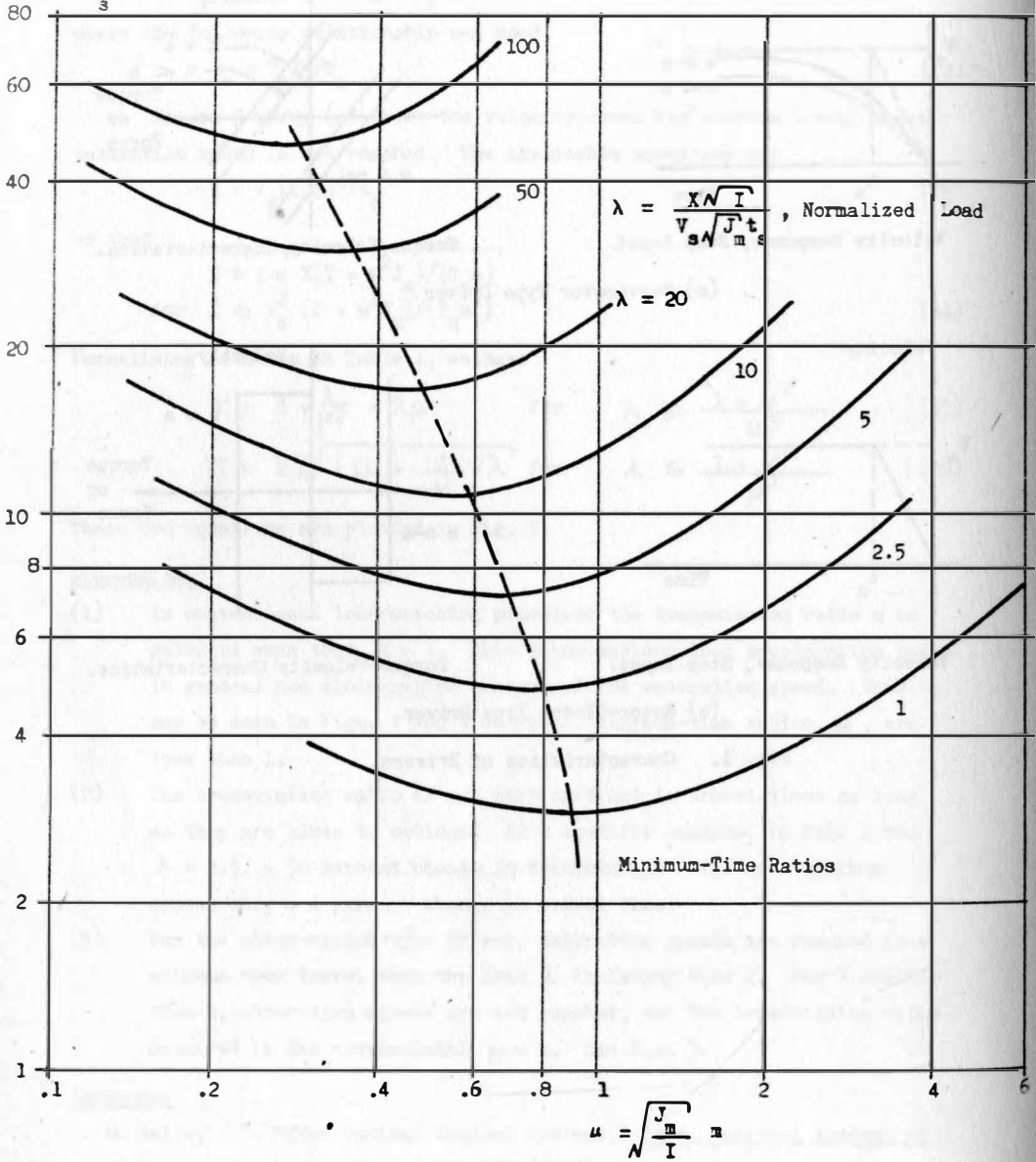


Fig. 2. Travel Times Vs. Transmission Ratios, Servomotor Driver.

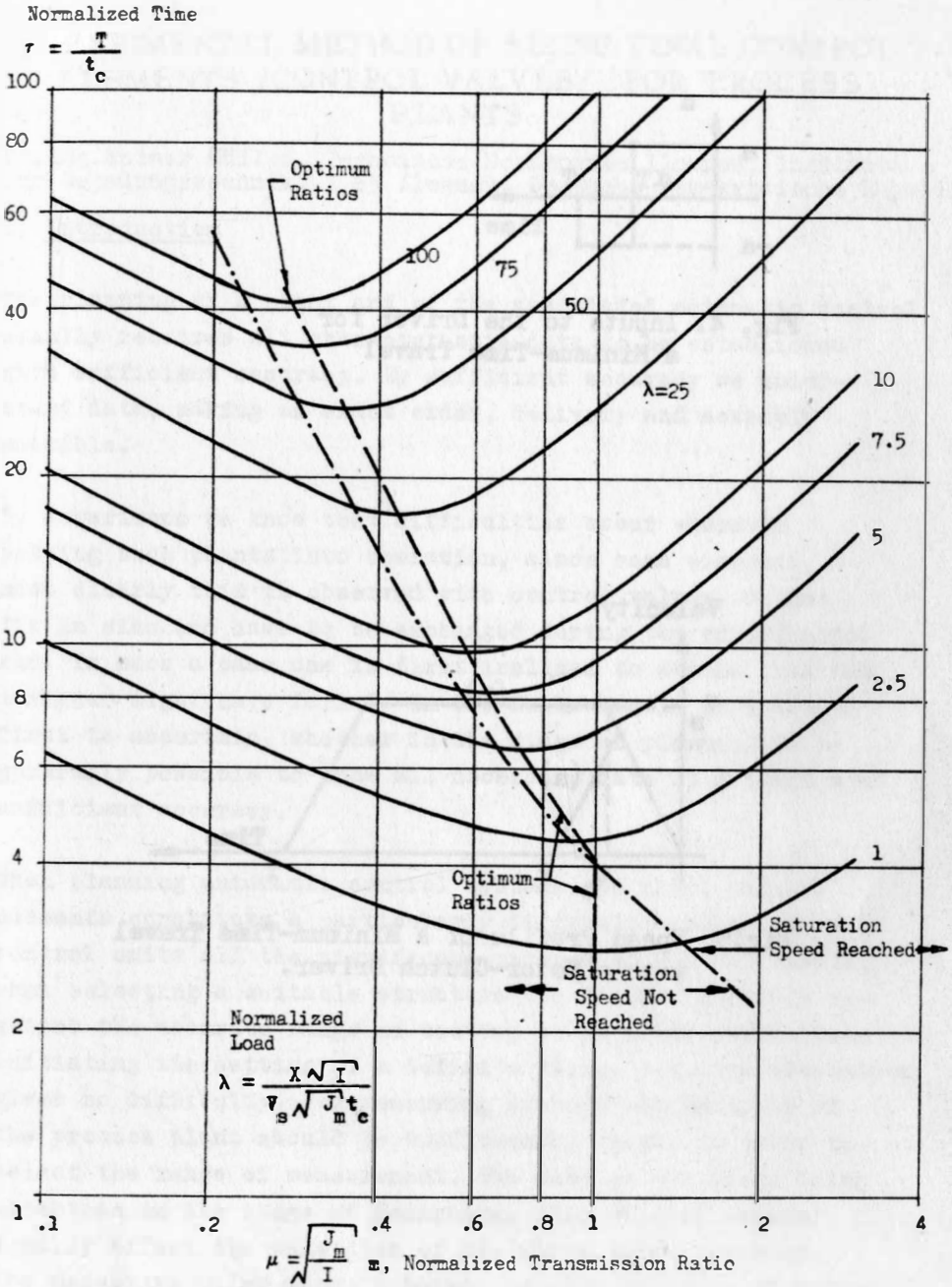


Fig.3. Travel Times Vs. Transmission Ratios, Motor-Clutch Driver.



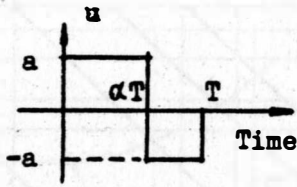


Fig. 4. Inputs to the Driver for a Minimum-Time Travel

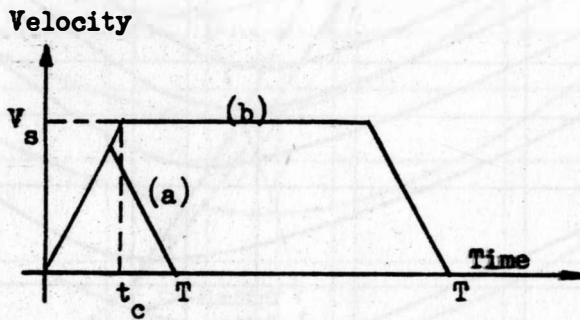


Fig.5. Speed Profile of a Minimum-Time Travel with a Motor-Clutch Driver.

## EXPERIMENTAL METHOD OF SIZING FINAL CONTROL ELEMENTS /CONTROL VALVES/ FOR PROCESS PLANTS

Dr. Ing. Rainer Müller, Technische Hochschule Ilmenau, Institut für Regelungstechnik, X 63 Ilmenau, Deutsche Demokratische Republik

### 1. Introduction

The planning of a plant and of the associated automatic control usually requires all characteristic data to be established with sufficient accuracy. By sufficient accuracy we understand data, making an exact order, delivery and assembly possible.

By experience we know that difficulties occur whenever putting such plants into operation, since some elements, most clearly this is observed with control valves, do not fit in size and have to be exchanged during the experimental run. In such a case one is first inclined to assume that the designer might have failed. In the following it is intended first to ascertain, whether in the stage of planning it is generally possible to know all necessary data of a plant with sufficient accuracy.

When planning automatic control systems the final control elements constitute a particularly difficult problem. With control units all the significant parameters are adjustable, when selecting a suitable structure the designing merely requires the accurate range of setting to be established. When initiating the setting of a definite value, i.e. the adaptation gives no difficulty. For measuring systems one variable of the process plant should be sufficiently known, in order to select the range of measurement. The data on the plant being uncertain in the stage of designing, this will of course equally affect the selection of the range of measurement. The necessary valve size, however, depends on pairs of values of pressure drop and controlled flow. Both are data, afflicted with appreciable uncertainties (errors) in the stage of

designing. Thus two possible errors enter into the valve sizing.

Now, let us deal more closely with the errors in calculating the sizing data in the stage of planning.

## 2. Uncertainty of the sizing data

For investigating the error a division of the applications into two groups is advisable. The first group comprises those cases, where the controlled flow represents a main variable of the process, e.g. the feed water flow of a boiler. This main variable is expected and supposed to be predetermined with tolerable accuracy. The second group embraces correction factors of the process. These are manipulated flows, which merely serve to control the state variables of the process, the value of the former being of no or only of a slight significance. Such controlled flows are nearly always small compared to the main flows of the process. The water spray for the temperature control of the superheated steam of boilers represents a typical example for that. Similar manipulated flows exist for heating or cooling chemical reaction processes.

While predicting the total process errors affect such correction flows considerably more than the main variable, since small changes of the main variables give rise to changes in the correction flows, which relative to these are great. The consequence was that in many cases the controlled flows cannot be planned with the accuracy required for planning a final control element. For the example of the temperature control of superheated steam by way of the injection of spray water the following error estimation is carried out.

### Error estimation for the controlled flow

Based on a heat balance around the whole superheater including the injection cooler

$$M_W = \frac{\Phi M_D (i_{DA} - i_{DE})}{i_{DA} - i_W} \quad (1)$$

is obtained for the spray water flow.

For the heat input contained therein

$$\Phi = \alpha A (\dot{v}_{Rm} - \dot{v}_{Dm}) \quad (2)$$

can be written for the heat transfer coefficient due to the contamination of the heating surface deviations of the gas velocity and inequal velocity distribution across the section

$$\frac{\Delta \alpha}{\alpha} = 0,1 \quad (3)$$

is set up.

Owing to changes in the air conditions during combustion or owing to the contamination of radiation heating surfaces as well as by changes of the position of flames an error of  $\Delta \dot{v}_{Rm} = \pm 100^\circ$  is assumed for the flame temperature. Moreover the variation of the steam temperature enters into the difference of temperature  $\Delta \dot{v}_m$ , here taken as the difference of average temperature, in order to simplify the calculation. In considering a controlled superheater the downstream temperature is assumed to be kept constant. The variations of the upstream temperature result in an error of the average steam temperature, which, compared to the error of flame temperature, is, however, negligibly small. With a mean difference in temperature of  $\Delta \dot{v}_m = 300^\circ$  as a relative error of the difference in temperature

$$\frac{\Delta \Delta \dot{v}_m}{\Delta \dot{v}_m} \approx 0,3 \quad (4)$$

and thus as an error of the heat input

$$\frac{\Delta \Phi}{\Phi} \approx 0,1 + 0,3 = 0,4 \quad (5)$$

is obtained.

Assuming the steam flow  $M_D$ , the downstream temperature  $\dot{v}_{DA}$  and/or the outlet enthalpy  $i_{DA}$  to be given quantities, for which no error is to be considered, the error of the spray water flow is obtained from equ. (1)

$$\Delta M_W = \frac{\Delta Q \pm M_D \Delta i_{DE}}{i_{DA} - i_W} \quad (6)$$

From experience we know that the temperature of the spray water and thus the enthalpy  $i_W$  are practically constant, so that no variations must needs be taken into account. Superheaters in boilers are usually designed such that the spray water flow is only used for correcting small differences between heat input and heat requirement. On this assumption

$$\frac{\Delta \Phi}{\Phi} \approx \frac{\Delta \Phi}{M_D (i_{DA} - i_{DE})} \quad (7)$$

is justified.

By means of the injection ratio  $\epsilon = M/M_D$  the error of the spray water flow can relatively be given

$$\frac{\Delta M_W}{M_W} = \frac{\left( \frac{\Delta \Phi}{\Phi} \pm \frac{\Delta i_{DE}}{i_{DA} - i_{DE}} \right) (i_{DA} - i_{DE})}{(i_{DA} - i_W) \cdot \epsilon} \quad (8)$$

from which

$$\frac{\Delta M_W}{M_W} = \frac{i_{DA} - i_{DE}}{\epsilon \cdot (i_{DA} - i_W)} \cdot \sqrt{\left( \frac{\Delta \Phi}{\Phi} \right)^2 + \left( \frac{\Delta i_{DE}}{i_{DA} - i_{DE}} \right)^2} \quad (9)$$

is derived.

The following numerical example is assumed:

steam pressure $p$	= 140 kp/cm <sup>2</sup>
upstream temperature $\dot{v}_{DE}$	= 420° C
upstream enthalpy $i_{DE}$	= 736 kcal/kg
downstream temperature $\dot{v}_{DA}$	= 500° C
downstream enthalpy $i_{DA}$	= 794 kcal/kg

enthalpy of spray water  $i_w = 200 \text{ kcal/kg} =$   
 average value of the injection ratio  
 $\epsilon = 0.03.$

Substituting in equ. (9) we thus obtain

$$\frac{\Delta M_W}{M_W} = \frac{794 - 763}{0.03 (794 - 200)} \sqrt{0.4^2 + \left(\frac{16}{794 - 736}\right)^2} \approx 1.6 \quad (10)$$

This rough error estimation showed that the error of the spray water flow solely from the error of the operating data far exceeds 100%, though a relatively small error was assumed for the heat-transfer coefficient.

For radiation superheaters the temperature enters in the fourth power. Thus an error of the flue-gas temperature takes a stronger effect. Calculating with the following values:

mean flue-gas temperature  $\bar{t}_{Rm} = 1200^\circ\text{K}$

error (uncertainty) of the  
 flue-gas temperature  $\bar{t}_R = 100^\circ$

average steam temperature  $\bar{t}_{Dm} = 750^\circ\text{K}$

relative error of the radiation  
 coefficient  $\Delta K/K = 0.1$

$$\frac{\Delta \phi}{\phi} = 0.55 \text{ is obtained.}$$

Substituting in equ. (9) results in

$$\frac{\Delta M_W}{M_W} = \frac{794 - 736}{0.03 (794 - 200)} \sqrt{0.55^2 + \left(\frac{16}{794 - 736}\right)^2} \approx 2 \quad (12)$$

The assumed individual errors in no way constitute extreme assumptions. The numerical values involved are about twice as large as those occurring on plants in operation in form of variations between different normal operating conditions. This appears adequate as an error(uncertainty) between

prediction and plant in operation. The error of the predicted heat-transfer coefficient may, however, readily be taken essentially higher.

### Error estimation for the pressure drop

The error of the pressure drop on the final control element can be estimated from the error for the pressure drop available for the injection line and the pressure drop of the injection nozzles.

In general the pump is used for surmounting the static pressure. Thus the pressure drop for the injection line  $p_L$  is often small compared to the pump pressure  $p_p$ , so that

$$p_L = p_p - p_D \approx 0.1 p_p \quad (13)$$

can be set up.

For the pump pressure

$$p_p = c n^2 d^2 \quad (14)$$

thus holds good.

Assuming an asynchronous drive you can reckon on changes of speed of the order of 1% due to frequency and load variations. Furthermore the pump pressure depends on the tolerances of the constructional dimensions. Thus in equ. (14) only the impeller diameter  $d$  was written, but additional to this radii of curvature, burr etc. are significant, as well. Summing up 1% diameter tolerance is taken for the constructional tolerances. As an error of the final pump pressure

$$\frac{\Delta p_p}{p_p} = \sqrt{(2 \cdot 0.01)^2 + (2 \cdot 0.01)^2} \approx 0.03 \quad (15)$$

is justified.

Owing to deviations of the load control the steam pressure  $p_p$  is subject to variations. For this 3% are assumed.

The error of the pressure drop across the injection line referred to the pump pressure amounts to

$$\frac{\Delta P_L}{P_p} = \sqrt{\left(\frac{\Delta P_p}{P_p}\right)^2 + \left(\frac{\Delta P_D}{P_D}\right)^2} \quad (16)$$

Applying equ. (14) with

$$\frac{\Delta P_D}{P_D} \approx \frac{\Delta P_D}{P_p} \quad (17)$$

$$\frac{\Delta P_L}{P_L} = \frac{1}{0.1} \sqrt{0.03^2 + 0.03^2} \approx 0.4 \quad (18)$$

is obtained.

When neglecting the resistance of pipe line the pressure drop across the whole injection line is divided among the control and injection nozzles

$$P_L = P_d + \Delta P \quad (19)$$

With reference to the flow characteristic of the control valve the nominal injection flow should be

$$P_d \approx \Delta P \quad (20)$$

The pressure drop of the spray water nozzle is

$$P_d = K \xi \frac{q^2}{d^5} \quad (21)$$

With the small diameter of the spray water nozzles the burr removing condition and bore tolerances enter appreciably. Due to a slight burr on the bore the resistance coefficient can be changed considerably.

$$\frac{\Delta \xi}{\xi} = 0.2 \quad (22)$$



is thus arranged.

Considering the small diameter we calculate with an error of the nozzle diameter of

$$\frac{\Delta d}{d} = 0.05 \quad (23)$$

With a constant mass flow we obtain from it

$$\frac{\Delta P_d}{P_d} = \frac{\Delta \xi}{\xi} + 4 \frac{\Delta d}{d} = 0.2 + 4 \cdot 0.05 = 0.4 \quad (24)$$

as error of the nozzle pressure drop.

For the relative error of the pressure drop of the control valve

$$\frac{\Delta \Delta P}{\Delta P} = \frac{2 \Delta P_L}{P_L} \pm \frac{\Delta P_d}{P_d} \quad , \quad (25)$$

is obtained from the equations (19) and (20), and from (25)

$$\frac{\Delta \Delta P}{\Delta P} = \sqrt{\left(\frac{2 \Delta P_L}{P_L}\right)^2 + \left(\frac{\Delta P_d}{P_d}\right)^2} = \sqrt{(2 \cdot 0.4)^2 + 0.4^2} \approx 0.9 \quad (26)$$

is derived.

This error estimation shows that even the pressure drop for the control valve exhibits a considerable error. This error equally occurs not only with injection systems but also with other controlled flow systems, e.g. with the control of the water flow serving as a heat carrier in a heated vessel, great errors for the pressure drop of the heating system of the vessel and heat exchanger for heating the water, the inside diameters of the pipes and the coefficients of friction of the pipes equally show a considerable error.

### 3. Plot of the rangeability of a final control element

The operating principle of a throttling valve is characterized by three variables: pressure drop  $\Delta_p$ , manipulated flow  $Q$  and stroke  $y$ . As a rule the first two variables are given by the process plant. By the stroke of the final control element, i.e. by the ratio of net orifice to great area the control valve should enable the pairs of values for pressure drop and controlled flow required for the process plant to be realized. The process being performed with different loads, different conditions of abrasion(erosion) and contamination etc., a field of pairs of values for pressure drop and controlled flow usually arises, not easy to survey.

The flow-dependent pressure change due to the series connection of final control element and fixed resistances in the piping and the differences between the area and flow characteristics of a final control element resulting from this, were widely discussed in the literature. Additional to this there is a number of flow-independent changes of pressure, e.g. when reversing to a spare pump or with the pump pressure varying due to the change of speed of the drive. A pressure reduction valve working for example between two steam systems, the pressure may rise up to the lift-up pressure of the safety valves, independent of the flow through the pressure reduction valve.

Until now the usual pattern has been to select the control valves according to the nominal values of the pressure drop and flow rate while considering a safety addition. For the above reasons we think it advisable to gain a survey of the combination of values. For this purpose we suggest a diagram, showing a semi-logarithmic chart of the pressure drop vs. the controlled flow, so that the  $k_v$ -values constitute parallel straight lines. The pressure drop entering into the flow equations with a root, it seems advisable to select the scale

of ordinate half as large as the scale of abscissa (Fig. 1). For given Cv characteristics of the final control elements a correlation of the stroke of the final control element and the Cv-value can be realized by applying auxiliary rulers<sup>1;2;3</sup>.

Compared to the chart proposed by Kretzschmar<sup>4</sup>, in which the stroke is plotted versus the controlled flow with the pressure drop serving as parameter, the  $\Delta p$ -Q-chart offers advantages, when changes in pressure, independent of flow, occur.

#### 4. Determination of sizing data from measured results

The simplest and previously usual way of monitoring the operating principle of a final control element is the plotting of the effective flow characteristic. In Fig. 2 three flow characteristics typical of an unfavourable sizing of the final control element are represented on the basis of a valve with linear Cv characteristic. A skilled engineer putting plants into operation recognizes, in which way the sizing should be corrected. The effective flow characteristic, however, yields no adequate quantitative data on the necessary correction of the final control element. Moreover the plotting of the effective flow characteristic is often no single line (curve). Due to the changes in pressure independent of the controlled flow (manipulated variable) an area of possible effective flow characteristics is obtained. For the case of the temperature control of superheated steam two motions of control are represented in Fig. 3. Fig. 3 shows the dependence of the spray water flow on the steam flow. Since there may be different combustion and heating surface conditions for each steam flow, a range of the spray water flow belongs to each steam flow. Since the pressure drop across the whole injection line depends on the steam flow due to the load drop of the superheater, there result different flow characteristics for the changes in load and those in heating with constant steam flow.

Plotting a  $\Delta p$ -Q-chart constitutes a favourable possibility of determining the sizing data by measurement. Keeping the employment of an expensive engineering staff within reasonable limits requires an automatical measurement. For this purpose a logarithmic coordinate plotter has been developed, by means of which the  $\Delta p$ -Q-chart can be plotted immediately. A precondition for this is in that the measurement for adapting the final control elements is from the first intended to be performed, so that the measuring possibilities, i.e. connections, where pressure drops are taken as well as means of attaching a flow meter need not subsequently be installed and that, if necessary, measuring transmitters may be connected. By widely applying elements of commercial potentiometric tape recorders the coordinate plotter consists of two Poggendorff compensators, one of which controls the rotation of a roller and the other the motion of a carriage. The logarithm of the quantity to be measured is taken via the compensating potentiometers of the recorder, approximating the logarithmic characteristic by means of shunts between a multiple of tapping points.

In consequence of the gain dependent of the measured values of the potentiometer the compensator loop contains some difficulties in control dynamics. This necessitated the gain of the amplifier being changed in dependence of the brush position on the measuring potentiometer.

Thus another nonlinear potentiometer affecting the gain of the compensating amplifier was mechanically coupled with the recording system.

The recorder is connected to the plant for a period, during which all typical operating conditions can be assumed to have been passed through. With this a field more or less filled with ink is obtained in the  $\Delta p$ -Q-chart as the rangeability of the final control element. Since it may happen that the plant

remains at one operating point, recording cannot be effected with <sup>liquid</sup>ink; as otherwise difficulties may arise with the ink drying up or with the paper soaking up the ink. The record is thus made by means of a pencil or a ball point.

##### 5. Iterative preparation of investments

The introductory error estimation shows that in some cases the size of the final control elements cannot be planned rationally. Therefore an organizational form has to be found, enabling the adaptation to be prepared systematically. For this the plan provides a so-called initiating final control element, being selected with a considerable safety addition in accord with the data available. In order to achieve a great immunity to an incorrect sizing the initiating final control element mostly obtains an equal percentage characteristic. On parallel lines with this runs an order given for a corrected final control element, which may already be included in the production program of the manufacturer, but the final size of which, especially of the inner valve is not established until measured results are obtained from the test run. The test run requires a final control element to have been installed before. The measured results realized this way do not depend on the sizing of the initiating final control element. The intended adaptation thus constitutes an iterative process. In practice you can, however, nearly always do with one step of iteration.

##### 6. Experimentally plotted $\Delta p$ -Q-chart

Fig. 4 shows a measured  $\Delta p$ -Q-chart of the temperature control of superheated steam of a 100 MW steam power plant (Fig. 5). For this plant the initiating control valve was selected too small. The necessary controlled flows were obtained by

increasing the upstream pressure. In the  $\Delta p$ - $Q$ -chart two superposed rangeabilities are thus plotted. In order to render it more visible the chart initially recorded by means of a pencil is traced with ink.

The Figs. 6 and 7 represent charts recorded on the pressure-control valve of a steam heating plant. The record was made with a ball point pen, the charts were not traced. When measuring steam flows the plotting as an equivalent water flow seems advisable with reference to the  $k_V$ - values ( $C_v$ -values) of the valves.

## 7. Flow characteristics

As previously described<sup>1;2;3</sup> the flow characteristic of the final control element can easily be plotted from the  $\Delta p$ - $Q$ -chart by using an auxiliary ruler. Since in the presence of flow-independent changes in pressure the rangeability represents no curve but an area, we usually confine to plotting the characteristics for the two outlines of the range of control in horizontal direction. With this all intermediate states are assumed to result in flow characteristics, radially distributed within the range thus localized (Fig. 6 and 7).

In general this requirement is not met. In the Fig. 6 and 7 the motions of control discussed by means of Fig. 3 were thus qualitatively plotted.

## References:-

- 1 Mueller, J. and R. Mueller: *Stelleinrichtungen für Stoffströme*. Berlin: VEB Verlag Technik 1967
- 2 Mueller, R.: *Arbeitsblatt zur Auslegung von Regelventilen* msr 8 ap (1965) H. 4, S.75-78

- 3 Mueller, R.: Anpassung von Stellventilen, msr 11 ap(1968)  
H. 3, S. 43-45
- 4 Kretzschmer: Die Bemessung von Regelventilen, Regelungs-  
technik 7(1959) H. 10, S. 351-355

### List of symbols

A	heating surface
C	constant
K	combined radiation coefficient
M	mass flow
Q	flow volume
d	diameter
i	enthalpy
$k_v$	valve coefficient
n	speed
p	pressure, pressure drop
$\Delta_p$	pressure drop of the regulating valve
$\Delta$	deviation
$\phi$	heat flow
$\alpha$	heat-transfer coefficient
$\varepsilon$	injection ratio
$\xi$	resistance coefficient
$\vartheta$	temperature

### Indices

A	outlet
D	steam
E	inlet
L	line
P	pump
R	flue gas (boiler gas)
d	nozzle
m	mean value

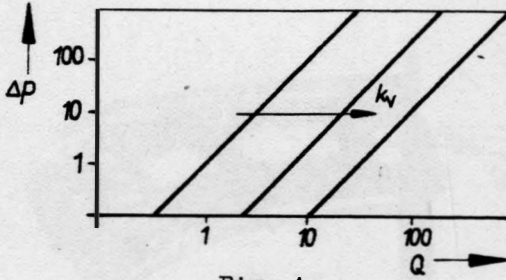


Fig. 1:

$\Delta p$ - $Q$ -chart representing the rangeability of throttling valves

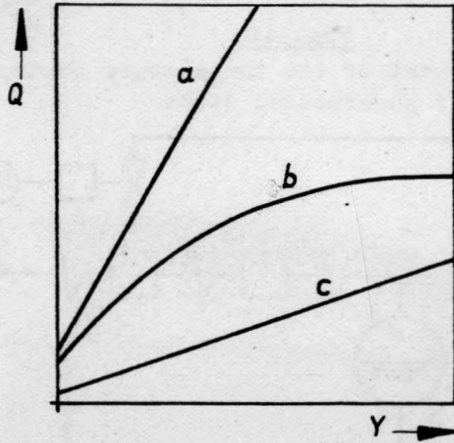


Fig. 2:

Typical flow characteristics

- a) too large a final control valve
- b) too large fixed resistances in the piping
- c) too small a final control element



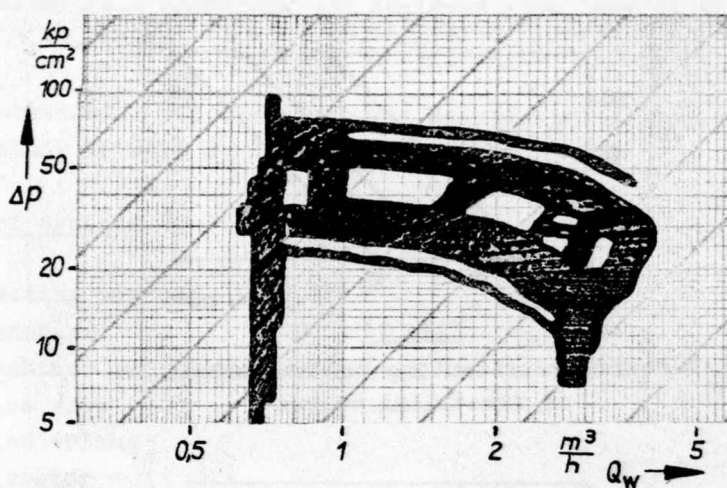


Fig. 4:

$\Delta p$ - $Q$ -chart of the temperature control  
of superheated steam

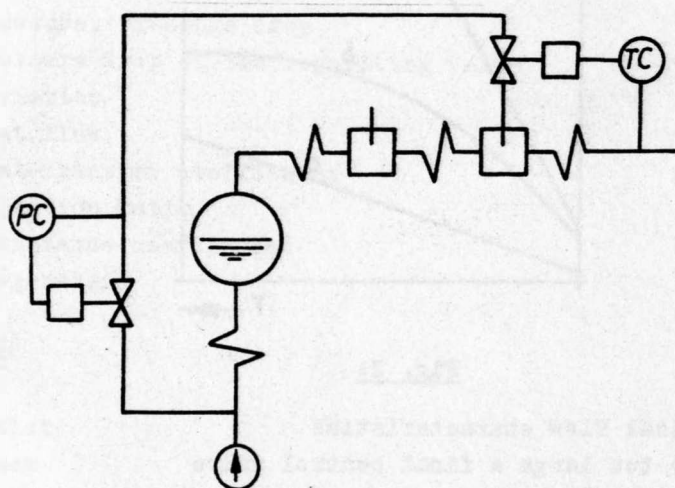


Fig. 5:

Part of the scheme of a plant

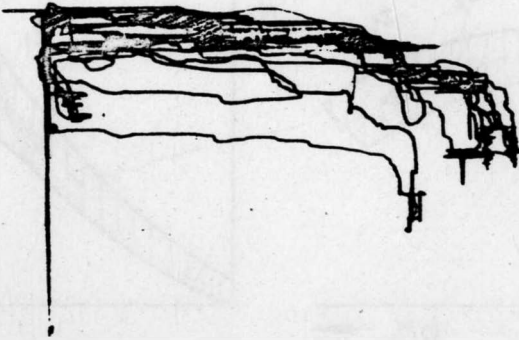
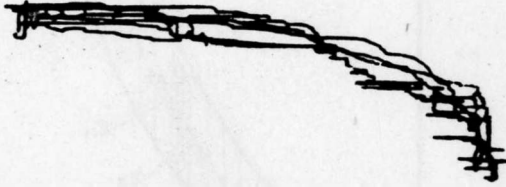


Fig. 6 and 7:

$\Delta p$ -Q-charts of a steam pressure control valve

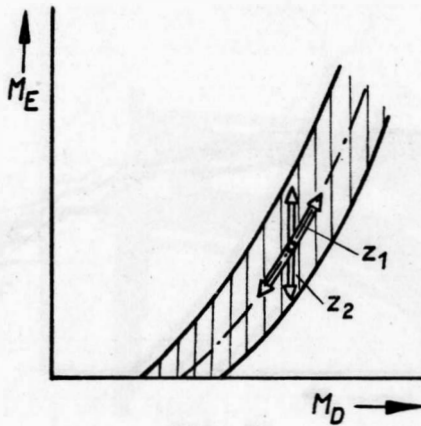


Fig. 3:

Operating motions of the temperature control

$z_1$  = change of the load

$z_2$  = change of the state of combustion

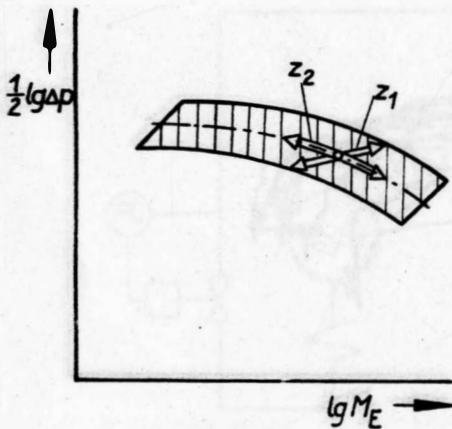


Fig. 8:

Operating motions  
of the temperature control  
in the  $\Delta p$ - $Q$ -chart

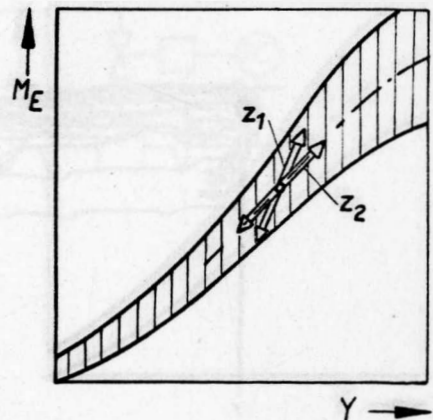


Fig. 9:

Flow characteristics (equal  
percentage flow characteristic)

